UDC 621
CODEN: MINSC5
In print: ISSN 1857 – 5293
On line: ISSN 1857 – 9191

MECHANICAL ENGINEERING SCIENTIFIC JOURNAL

МАШИНСКО ИНЖЕНЕРСТВО НАУЧНО СПИСАНИЕ

Volume 41
Number 1

Skopje, 2023

Mech. Eng. Sci. J.	Vol. **41**	No. 1	pp. 1–74	Skopje 2023
Маш. инж. науч. спис.	Год.	Број	стр.	Скопје

MECHANICAL ENGINEERING – SCIENTIFIC JOURNAL
МАШИНСКО ИНЖЕНЕРСТВО – НАУЧНО СПИСАНИЕ

Published by
Faculty of Mechanical Engineering, Ss. Cyril and Methodius University in Skopje, North Macedonia
Издава
Машински факултет, Универзитет „Св. Кирил и Методиј” во Скопје, Северна Македонија

Published twice yearly – Излегува два пати годишно

UDC: "St. Kliment Ohridski" Library – Skopje	УДК: НУБ „Св.. Климент Охридски“ – Скопје
Copies: 300	Тираж: 300
Price: 520 denars	Цена: 520 денари

Address	Адреса
Faculty of Mechanical Engineering	**Машински факултет**
(Mechanical Engineering – Scientific Journal)	(Машинско инженерство – научно списание)
Editor in Chief	Одговорен уредник
P.O.Box 464	пошт. фах 464
MK-1001 Skopje, Republic of North Macedonia	МК-1001 Скопје, Република Северна Македонија

Mech. Eng. Sci. J. is indexed/abstracted in INIS (International Nuclear Information System)
www.mf.ukim.edu.mk

MECHANICAL ENGINEERING – SCIENTIFIC JOURNAL
FACULTY OF MECHANICAL ENGINEERING, SKOPJE, REPUBLIC OF NORTH MACEDONIA

МАШИНСКО ИНЖЕНЕРСТВО – НАУЧНО СПИСАНИЕ
МАШИНСКИ ФАКУЛТЕТ, СКОПЈЕ, РЕПУБЛИКА СЕВЕРНА МАКЕДОНИЈА

Mech. Eng. Sci. J.	Vol.	No.	pp.	Skopje
	41	1	1–74	2023
Маш. инж. науч. спис.	Год.	Број	стр.	Скопје

TABLE OF CONTENTS
(С О Д Р Ж И Н А)

WELDING ENGINEERING
(Заварување)

658 – Martin Petreski, Aleksandra Krstevska, Zoran Bogatinoski
MECHANICAL TESTING OF HLAW WELDED JOINTS IN ACCORDANCE WITH EUROPEAN STANDARDS – THEORETICAL APPROACH
(Механичко испитување на заварени споеви изведени со хибридно заварување согласно со европските стандарди – теоретски пристап).....5–13

659 – Aleksandra Krstevska, Martin Petreski, Filip Zdraveski
INFLUENCE OF INDUSTRY 4.0 IN WELDING ENGINEERING – THEORETICAL APPROACH
(ВЛИЈАНИЕ НА ИНДУСТРИЈАТА 4.0 ВРЗ ЗАВАРУВАЊЕТО – ТЕОРЕТСКИ ПРИСТАП) 15–21

MECHANOTRONICS
(Механотроника)

660 – Slavčo Premčeski, Dame Korunoski, Anastasija Ignjatovska, Damjan Pecioski
DESIGN AND IMPLEMENTATION OF AN AUTOMATED SAFETY LOCK SYSTEM WITH MULTIPLE AUTHENTICATIONS AND ALARM PROTECTION
(Дизајн и имплементација на автоматизиран безбедносен систем за заклучување со повеќе автентикации и заштитен аларм) 23–28

661– Anastasija Ignjatovska, Damjan Pecioski, Dejan Šiškovski, Maja Anačkova, Simona Domazetovska
ANALYTICAL MODELING AND FEM SIMULATIONS OF ENERGY HARVESTING CANTILEVER BEAM
(Аналитичко моделирање и симулации на конзолен систем за собирање енергија со методот на конечни елементи) 29–36

662 – Damjan Pecioski, Anastasija Ignjatovska, Dejan Šiškovski, Simona Domazetovska, Maja Anačkova
DESIGN OF AN ENERGY HARVESTING SYSTEM USING PIEZOELECTRIC MATERIALS
(Дизајн на систем за собирање енергија со користење на пиезоелектрични материјали) 37–42

INDUSTRIAL DESIGN
(Индустриски дизајн)

663 – Ile Mirčeski, Dimitrij Georgievski
DESIGN PROCESS OF COMPLEX PRODUCT SHAPE WITH LATTICE VORONOI'S STRUCTURE USING CAx TOOLS
(Процес на дизајнирање сложени облици на производ со решеткави Вороноиеви структури и употреба на алатките CAx) 43–50

MOTOR VEHICLES
(Моторни возила)

664 – Stefani Josifovska, Vase Jordanoska
COMPARISON OF DIFFERENT MODELLING APPROACHES FOR VEHICLE VELOCITY CONTROL ON AN UPCOMING BOTTLENECK SECTION
(Споредба на различни начини на моделирање управување со брзината на возило при спојување на две сообраќајни ленти во една) 51–58

665 – Vasko Čangoski, Igor Ǵurkov, Darko Danev, Vase Jordanoska
VEHICLE HANDLING ENHANCEMENT EMPLOYING FOUR-WHEEL INDEPENDENT STEERING SYSTEM USING SLIDING MODE CONTROL
(Подобрување на управливоста кај возилата со систем за независно управување на четири тркала со примена на стратегијата со лизгачка површина) 59–70

Instruction for authors 71–74

Mechanical Engineering – Scientific Journal, Vol. **41,** No. 1, pp. 5–13 (2023)
Number of article: 658
In print: ISSN 1857–5293
Received: October 31, 2022
On line: ISSN 1857–9191
Accepted: March 15, 2023
UDC: 621.791.72/.75:[620.1:006.86
https://doi.org/10.55302/MESJ23411658005p

Original scientific paper

MECHANICAL TESTING OF HLAW WELDED JOINTS IN ACCORDANCE WITH EUROPEAN STANDARDS – THEORETICAL APPROACH

Martin Petreski, Aleksandra Krstevska, Zoran Bogatinoski

Faculty of Mechanical Engineering, "Ss. Cyril and Methodius" University in Skopje, P.O.Box 464, MK-1001Skopje, Republic of North Macedonia
martin.petreski@mf.edu.mk

A b s t r a c t: Hybrid laser arc welding is a relatively new welding process, whereby combining the advantages of two different processes, laser beam welding and gas metal arc welding, represents an excellent substitute for conventional welding processes, but has not yet been sufficiently elaborated and researched. Additional research should be carried out in terms of hybrid welding technologies, this leads to the creation and development of new standards and procedures that would confirm their validity. The mechanical tests that could be destructive and non-destructive are the primary indicator of the quality of the welded joint and the qualification of the welding technology. This paper presents the current procedure for mechanical testing of welded joints performed by hybrid laser arc welding and the design of the test specimens that depends on the type of the testing method and conditions in the relevant application standard. In the final part, general conclusions are drawn regarding the standards covering the welded joint quality performed by hybrid laser welding.

Key words: hybrid welding; test specimens; mechanical testing; standard; procedure

МЕХАНИЧКО ИСПИТУВАЊЕ НА ЗАВАРЕНИ СПОЕВИ ИЗВЕДЕНИ СО ХИБРИДНО ЗАВАРУВАЊЕ СОГЛАСНО СО ЕВРОПСКИТЕ СТАНДАРДИ – ТЕОРЕТСКИ ПРИСТАП

А п с т р а к т: Хибридно заварување со ласерски зрак и електричен лак е релативно нов процес на заварување кој преку комбинирање на предностите на два различни процеса, заварување со ласерски зрак и полуавтоматско заварување со топлива електродна жица под заштитен гас, претставува одлична замена за конвенционалните процеси на заварување, но сè уште не е доволно елаборирани истражен. Треба да се изведат дополнителни истражувања поврзани со технологиите за хибридно заварување, што доведува до создавање и развој на нови стандарди и процедури кои би ја потврдиле нивната валидност. Механичките испитувања се основен показател со кој се определува квалитетот на завареният спој и квалификација на технологијата на заварување и тие испитувања можат да се изведат со разорување и без разорување. Овој труд ја елаборира тековната постапка за механичко испитување на заварени споеви изведени со хибридно заварување со ласерски зрак и електричен лак, како и дизајнот на епруветите кој зависи од видот на испитувањето и условите на примена. Накрај се изведени генерални заклучоци во однос на стандардите кои го покриваат квалитетот на завареният спој изведен со хибридно заварување со ласерски зрак и електричен лак.

Клучни зборови: хибридно заварување; епрувети; механичко испитување; стандарди; процедури

1. INTRODUCTION

Today's globalization is characterized by an accelerated process movement of capital, resources, products and services, resulting in a completely new world trade structure, economic and financial flows, internationalization of production, and acceleration of technical and technological development. As a part of mechanical engineering, the welding have not been lagging in technological development, new welding techniques and technologies are constantly being introduced, which would result in reduced production costs and improved technical characteristics of the welded joints [1].

Hybrid laser arc welding (HLAW) is a relatively new welding process, whereby combining the

advantages of two different processes: laser beam welding – LBW, and semi-automatic welding processes such as gas metal arc welding – GMAW, and flux-cored arc welding – FCAW, represents an excellent substitute for conventional welding processes [2, 7].

The implementation of new welding techniques and technologies leads to the creation and development of new standards and procedures that would confirm their validity.

Mechanical tests are a primary indicator that determines the mechanical properties of welded joins, and they can be done destructively or non-destructively. The tests give results that, if within predetermined needs and criteria, guarantee the safety of the welded structure, but if the results prove to be 'poor', they indicate defects in the welded joint and require corrective actions to meet the required criteria.

The mechanical testing of the welded joints can be performed in two ways, on a fully welded structure or test pieces – test specimens made from a part of the welded structure, and the second way, laboratory test specimens prepared and made under the general conditions of welding in production, which they shall represent.

Depending on the required criteria, the mechanical testing of the welded joint can be performed on:

– Test specimens are entirely made of weld metal (made in molds). The obtained results will define the weld metal's mechanical properties without considering the base material influence;

– Test specimens are made of welded joints where the base material has been melted and with a certain percentage mixed in the molten mixture during the welding process. The percentage of participation of the base material in the weld metal depends on the welding procedure and welding parameters such as the welding current, voltage, diameter of the electrode-welding wire, welding speed, welding position, etc.

In this paper, the current procedure for mechanical testing of welded joints performed by hybrid laser arc welding HLAW is presented. The procedures for the preparation of test specimens for mechanical testing have been elaborated in detail depending on the welded joint as well as the type of mechanical testing (tensile test, bending, toughness test, etc.).

2. PRODUCTION OF TEST PIECES – WELDED SPECIMNES

The production of the test pieces – welded specimens, must be carried out in accordance with the prescribed norms and standards for the welding procedure as well as the type of material which is welded, while taking care that they are fully prepared and made under conditions that correspond to the production or assembly of the welded structure.

In order to determine the quality of the welded specimens and their mechanical properties and thus qualify the welding technology, it is necessary to carry out destructive and non-destructive testing after the welding process. The following types of tests are mainly performed to determine the quality of the welded specimens:

- Non-destructive testing of welded specimens:
  - Visual and dimensional control.
  - Liquid penetrant testing.
  - Magnetic particle testing.
  - Ultrasonic inspection.
  - Radiographic inspection.
- Destructive (mechanical) testing of welded specimens:
  - Tensile test.
  - Bend test.
  - Impact testing.
  - Hardness testing.
  - Metallographic inspection of the weld and HAZ.

The testing procedures for welded specimens performed by hybrid laser arc welding – HLAW, must be performed in accordance with the standard EN ISO 15614-1, more precisely with standard EN ISO 15614-14 – Specification and qualification of welding procedures for metallic materials – Welding procedure test – Part 14: Laser-arc hybrid welding of steel, nickel and nickel alloys [3, 4].

This standard proves the validity of the welding technology of the test piece and a welding procedure qualification record (WPQR) is issued based on it. For the purpose of complete inspection, the test piece should have sufficient size to ensure good heat distribution and sufficient surface area to be able to produce all the required test specimens. The rolling direction should also be marked on the welded specimen for caution when the test specimens are produced from the heat-affected zone [3].

In addition, the operator of the welding equipment should be certified according to the standard EN ISO 14732, while the welding parameters

should be in accordance with the preliminary welding procedure specification – pWPS [5, 6].

The dimensions and shape of the welded specimens depend on the type of the weld, for a butt weld the following dimensions are required (Figure 1):

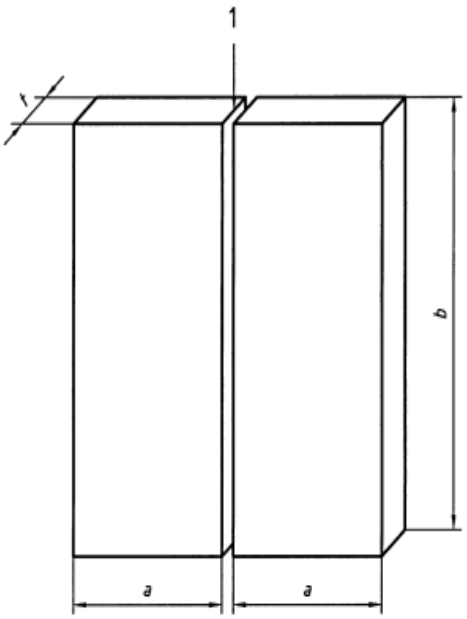

Fig. 1. Dimensions of a test piece for a butt joint in plate with partial or full penetration [4]
1 – Preparation of the groove and positioning in accordance with pWPS; *t* – material thickness; *a* – minimum 150 mm; *b* – minimum 350 mm

3. EXAMINATION AND TESTING OF TEST PIECES – WELDED SPECIMENS

Welded specimens after the welding process are tested with destructive and non-destructive tests in order to determined the quality of the welded joint. Depending on the type of weld, the test pieces should be in accordance with Table 1.

3.1. *Location and taking of test specimens*

Before being cut out of the test piece, test specimens should be marked into several locations depending on how many and what types of test specimens are needed to test the mechanical characteristics of the welded joint.

The test specimens shall be cut out, wherever possible by a mechanical process, and machined to the required dimensions. If the test specimens are cut from the test piece by a thermal process, they must be wide enough to ensure that the heat-affected zone can be completely machined off.

T a b l e 1

Examination and testing of the test pieces [4]

Test piece	Type of test	Extent of testing	Footnote
Butt joint with full penetration	Visual	100 %	–
	Radiographic or ultrasonic	100 %	a
	Surface crack detection	100 %	b
	Transverse tensile test	2 specimens	–
	Transverse bend test	4 specimens	c
	Impact test	2 sets	d
	Hardness test	Required	e
	Macroscopic examination	1 specimen	–
T-joint with full penetration	Visual	100 %	f
Branch connection with full penetration	Surface crack detection	100 %	b and f
	Ultrasonic or radiographic	100 %	a, f and g
	Hardness test	Required	e and f
	Macroscopic examination	2 specimens	f
Fillet welds	Visual	100 %	f
	Surface crack detection	100 %	b and f
	Hardness test	Required	e and f
	Macroscopic examination	2 specimens	f

[a] Ultrasonic testing shall not be used for $t < 8$ mm and not for material groups 8, 10, 41 to 48.

[b] Penetration testing or magnetic particle testing. For non-magnetic materials, penetration testing.

[c] For bend tests, see 7.4.3.

[d] 1 set in the weld metal and 1 set in the HAZ for materials ≥ 12 mm thick and having specified impact properties. Application standards may require impact testing below 12 mm thick. The testing temperature shall be chosen by the manufacturer with regard to the application or application standard but not be lower the parent metal specification. For additional test see 7.4.5.

[e] Not required for parent metals: sub-group 1.1. and groups 8, 41 to 48.

[f] Tests as detailed do not provide information on the mechanical properties of the joint. Where these properties are relevant to the application an additional qualification shall also be held, e.g. a butt weld qualification.

[g] For outside diameter ≤ 50 mm no ultrasonic test is required.

[F] For outside diameter > 50 mm and where it is not technically possible to carry out ultrasonic examination, a radiographic examination shall be carried out provided that the joint configuration will allow meaningful results.

The test specimens for mechanical testing should be taken after all non-destructive testing has been carried out and which has passed the relevant inspection criteria. If the test piece has imperfections within the acceptable tolerance for non-destructive testing, it is acceptable to take the test specimens from locations not provided within the standard.

The location for the test specimens depends on the type of the weld, for a butt weld it should be in accordance with Figure 2.

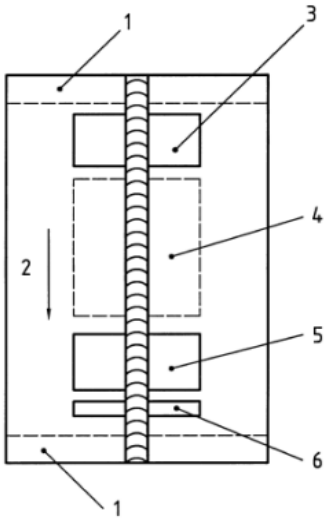

1. Discard 25 mm.
2. Welding direction.
3. Area for:
   – 1 tensile test specimen,
   – bend test specimens.
4 Area for:
   – impact and additional test specimens if required.
5. Area for:
   – 1 tensile test specimen
   – bend test specimens.
6. Area for:
   – 1 macro test specimen;
   – 1 hardness test specimen.

Fig. 2. Location of test specimens for a butt joint in plate [4]

3.2. *Tensile tests*

The tensile test is the most widely applied static test that provides a lot of information on the mechanical characteristics of the material under test. The tensile test is carried out to determine the tensile strength (Rm), breaking strength, contraction and elongation, yield strength (ReH), young's modulus and proportional limit stress [9].

The basic principle in the design of the welded structures is that the weld strength should be equal or higher than the base material strength. The test specimen must be made of the same material as the structure, while separating the test specimens from the base material, care should be taken for structural changes that would affect the final test results.

Tensile test specimens can be technical or standardized. The technical test specimens are tested in the state of application of the product, without special machining of the measurement length. On the other hand, the standard tensile test specimens should be made in accordance with standard EN ISO 4136, and they can have a cylindrical or prismatic cross-section [8].

The standard allows the test specimens to be taken from locations with minimum imperfections acceptable in non-destructive testing.

The symbols and abbreviated terms to be used for the tensile test specimens are specified in Table 2 and represented in Figure 3.

The test specimen should be taken transversely from the welded joint, which after machining, the weld axis should be in the middle of the parallel length (Lc) of the test specimen [8].

Additional heat treatment shall not be applied to the welded joint or to the test specimen unless previously specified, in case of heat treatment, any details shall be recorded in the test report. If the test specimens are cut from the welded plate with a thermal process, cuts should be made at a minimum distance of 8 mm from the surfaces of the final parallel length (Lc) of the test specimen [8].

T a b l e 2

Symbols and abbreviated terms for tensile test specimens [8]

Symbol	Terms	Unit
b	Width of the parallel length	mm
b_1	Width of shoulder	mm
d	Diameter of the plug	mm
D	Outside diameter of the pipe	mm
L_C	Parallel length	mm
L_O	Original gauge length	mm
L_S	Maximum width of the weld after machining	mm
L_t	Total length of the test specimen	mm
r	Radius of shoulder	mm
t	Thickness of the welded joint	
t_s	Thickness of the test specimen	mm

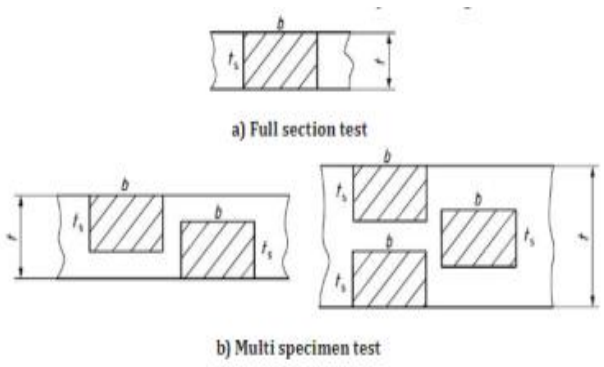

Fig. 3. Location of test specimens depending on the thickness of the welded joint [8]

In general, the thickness of the tensile test specimen (t_s), should be equal with the base material thickness near the welded joint (Figure 3a). If the base material has thickness >30 mm and the application requires testing of full thickness, several test specimens should be produced from different levels to cover the full thickness of the welded joint (Figure 3b).

The dimensions and shape of the test specimen shall be in accordance with those given in Table 3, with reference to the symbols in Figure 4 and Table 2. The thickness of the test specimen should be constant along the parallel length (Lc) [8].

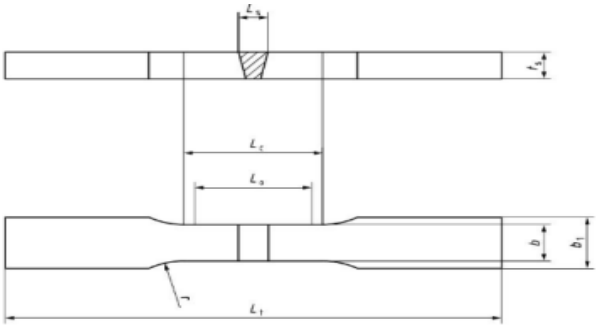

Fig. 4. Tensile test specimen for a butt joint in plate [8]

Table 3

Dimensions of the tensile test specimens for a butt joint [8]

Denomination		Symbol	Dimensions
Total length of the test specimen		L_t	To suit particular testing machine
Width of shoulder		b_1	b + 12
Width of the parallel legth	plates	b	12 for $t_s \leq 2$ 25 for $t_s > 2$
	pipes	b	6 for D ≤ 50 12 for 50 < D ≤ 168,3 25 for D > 168,3
Parallel length [a b]		L_C	≥ L_s + 60
Radius at shoulder		r	≥ 25

3.3. *Bend test*

The bend test aims to check the deformation capabilities of the welded joint, and it is a part of technological tests, while the bending strength represents the essential characteristics of resistance to bending. This test should be in accordance with standard ISO 5173.

The standard specifies 9 types of bend test specimens made transversely and longitudinally to the welding direction. Usually, there are made test specimens for transverse root and face bend tests of butt welds, but depending on the base material thickness, lateral test specimens are made for side bend test in such a way that after machining the weld axis will remain in the center of the test specimen [10].

The symbols and abbreviated terms to be used for the bend test specimens are specified in Table 4 and represented in Figures 5 and 6.

Table 4

Symbols and abbreviated terms for bend test specimens [10]

Symbol	Description	Unit
A	Min. elongation after destruction depending of the material	%
b	Test specimen width	mm
d	Internal roller diameter (presser)	mm
I	Distance between the rollers	mm
L_f	Starting distance between the roller contact and the weld axis	mm
L_s	Maximum weld width after treatment	mm
L_t	Test specimen total length	mm
r	Test sample edges radius	mm
t	Welded sample thickness	mm
Ts	Test specimen thickness	mm
α	Bending angle	°

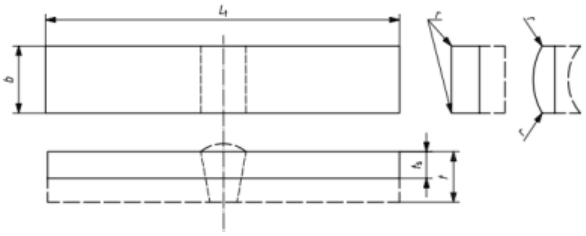

Fig. 5. Transverse face bend test specimen for a butt weld [10]

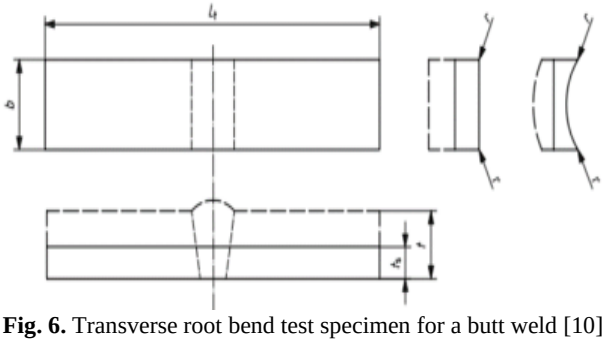

Fig. 6. Transverse root bend test specimen for a butt weld [10]

Heat treatment shall not be applied to the welded joint or the test specimen unless previously specified, if a thermal process is used to extract the test specimen from the welded plate, the cuts shall be made at the minimum distance of 3 mm from the test specimen [10].

The test should be carried out by placing the test specimen on two parallel supports, where the weld will be in the middle and is bent by applying force from an upper roller. The bending takes place continuously until a 2 mm crack appears, after which the bending angle is measured. Otherwise, the bending takes place until the test specimen sides are parallel, up to a bending angle of 180°.

In general, the test specimen thickness for transverse root and face bend test (t_s), shall be equal to the thickness of the base material near the welded joint (Figure 7a). If the base material thickness is greater than 10 mm, the test specimen thickness shall be machined from one side to a thickness equal to 10 ± 0.5 mm, while the root or face of the weld shall be in tension zone. When the application requires testing of a full thickness >10 mm, several test specimens shall be taken in order to cover the full thickness of the welded joint (Figure 7b). The same procedure shall be for the side bend test.

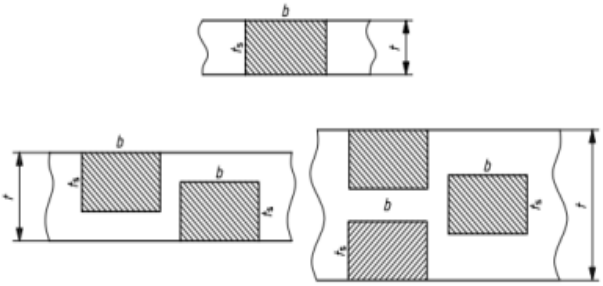

Fig. 7. Root and face bend test specimens for a butt weld [10]

In terms of the dimensions, the width (b) of the test specimen for transverse root or face bend test shall be $4t_s$ or greater, unless otherwise specified in the relevant application standard. The total length (L_t) of the test specimens shall be equal to the required value, i.e. from 250 mm to 450 mm for test specimen thickness up to 30 mm, on the other hand, the dimensions are related to the diameter of the upper roller and distance between supports [10, 11].

3.4. *Impact test*

The purpose of this test is to determine the toughness of the weld and HAZ, therefore the test specimen with V or U-notch shall be used, according to standard ISO 9016 (Figure 8).

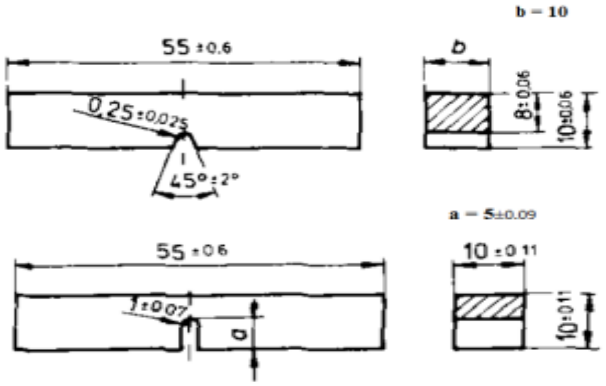

Fig. 8. Impact test specimens with V or U notch [12]

The Charpy impact test is performed on a Charpy pendulum, which should be constructed and installed according to standard EN 10045-2.

The test shell be carried out at the specified temperature, usually 23°C ± 5°C. If the test should be performed at high or low temperatures, the test specimens must be placed in an environment that will ensure the required temperature. The test specimen should be examined immediately afterward within 5 seconds.

The locations for making the test specimens and the temperature at which they will be tested should be in accordance with standard ISO 15614, while the dimensions and the test principle should be in accordance with standard EN ISO 9016 [4]. However, the test temperature, type, location and size of the test specimen, and notch orientation shall be in accordance with the required application.

Impact test specimens should have the following characteristics:

– 1st character U: Charpy U-notch.
V: Charpy V-notch.

– 2nd character W: Notch in the weld metal; the reference line is the centre line of the weld at the position of the test specimen.
H: Notch in the heat affected zone; the reference line is the fusion or the joint line (notch will include HAZ).

– 3rd character S: Notched face parallel to the surface.
T: Notch through the thickness.

– 4th character a: Tthe distance between the notch and the reference line.

– 5th character b: The distance between the weld joint face to the nearer face of thetest specimen.

In order to test a fully welded joint, the standard ISO 15614-14 requires the test specimens with VWT and VHT marking. From each specified location, each set shall be comprised of three specimens (Figure 9).

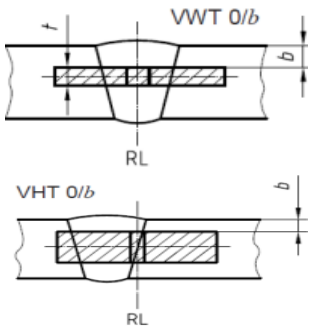

Fig. 9. Locations of the impact test specimens

The test specimens with Charpy V-notch shall be used and sampled from a maximum of 2 mm below the surface of the base material and transverse to the weld.

The absorbed energy shall be in accordance with the appropriate base material. The average value of the three specimens shall meet the specified requirements. For each notch location one individual value may be below the minimum average value specified, provided that it is not less than 70 % of that value [4].

The impact test specimens are made by machining from the middle part of the welded plate, Figure 2 zone 4, while the dimensions and its tolerances shall be in accordance with standard EN ISO 9016 (Table 5).

T a b l e 5

Dimensions and tolerances of impact test specimens [12]

Term (description)	U-notch test specimen		V-notch test specimen	
	Nominal dimensions	Machining tolerances	Nominal dimensions	Machining tolerances
Length	55 mm	± 0.60 mm	55 mm	± 0.60 mm
Heigth	10 mm	± 0.11 mm	10 mm	± 0.60 mm
Width				
─ standard test specimen	10 mm	± 0.11 mm	10 mm	± 0.11mm
─ rediced thickness test specimen	/	/	7.5 mm	± 0.11mm
─ rediced thickness test specimen	/	/	5 mm	± 0.06 mm
Notch height	5 mm	± 0.09 mm	8 mm	± 0.06 mm
Notch radius	1 mm	± 0.07 mm	0.25 mm	± 0.025 mm
Notch angle	/	/	45°	± 2°
Distance between the notch axis and the ends of the test specimens	27.5 mm	± 0.42 mm	27.5 mm	± 0.42 mm
Angle between the planes of the welded sample and the test specimen	90°	± 2°	90°	± 2°

3.5. *Hardness test*

According to the standard ISO 15614-14, the welded joint performed by hybrid laser arc welding is not subject to a hardness test, unless otherwise specified in the relevant application standard. If the hardness test is required should be done according to standard EN 9015-1 [4].

The hardness of the welded joint should be measured by Vickers method by applying a load of 98N (HV 10) on polished and etched test specimens whose test face is perpendicular to the weld axis. Normally, the test shall take the form of rows of hardness measurements, one for fillet welds and at least two rows for butt welds, the first one in the root area, and the second one in the cover pass area [11].

Hardness values should be determined for the weld metal, HAZ and base material in order to evaluate the range of hardness values across the welded joint [3].

The number of rows depends not only of the type of the weld, but also on thickness of the base material. For material thickness ≤ 5 mm, only one row is performed at a depth of < 2 mm below the upper surface of the welded joint. For a base material thickness over 5 mm, two rows should be performed at a depth of < 2 mm below the lower and upper surfaces of the welded joint [4]. Should this be insufficient for an adequate assessment of the welded joint hardness, additional rows shall be performed in the area between the root and cover pass. The arrangement of the rows of hardness measurements shall be as shown in Figure 10 [4, 11].

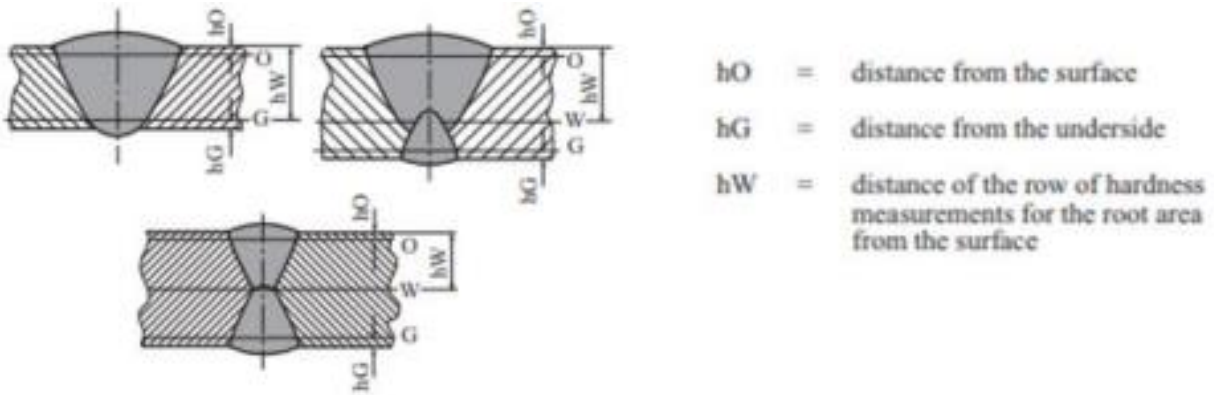

Fig. 10. Hardness testing with rows of hardness measurements [11]

For hardness test, certain guidelines should be met, for each row, the measurements should be done in three zones, the weld (3), the HAZ (2), and the base material (1), and at least 3 individual indentations should be taken in each area (Figure 11). In the HAZ the first indentation shall be placed as close to the fusion line as possible [4, 11, 14].

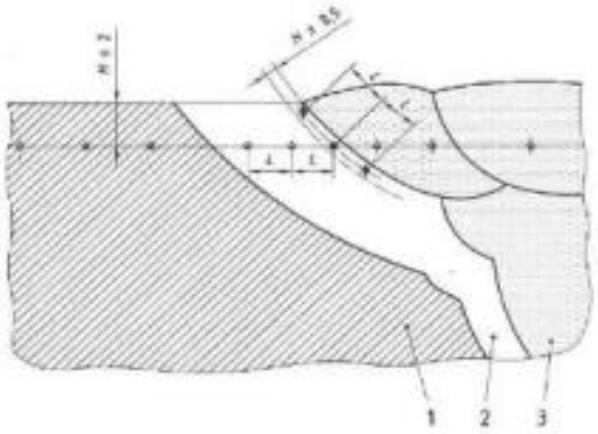

Fig. 11. Location of the indentations in butt welds in ferrous metals [13]

4. CONCLUSION

The introduction of new welding techniques and technologies leads to creation and development of new standards and procedures that confirm the quality of the welded joint.

Hybrid laser arc welding – HLAW, is a relatively new welding process that provides several advantages over conventional welding processes but has not yet been sufficiently elaborated and researched. For a better understanding of the hybrid process, additional research should be carried out in the field of welding technology, and the only way for verification is the production and testing of test specimens according to the prescribed norms and standards.

The test specimens used to prove the quality and mechanical characteristics of the welded joint performed by HLAW process are very similar to the test specimens of the conventional welding processes. However, there are certain deviations and additions that are prescribed in standard ISO 15614-14: Specification and qualification of welding procedures for metallic materials – Welding procedure test – Part 14: Laser-arc hybrid welding of steels, nickel and nickel alloys. According to standard ISO 15614-14, the mechanical tests that can be destructive and non-destructive are the primary indicator of the quality of the welded joint and the qualification of the welding technology.

The test specimens for tensile test of the welded joint are prescribed in standard ISO 4136

and they can be technical or standardized, the second type can have a cylindrical or prismatic cross-section, heat treatment shall not be applied to the welded joint or to the test specimen unless previously specified.

The bend test aims to check the deformation capabilities of the welded joint and should be performed according to standard ISO 5173, the dimensions of the test specimens depend on the base material thickness. Heat treatment shall not be applied to the welded joint or the test specimen unless previously specified.

The impact test of the welded joint is performed by the Charpy method on square cross-section test specimens with a V or U-notch and manufactured according to the standard ISO 9016.

The locations for making the test specimens and the temperature at which they will be tested should be in accordance with standard ISO 15614-14, more precisely, from each location set of three test specimens with marked VWT and VHT should be made.

According to the standard ISO 15614-14, the welded joint performed by hybrid laser arc welding is not subject to a hardness test, unless otherwise specified in the relevant application standard. If the hardness test is required should be done according to standard EN 9015-1, in the form of rows of hardness measurements in the weld metal, HAZ, and base material.

REFERENCES

[1] Agrawal, B. P.; Kumar, R. (2016): Challenges in application of pulse current gas metal arc welding process for preparation of weld joint with superior quality. *Int. J. Eng. Res. Technol.*, Vol. 5, Iss. 1, pp. 319–327.

[2] Rao, Z. H.; Liao, S. M.; Tsai, H. L. (2011): Modelling of hybrid laser – GMA welding: review and challenges. *Sci. Technol. Weld Join*, Vol. 16, Iss. 4, pp. 300–305.

[3] International Organization for Standardization (2017): *ISO 15614-1:2017. Specification and qualification of welding procedures for metallic materials – Welding procedure test – Part 1: Arc and gas welding of steels and arc welding of nickel and nickel alloys*.

[4] International Organization for Standardization (2013): *ISO 15614-14:2013. Specification and qualification of welding procedures for metallic materials — Welding procedure test — Part 14: Laser-arc hybrid welding of steels, nickel and nickel alloys*.

[5] International Organization for Standardization (2013): *ISO 15609-6:2013. Specification and qualification of welding procedures for metallic materials — Welding procedure specification — Part 6: Laser-arc hybrid welding*.

[6] International Organization for Standardization (2013): *ISO 14732:2013. Welding personnel — Qualification testing of welding operators and weld setters for mechanized and automatic welding of metallic materials*.

[7] Petreski, M.; Runchev. D.; Vrtanoski, G. (2021): Hybrid laser arc welding – state of the art in technology. Practice. *Zavarivanje i zavarene konstrukcije*, Vol. **66**. No. 3, pp. 115–124.

[8] International Organization for Standardization (2012): *ISO 4136:2012. Destructive tests on welds in metallic materials – Transverse tensile test*.

[9] Adžiev, T. (1995): *Mašinski materijali*, Kniga 2, Univerzitet "Sv. Kiril i Metodij", Skopje.

[10] International Organization for Standardization (2009): *ISO 5173:2009. Destructive tests on welds in metallic materials — Bend tests*.

[11] Germanischer Lloyd Aktiengesellschaft (2000): *Rules for Classification and Construction – Materials and Welding.* Hamburg, Germany.

[12] International Organization for Standardization (2012): *ISO 9016:2002. Destructive tests on welds in metallic materials — Impact tests — Test specimen location, notch orientation and examination*.

[13] International Organization for Standardization (2012): *ISO 9015-1:2013. Destructive tests on welds in metallic materials – Hardness testing – Part 1: Hardness test on arc welded joints*.

[14] Sokolov, M.; Salminen, A.; Kuznetsov, M.; Tsibulskiy, I. (2011): Laser welding and weld hardness analysis of thick section S355 structural steel. *Mater. Des.*, Vol. **32**, Iss. 10, pp. 5127–5131.

Mechanical Engineering – Scientific Journal, Vol. **41,** No. 1, pp. 15–21 (2023)
Number of article: 659
In print: ISSN 1857–5293
Received: January 9, 2023
On line: ISSN 1857–9191
Accepted: January 25, 2023
UDC: 621.791.7:658.58-027.44
https://doi.org/10.55302/MESJ23411659015k

Original scientific paper

INFLUENCE OF INDUSTRY 4.0 IN WELDING ENGINEERING – THEORETICAL APPROACH –

Aleksandra Krstevska, Martin Petreski, Filip Zdraveski

Faculty of Mechanical Engineering, "Ss. Cyril and Methodius" University in Skopje, P.O.Box 464, MK-1001 Skopje, Republic of North Macedonia
aleksandra.krstevska@mf.edu.mk

A b s t r a c t: Today we are involved in the fourth industrial revolution which aims towards autonomous working smart factories operating in smart manufacturing of smart industry. In this paper is discussed about Industry 4.0 and the influence of this new technological revolution in welding engineering. Smart factories are aiming for smart production using humanles and paperless technologies and accordance to that is analyzed the influence on welding engineering. Interconnectivity among welding power sources, software, and manufacturing decision-makers makes possible the integration of Industry 4.0 in welding environment. Working together with the "Internet of Things" and "Industry 4.0" the possibility for implementing sensor technology to provide real-time welding process monitoring and high-quality production has been met.

Key words: Industry 4.0; welding engineering; weld monitoring

ВЛИЈАНИЕ НА ИНДУСТРИЈАТА 4.0 ВРЗ ЗАВАРУВАЊЕТО – ТЕОРЕТСКИ ПРИСТАП –

А п с т р а к т: Денес сме инволвирани во четвртата индустриска револуција која се стреми кон автономни паметни фабрики кои работат во паметно производство на паметна индустрија. Во овој труд е дискутирано за Индустријата 4.0 и нејзиното влијание врз заварувањето. Паметните фабрики се стремат кон паметно производство користејќи технологии без луѓе и хартија и соодветно на тоа се анализира влијанието врз заварувањето. Меѓусебната поврзаност на изворите на енергија за заварување, софтверот и одлуките поврзани со производството го овозможи интегрирањето на Индустријата 4.0 во областа на заварувањето. Заедничкото користење на "Интернет на нештата" и "Индустрија 4.0" ја отвора можноста за имплементирање на сензорната технологија во следењето на заварувачкиот процес во реално време, а со тоа и задоволување на потребата од завар со висок квалитет.

Клучни зборови: Индустрија 4.0; заварување; мониторинг на завар

1. INTRODUCTION

This paper discusses about the technological industrial revolutions especially about the fourth industrial revolution and its emphasis on welding engineering. All of the industrial revolutions are defining the process of change from a handicraft economy to one dominated by industry and machine manufacturing. These technological changes introduced new ways of working and living and fundamentally transformed society. Every industrial revolution indicates the technical progress of industry.

Welding presents a major joining process in modern manufacturing, primarily used for the creation of metal structures and components, as well as maintenance and repair operations. It is playing a significant role in manufacturing, especially in industries that use complex metal components and structures.

Until now, little importance has been given to Industry 4.0 and its impact on welding engineering. Recent developments in welding engineering have shown the need for an automated weld monitoring

system and as result of that it brings digital connectivity to the welding engineering. The role of the automated weld monitoring system is to deliver a diagnosis of weld quality, so needs to be able to track welding parameters: current, voltage, gas flow rate, wire feed speed, and take multiple measurements every second. Using patented algorithms to analyze the real-time welding data, modern weld monitoring measurement systems can detect when a problem arises [1].

2. REVIEW OF THE INDUSTRIAL REVOLUTIONS

The historical timeline of technical progress is presented in Table 1 [2]. All these four revolutions significantly affected on the organization of work in companies and influenced on the development of civilization and the quality of peoples life.

T a b l e 1

History of technical progress [2]

Industrial revolution	Time period	Technology
First	1784 – mid 19th century	Water and steam – powered mechanical manufacturing
Second	Late 19th century – 1970s	Electric – powered mass production based on the division of labor (assembly line)
Third	1970s – today	Electronics and information technology drives new levels of automation of complex tasks
Fourth	Today	Sensor technology, interconnectivity and data analysis allow mass customization, integration of value chains and greater efficiency

Industry 1.0 was established in England at the end of the 18th century and mid of the 19th century, to 1840, and is related to the mechanization of production and vast usage of steam power. The revolution impacted the textile industry, mining and agriculture marking the first major transition from handicraft economy to one involving the use of machines in the manufacturing processes.

The second industrial revolution (2.0) began in the late of the 19th century, around 1870s, also known as the "Technological Revolution Era", involving industrial processes that used machines powered by electrical energy. In this second revolution Henry Ford, known as the father of automotive mass manufacturing, was the first to bring the idea of mass production. Starting from using conveyor belts for pigs to implementing these principles into the production of automobiles and creating a system where all vehicles are produced step by step on a conveyer belt.

The third industrial revolution started in 1969 where programable logic controllers were implemented on programable digital machines [3]. Start of digital revolution that marked the history of humanity. This revolution period introduced digitalization of production, computing devices and the use of new energy harvesting sources.

The fourth industrial revolution was initiated with its official use in 2011 as a name for a digital manufacturing project at the Hannover Messe, and today we are witnessing this Fourth Industrial Revolution. The fourth industrial revolution, also known as Industry 4.0, indicates the present phase of technical progress as a result of progress in information technology.

These technological revolutions and the transition from one period to another did not happen suddenly. In the second half of Industry 3.0 the progress of artificial intelligence is noted which is integral part of the following Industry 4.0 as a foundation for entering in the next technological industrial revolution.

3. INDUSTRY 4.0

The most used technical terms in the past years as "Internet of Things" and "Industry 4.0" are defining the new industrial revolution. The Industry 4.0 aims towards autonomous working smart factories and this is done by equipping almost everything with information and communications technologies of modern PCs. The last step is to connect them to a cyber-world, the internet. With the IoT all the manufacturing informations are stored in cloud. Intelligent software tools manage and control manufacturing processes and organize the supply chain. The end product will be produced on demand by additive manufacturing [4].

Production tools and manufacturing equipment as physical objects need to be digitally connected with the virtual world. Bauernhansl *et al*. [5] identified three key areas which will raise the economic benefit:

– The use of IoT and the digital services within the whole value chain.
– The change in hardware design from mechatronic to cyber-physical systems to make a comprehensive industrial-based network possible.
– Data generation, real-time "Big Data" analysis and development of prediction models for optimization control systems within the value chain.

The new fourth revolution gives the foundation of "smart factory" where we are witnessing the transformation from manufacturing industry. Not only automation and data exchange in manufacturing technologies, but beyond that, it is oriented towards the chain between the end points, including storage, logistics, recycling, energy systems, etc. With the implementation of cyber-physical systems, intelligent networks, intelligent logistics promote the establishment of smart factories operating in smart manufacturing of smart industry.

Industry 4.0 is based on nine technological pillars (Figure 1) [2] and aims to creation of digital production companies based on humanless and paperless technologies.

Fig.1. Technological pillars of Industry 4.0 [2]

On Table 2 are given nine technological pillars of Industry 4.0 and how they are implemented in this new era of the fourth technological revolutions.

Table 2

Technological pillars of Industry 4.0 [2]

Autonomous robots	Autonomous, cooperative robots, intelligent operation, standardizes interfaces
Simulation	Simulation of value networks, optimization of real-time data originated from intelligent systems
Horizontal and vertical system integration	Complete enterprise data-integration based on data transfer standards, preconditions for establishing a fully automated value chain (from the supplier to the customer, from management to the workshop)
The Industrial Internet of Things	The network of machines and products, multidirectional communication between the network members
Cyber-security	Operation in networks and open systems, organizing intelligent machines, products and system into a network
Cloud based systems	The management of large amount of data in open systems, real-time communication between manufacturing systems
Additive manufacturing	3D printing for producing prototypes and individual components
Augmented reality	For maintenance, logistics, various standardized operation processes, display
Big data and analytics	The full evaluation of available data, the support of real-time decision making and optimization.

As a result of manufacturing automation, better utilization of assets and efficient stock management is reduced manufacturing time and is noted growth of productivity. With the implementation of robots is expected improvement of flexibility and with real-time quick interference in case of errors with the help of advanced sensor technology and artificial intelligent is improved quality. Thanks to the advanced simulation devices and solutions efficiently fulfilling to the customers needs is reduced the lead time between plans and their realization [6].

4. INDUSTRY 4.0 IN WELDING ENGINEERING

The fourth industrial revolution impacts also on welding engineering. One of the developments in Industry 4.0 is the robotization of welding by implementing sensor technology, application of artificial intelligence, the development of standardized robot interfaces, interface for open-source programming, remote diagnosis via the Internet, maintenances, intelligent forecast of the need for part replacement [7]. Industry 4.0 represents "smart factories" where industrial welding robots are connected to a network and exchange information to improve their work. In Industry 4.0 are implemented cyber physical systems, systems that can connect the digital world with the physical world and optimize results thanks to continuous data analysis.

Welding parameters must be digitalized, and that means that welding machine needs to be equipped with hardware and software that will play the key role of the welding machine. This will arise ultrahigh speed data communication within the welding machine, but also the internet and the development of strategies for securing data and cyber-security. The influence of all four industrial revolutions on welding is shown on Figure 2 [12].

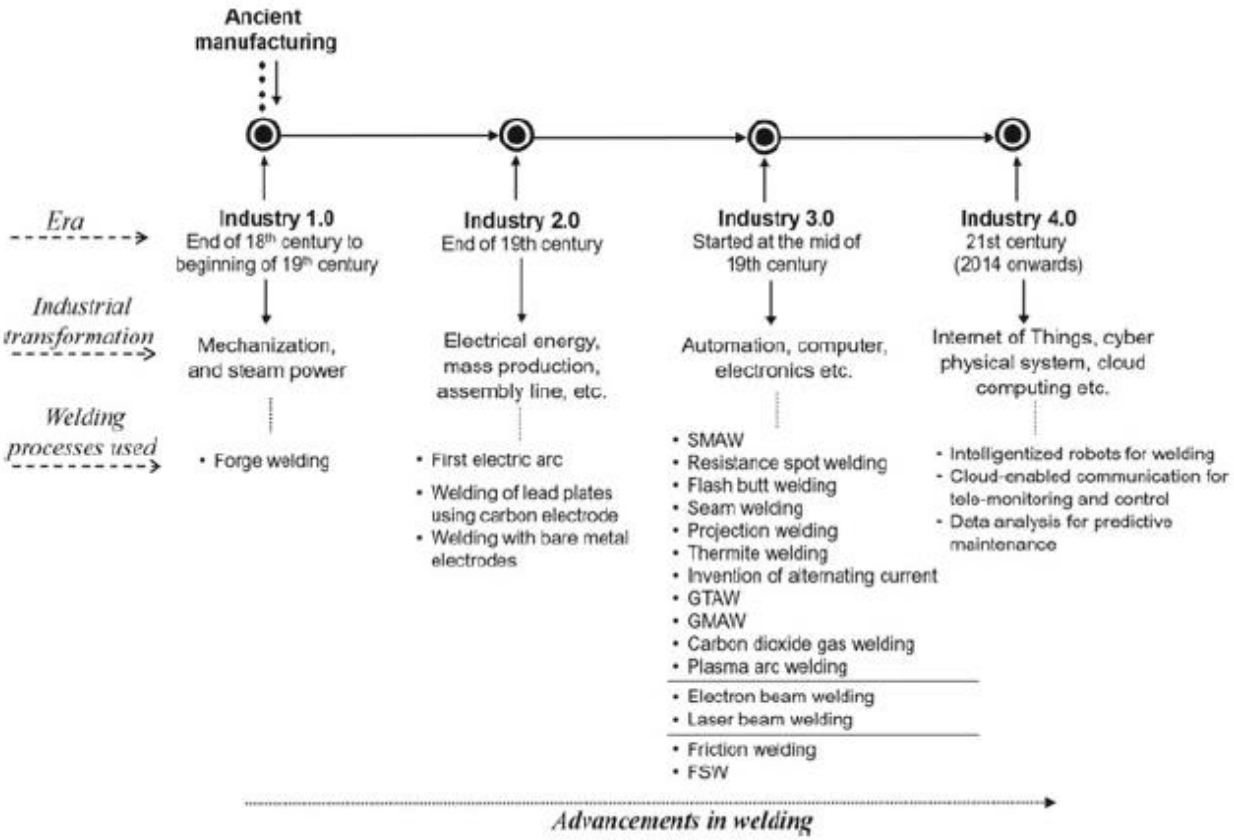

Fig 2. Evolution of technological revolutions and welding [12]

The developments of welding equipment influenced by Industry 4.0 contributed to the improvements in welding environment. Working together with the industrial internet of things and the cloud-based systems for data transfer, the following benefits can be observed: guaranteed and increased quality, increased productivity, cost reductions, management [8].

Interconnectivity among welding power sources, software, and manufacturing decision-makers makes possible the integration of Industry 4.0 in welding environment. The connection between intelligent power sources, robots, data collection, storage systems and weld monitoring software need to be integrated together so that can define the whole welding process. The software needs to track the whole welding procedure specification: wire feed speed, amps, volts, weld duration and heat input, and the monitoring software needs to record the prescribed welding parameters. The software for welding machines is designed to increase welding efficiency whether is done by a robot or a human

operator. By implementing Industry 4.0 all the human experience and the knowledge needs to be digitalized, between material selection, welding procedures, interaction with the heat source, metallurgy and joint properties. The welding machines need to be equipped with powerful microprocessor where the electronics will have to operate in a very harsh, dirty and dusty industrial surrounding.

The control of welding parameters needs real time response and powerful hardware. The use of real-time monitoring allows avoiding defects and producing high quality joints. To illustrate, the use of arc sensors in GTAW system with automatic voltage control system is shown on Figure 3 [9]. The arc sensor controls the arc length with an automatic voltage control system as it can measure the position of the electrode over the joint groove.

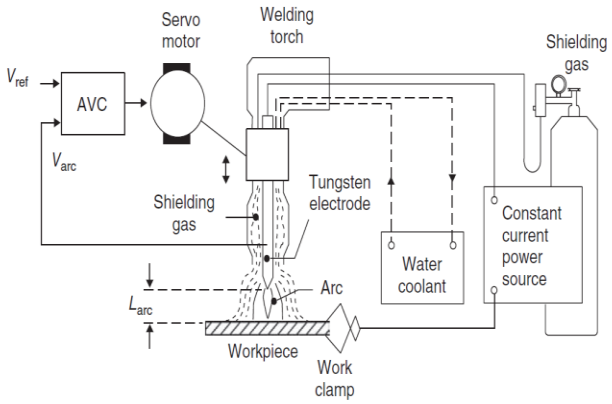

Fig. 3. GTAW system with automatic voltage control system [9]

When discussed about weld monitoring system, optical sensing systems have been developed to monitor and sense welding processes. One system that uses optical sensors is the stroboscopic video camera system (Figure 4) who can capture a video image from the process and it is designed for high temperature conditions such as welding processes. The stroboscopic video camera system consists of a laser unit, camera unit, and system controller [10]. The system can measure a two-dimensional weld pool boundary. Figure 4 shows the designed measurement system diagram, where the camera observes the weld pool at an angle to the direction of the weld and the laser is projected in the opposite direction [10].

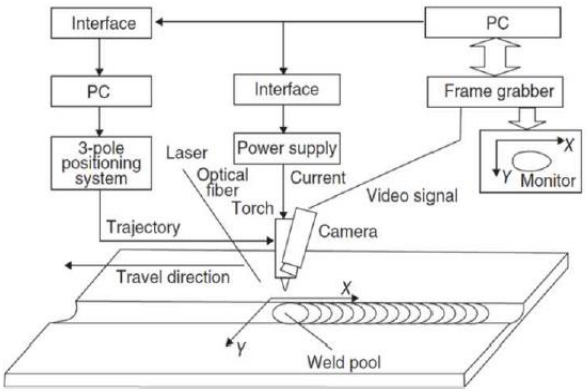

Fig. 4. Stroboscopic video camera system [10]

Another method is the ultrasonic technique in online weld monitoring for monitoring the welding process in real time and determining the weld joint penetration and joint tracking. On Figure 5 is shown the weld pool depth measurement using two shear wave probes asymmetrically disposed around the electrode center line. On Figure 5 is also given schematic diagram of the signals generated due to ultrasonic beam spread, where A is the penetration control signal, B is joint tracking signal, and C is the possible quality indication signal [11].

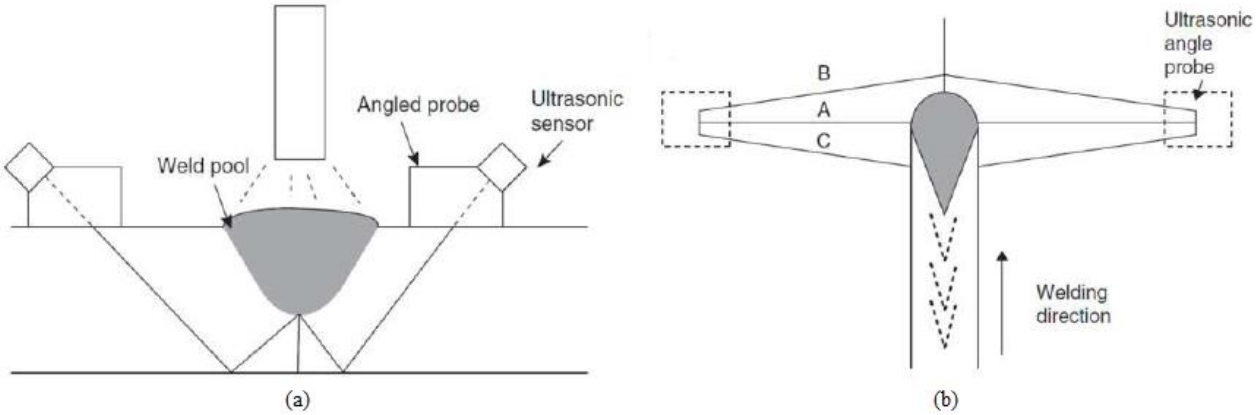

Fig. 5. Ultrasonic method for online weld monitoring [11]

With the ultrasonic method can be detected all existing welding defects in real time by a multifunctional ultrasonic sensor at real welding speed. The technology provides a real non-contact and remote access approach for real-time welding monitoring which plays an important role in development the next-generation intelligent welding machine [1].

In Industry 4.0 a step forward is done with automation of friction stir welding processes by utility of data in online process monitoring and control. The data from the welding process is used for online prediction of weld quality and control of the weld, presented on Figure 6 [12]. With implementation of the pillars of I4.0 to friction stir welding a weld quality can be predicted: tensile strength of the weld in real time and control of quality. For all the quality measuring parameters are used different signals so the utilization of sensors and proper signal processing techniques is the foundation of implementing Industry 4.0 in welding processes.

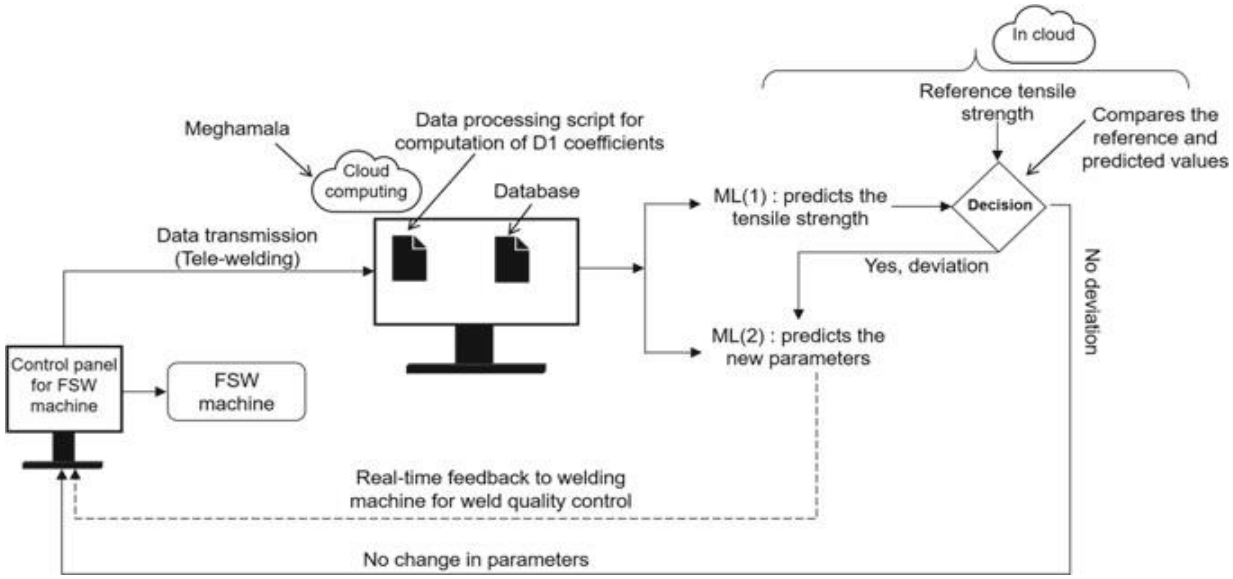

Fig. 6. FSW schematic diagram for real-time weld quality prediction and control [12]

5. CONCLUSION

The fourth industrial revolution has influenced welding engineering. It has become important to achieve efficiency in production, transparent planning, quality management, final costing, and effectiveness of the company. By intelligent weld monitoring the factory will provide documentation of the welding parameters, real-time parameter monitoring on the welding machine, and precise specifications from component management. With the weld management a consumption values for power, shielding gas, welding consumables and welding time are recorded to recognize potential savings and can influence on cost reductions.

The impact of Industry 4.0 in welding engineering is resulting in advanced welding technology helping factories to improve their efficiency and productivity. Advanced welding technology plays an essential role in creating lean manufacturing processes. It is important not only to achieve efficiency in production but also to obtain appropriate effectiveness of the factory. With the right type of technology, it can be eliminated workflow delays and duplications and accelerate entire processes through the automation of individual tasks.

REFERENCES

[1] Kah, P.; Layus, P.; Hiltunen, E.; Martikainen, J. (2014): Real-time weld process monitoring. *Advanced Materials Research*, 933, 117–124. 10.4028/www.scientific.net/AMR.933.117.

[2] Rüssmann, M. *et al*. (2015): *Industry 4.0: The Future of Productivity and Growth in Manufacturing Industries.*

[3] Zakoldaev, D.; Shukalov, A.; Zharinov, I. (2019): From Industry 3.0 to Industry 4.0: Production, modernization and creation of innovative digital companies. IOP Conference Series: *Materials Science and Engineering*. **560**, 012206. DOI 10.1088/1757-899X/560/1/012206.

[4] Ersoy, Y. (2022): The advantages and barries in implementing of Industry 4.0 and key features of Industry 4.0. *The Journal of International Scientific Researches*, **7** (3), 207–214.

[5] Bauernhansl T.; Krüger J.; Reinhart G.; Schuh G. (2016): WGP-Standpunkt Industrie 4.0, *WGP e.V*.

[6] Zawadzki, P.; Żywicki, Z. (2016): Smart product design and production control for effective mass customization in the Industry 4.0 concept. *Management and Production Engineering Rev*iew. **7** (3), pp. 105–112. DOI:10.1515/mper-2016-0030

[7] Farkas, A. (2012): A mesterséges intelligencia szerepe a hegesztés robotosításában. *26. Hegesztési Konferencia, Budapest*, 2012, Május 10–12, pp. 45–51. ISBN: 978-615-5018-28-2

[8] Farkas, A. (2018). Impact of Industry 4.0 on robotic welding. IOP Conference Series: *Materials Science and Engineering*. Vol. **448**: *XXIII International Conference on Manufacturing (Manufacturing 2018) 7–8 June 2018, Kecskemét*, Hungary. DOI 10.1088/1757-899X/448/1/012034

[9] Cook, G. E.; Strauss, A. M.; Lammlein, D. H.; Fleming P. A. (2008): Arc sensors in weld monitoring, In: Y. M. Zhang, ed., *Real-time Weld Process Monitoring.* Woodhead Publishing Ltd., Cambridge, pp. 15–43. DOI: 10.1533/9781845694401.1.15

[10] Saeed, G.; Song, H. (2008): Optical sensors in welding, In: Y. M. Zhang, ed., *Real-time Weld Process Monitoring*, Woodhead Publishing Ltd., Cambridge, pp. 45–73. DOI: 10.1533/9781845694401.1.45

[11] Shao, J.; Yan, Y. (2008): Ultrasonic sensors in welding, In: Y. M. Zhang, ed., *Real-time Weld Process Monitoring*, Woodhead Publishing Ltd., Cambridge, pp. 104–128. DOI:10.1533/9781845694401.1.104

[12] Mishra, D.; Pal, S. K.; Chakravarty, D. (2021): Industry 4.0 in welding. In: Davim, J. P. (ed.) *Welding Technology. Materials Forming, Machining and Tribology*. Springer, Cham. https://doi.org/10.1007/978-3-030-63986-0_8

Mechanical Engineering – Scientific Journal, Vol. **41,** No. 1, pp. 23–28 (2023)
Number of article: 660
In print: ISSN 1857–5293
Received: Novembet 16, 2022
On line: ISSN 1857–9191
Accepted: December 26, 2022
UDC: 683.336.5:681.518.52]:004.896.056.523
https://doi.org/10.55302/MESJ23411660023p

Original scientific paper

DESIGN AND IMPLEMENTATION OF AN AUTOMATED SAFETY LOCK SYSTEM WITH MULTIPLE AUTHENTICATIONS AND ALARM PROTECTION

Slavčo Premčeski[1], Dame Korunoski[2], Anastasija Ignjatovska[2], Damjan Pecioski[2]

[1]*Student at Faculty of Mechanical Engineering, "Ss. Cyril and Methodius" University in Skopje*
[2]*Faculty of Mechanical Engineering, "Ss. Cyril and Methodius" University in Skopje,*
P.O.Box 464, MK-1001Skopje, Republic of North Macedonia
slavco.premceski@gmail.com

A b s t r a c t: As a result of continuous technological development, repetitive manual tasks can be performed by automated systems which are required to meet the challenges and requirements of the modern world. An ordinary lock can be upgraded with programmable components so that it can be controlled by electrical power. This kind of lock would also allow a higher level of flexibility when dealing with multiple users of an object. This paper proposes a combination of electronic components and a mechanical lock controlled by an Arduino controller. There are three main subsystems: an authentication system, an output system (locking mechanism), and an alarm system. The proposed standard password authentication can be performed by both, physical input on a keypad or through bluetooth communication via a mobile application. The alarm subsystem allows additional safety from unauthorized access. The locking mechanism is driven by a servo motor and can be implemented on several types of access points such as doors, drawers, safes, and so on.

Key words: automation; safety lock; alarm; design; Arduino controller

ДИЗАЈН И ИМПЛЕМЕНТАЦИЈА НА АВТОМАТИЗИРАН БЕЗБЕДНОСЕН СИСТЕМ ЗА ЗАКЛУЧУВАЊЕ СО ПОВЕЌЕ АВТЕНТИКАЦИИ И ЗАШТИТЕН АЛАРМ

А п с т р а к т: Како резултат на постојаниот технолошки развиток, повторливите мануелни активности можат да се извршуваат со помош на автоматизирани системи кои имаат за цел да ги совладаат потребите и предизвиците на модерниот свет. Системот на обична брава може да се надгради со програмабилни компоненти и на тој начин таа да може да се управува со помош на електрична енергија. Ваквата брава исто така би била пофлексибилна во случај на повеќе корисници на некој објект. Во овој труд се предлага дизајн на автоматизирана брава кој комбинира електронски компоненти и механички систем за заклучување управуван од Ардуинов контролер. Се состои од три главни потсистеми: автентикациски систем, излезен систем (механизам за заклучување) и систем за аларм. Предложената проверка може да биде изведена со физички внес на лозинка на тастатура или преку комуникацијата „bluetooth" со мобилна апликација. Алармниот систем овозможува додатна безбедност од пристап на неовластени лица. Механизмот за заклучување е управуван од сервомотор и може да се примени на различни видови пристапни точки, на пример врати, фиоки, сефови итн.

Клучни зборови: автоматизација; безбедносно заклучување; аларм; дизајн; Ардуинов контролер

1. INTRODUCTION

User authentication is a useful tool for ensuring limited access to a device by verifying the user's identity. Only the user(s) that know the password can enter the access point. The motivation behind this idea comes from the necessity of an automated lock system that allows the privacy of user authentication within a physical domain. It enables easier control of the desired access point (door), without the concern of where someone has left their keys. There are diverse designs that allow automatic door authentication and access. I. Yugashini *et al*. [1] proposed a complex algorithm of face recognition

using a magnetic door. If the user were to be recognized, the controller would send a signal to unlock the door. The system incorporates a GSM (Global System for Mobile communication) modem that sends a message to the host if the face of the person trying to enter has not been recognized. The system ranges from home appliances to large-scale installations. Its drawback is the rare use of GSM applications and the cost of the algorithm. O. Doh and I. Ha [2] proposed a digital lock system controlled by a Raspberry Pi computer. The validation of the user can be achieved through a standard password, bluetooth communication or facial recognition. If an intruder tries to open the door with an impact, the system can detect it, take a picture of the intruder, and send it to the server through wireless communication. The computer serving as a controller is much more powerful, but also less cost-effective. P. Bhushan *et al.* [3] proposed a complex door lock system that incorporates a server installed on the door. Authentication is done by combining RFID (Radio Frequency Identification) and biometrics. The server controls the digital lock and communicates with the smartphone. Its downside is using a whole server just to control a door which is not effective. S. Goswami *et al*. [4] proposed a door lock system controlled by an "8051 controller". In this paper, the proposed system is powered by AC (alternating current) voltage. The authentication is performed by inputting a password through a 7-segment display. T. H. Thoung and Dr. Z. Ma Ma Myo [5] proposed a system that is implemented on university entry counters. A PIR (passive infrared) sensor detects a person's motion and opens the entry with the use of a stepper motor. This paper, however, does not focus on safety and authentication. A more elegant and more complex approach was proposed by T. Adiono *et al.* [6], whose paper revolves around the idea of smart home application. The main controller is a Raspberry Pi computer, where the validation of the user is performed over a smart application that connects to the controller through cloud storage. It is GPS (Global Positioning System) based, meaning that the phone sends its coordinates to the user. The lock serves as an on/off solenoid switch that receives a signal from another controller through the main host. This kind of system has two controllers and GPS is rarely used for safety lock applications. H.-S. Lee and L.-C. Hsieh [7] proposed a design of a mechanism for car-door opening. The actuator for this design is a DC (direct current) motor. Its motion is converted to linear with a worm gear, which then transfers its output motion to a screw pair. This enables linear motion of the screw slider, which matches the kinematic requirement of a car-door. This paper does not focus on the control of the motion, but rather on the motion itself. Downs *et al*. [8] designed a residential door opener that enables motion with a wire and set of pulleys. Their concept also includes detailed technical documentation and dynamic analysis as proof of concept. The motion is performed by a motor which is controlled by an Arduino controller. This paper focuses on the motion of the mechanism, rather than the safety of the object.

A review of relevant literature shows that distinct types of systems have their own deficiencies, which mainly revolve around complexity and cost-effectiveness. This paper, which is a part of a bachelor's degree thesis, proposes a design of an automated safety lock with an equivalent safety level while keeping low costs and simplicity.

2. METHODOLOGY

Developing a safety system that is reliable and grants a high-security level, which is low-cost and effective, is the aim of this paper. Such a system requires automatic actuation and control, as well as real-time information sharing. In this regard, low-budget equipment has been chosen for the prototype of this system. In the proposed system, the required manual task for unlocking a mechanical lock is substituted with an electrical signal from an Arduino controller. Figure 1 shows a block diagram of the overall system architecture and its levels of communication. The locking mechanism will be presented more specifically in the next section. The user could cross the access point over two different and independent ways of authentication. The first authentication is standard, by inputting a previously memorized password. The user could enter the password on a keypad, and once the password is confirmed by the controller, the access point would automatically unlock. The system has indicators of the state of the access point. There would be two indicators, one showing the locked state and the other one showing the unlocked state.

The second authentication can be achieved via Bluetooth communication. The proposed system incorporates wireless access which can be achieved by a smartphone application through another previously memorized password. When the password is confirmed and the connection is established, a simple command on the smartphone would unlock the access point.

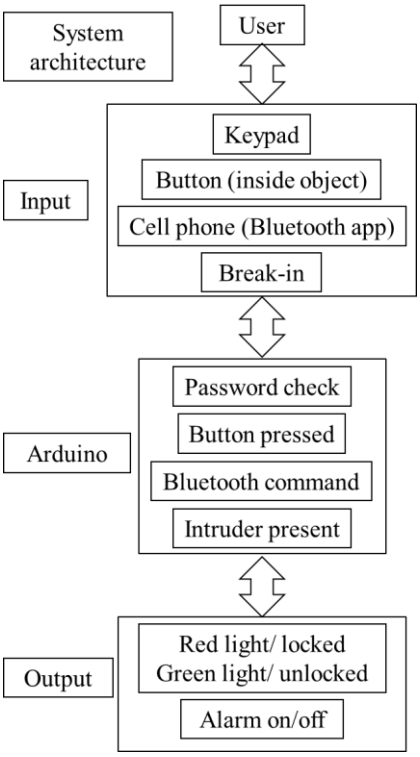

Fig. 1. Integrated architecture of the proposed system

The alarm subsystem works only when the access point is locked. Alarm sensing would be placed on every possible place that could be a subject of a violent and unauthorized break-in. The sensing is performed with a thin ultrasound layer from the top to the bottom of the access point, constantly measuring the distance. If an intruder were to pass, the detected distance would change. Then, a sound reaction would automatically be triggered. The alarm subsystem can be turned off by a command on the application or by typing the correct password on the keypad. The proposed architecture also includes another capability (button) found on the inside of the access point. This button allows (un)locking of the access point and could only be performed from the inside of the object.

Figure 2 shows a block diagram of the Bluetooth communication part of the authentication subsystem. As long as the connection is established, each command performs an adequate operation.

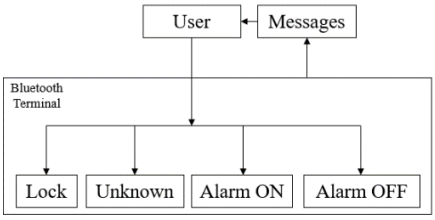

Fig. 2. Architecture of the subsystem for wireless communication

3. DESIGN OF THE SYSTEM

a) *System architecture*

The chosen components and their features are shown in Table 1. The system consists of eight components:

- Arduino which controls the system,
- diodes that show the state of the lock,
- an actuator that enables lock control,
- a button that allows control of the lock from the inside,
- a Bluetooth module that is used for wireless communication,
- an alarm subsystem that consists of an ultrasonic distance sensor and a buzzer; multiple sensors could be used to cover all possible entry points,
- a buzzer that generates a high-frequency sound in case the sensor detects an intruder.

T a b l e 1

Electrical components and their features

Component	Specification	Function
Diodes	Red and green	Shows state
Button	3 terminals	Inside-control
Keypad	HC-543 4×4	Authentication
Motor	SG90 Servo	Mechanism control
Controller	Arduino MEGA 2560	Controls the system
Bluetooth device	HC-05 module	Authentication and control
Alarm sensor	HC-SR04 ultrasonic distance sensor	Intruder detection
Buzzer	Active 5v digital	Alarming

b) *Design of the mechanism*

The proposed mechanism is controlled by a SG-90 model servo-motor. The most suitable type of mechanism is the slider-crank mechanism. The functional part of the lock is designed to be of a cylinder type. The whole mechanism is assembled in a box that can be mounted on or inserted into the access point. The internal view of the assembly is shown in Figure 3 and the length and legend of the mechanical components is given in Table 2.

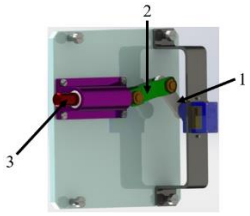

Fig. 3. Internal view of the designed mechanism

T a b l e 2

Mechanical components and their length

Component	Length (mm)	Legend
Crank	26	1
Connecting rod	36	2
Slider	75	3

4. ANALYSIS OF THE SYSTEM

a) *Kinematic analysis*

The kinematic analysis is performed to verify the reliability of the proposed model. Figure 4 shows the kinematic diagram of the proposed model.

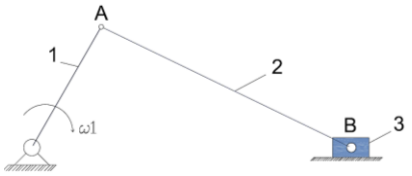

Fig. 4. Schematic diagram of the mechanism

A Simulink model is built using the schematic diagram of a crank mechanism with one degree of freedom. Kinematic analysis of the mechanism is performed using Simulink and the obtained results are shown in Figure 5 which shows the position change of the locking cylinder with one degree of movement freedom.

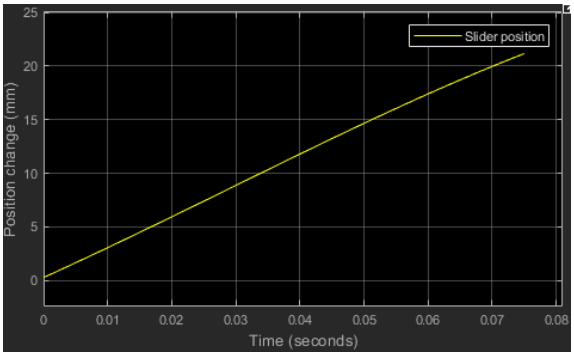

Fig. 5. Change of position of the slider

Within Figure 6 the relative change of position of the cylinder slider shown on the *y*-axis is approximately 21 mm ($p \approx 21$ mm). The total time for which the simulation takes place is shown on the *x*-axis and it is 0.075 s. These results have been achieved for a change of angular position of the motor shaft of 45° ($\alpha = 45^\circ$).

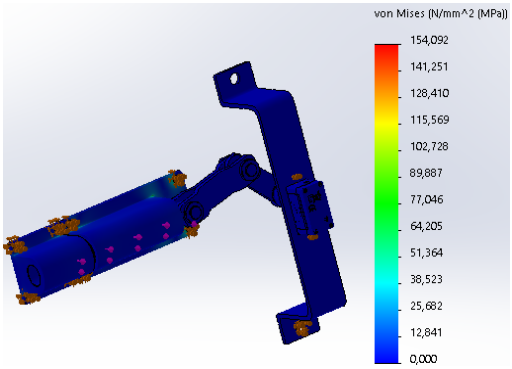

Fig. 6. FEA analysis results

b) *Dynamic analysis*

After the combination of design and kinematic analysis, a dynamic analysis is essential to check the stress strength of the mechanism. Consider a case when an intruder is trying to open the door by force. To check if this is possible, FEA (finite element analysis) using the SolidWorks Simulation module is performed. The break-in force is an input to the analysis, while the highest stress value is an output and a result of the simulation. The input force is obtained according to the fastest recorded acceleration generated by a human being [9, 10]. The obtained result is:

$$a \approx 10 \ \frac{\mathrm{m}}{\mathrm{s}^2}. \tag{1}$$

This would be a theoretical case because a person cannot achieve this acceleration when hitting a door with the whole body. A person with a mass equal to 100 kg would generate a force of:

$$F = ma = 1000 \ \mathrm{N}. \tag{2}$$

The results from the analysis are shown in Figure 6. From the analysis, the highest stress value using the Von Mises principle for calculation is 154 MPa. The stressed part would be designed of a low-carbon structural steel (S185). The value of the maximum stress allowed for the used material for the mechanism is 185 MPa.

The safety factor can be calculated as a proportion of the maximum stress value allowed and the highest stress value of the analysis. For this analysis, it has a value of:

$$S = \frac{\sigma max}{\sigma ob} \approx 1.2\,. \qquad (3)$$

Since $S > 1$, the mechanism can withstand the projected impact force, hence the dynamic analysis is successful and completed.

5. EXPERIMENTAL RESULTS AND DISCUSSION

The experimental results are defined by 4 cases*:*

1. Correct keypad password.
2. Incorrect keypad password.
3. Wireless unlocking and alarm commands.
4. Illegal break-in.

Figure 7 shows the experimental setup of the designed safety lock system. The mechanism is locked by default, and the red diode is turned on.

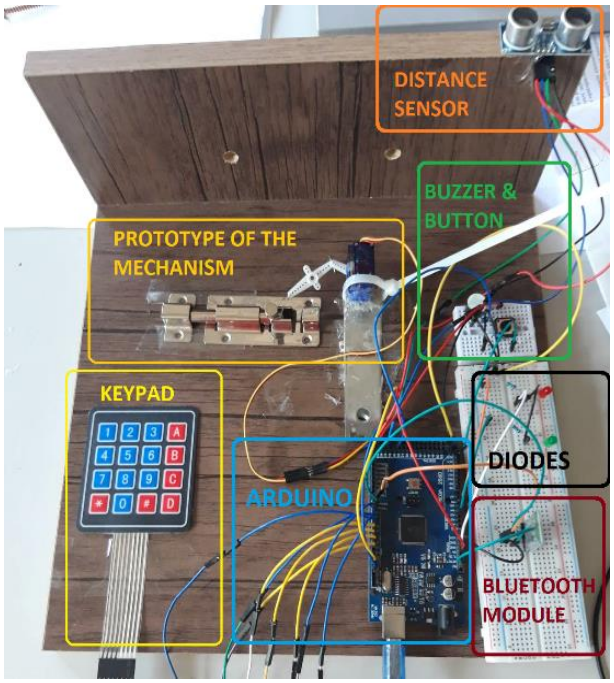

Fig. 7. Experimental model of the safety lock system

In the first case, the user enters the password from the keypad. When the password is confirmed, the mechanism unlocks, while the green light turns on. The user can enter the access point, and then simply press the button from the inside to lock the mechanism.

For the second case, if the password is incorrect, the red-light blinks and the buzzer beeps three times as a warning. The password automatically resets.

The third case is represented by pressing the commands on the phone app. Previously, a connection must be established via Bluetooth, which also requires a password. The mechanism is controlled by pressing the commands “OPEN” and “CLOSE”. There are also commands for the alarm control.

In the fourth case, the experiment included a purposeful unauthorized break-in. When the sensor detects intrusion, the response is automatically triggered. The alarm can be turned off in two ways: By inputting the correct password through the keypad, or by pressing the command “AL OFF” on the interface of the phone application, as can be seen in Figure 8.

Fig. 8. Display of the smartphone application interface over bluetooth connection

In Figure 8, the display of the interface of the application is shown with multiple experiments and their corresponding messages.

6. CONCLUSION

In this paper, an automated safety lock system with multiple authentications and alarm protection has been designed. Its purpose is to improve the usability and security of an everyday repetitive manual task. The techniques used for its design are standard and cost-effective, so it can easily be commercialized.

The proposed system has all the features that the established solutions on the market do. The combination of the lock with the alarm is considered a great advantage since most of the existing solutions come independently of each other. Its downside is the inability to check whether someone has tried to hack the passwords. To improve it, a server that can save the messages from the module has to be added. The server would also have to be able to resend the messages to the host. Future efforts can improve safety while keeping the effectiveness and usability.

REFFERENCES

[1] Yugashini, I.; Vidhyasri, S.; Devi. K. G. (2013): Design and implementation of automated door accessing system with face recognition, *International Journal of Science and Modern Engineering* (IJISME), **1** (12), 10–13.

[2] Doh O.; Ha, I. (2015): A digital door lock system for the Internet of Things with improved security and usability, *Advanced Science and Technology Letters* Vol. **109**, pp. 33–38.
http://dx.doi.org/10.14257/astl.2015.109.08

[3] Bhushan, P.; Vishal, M; Sagar, S.; Mayur, P.; Patole, U. R. (2918): Automatic door lock system using PIN on android phone, *International Research Journal of Engineering and Technology* (IRJET) Vol. **05**, Issue 11, pp 1007–1011.
e-ISSN: 2395-0056.

[4] Goswami, S.; Choudhury, A.; Das, S.; Banerjee, T.; Ghosh, S. (2017): Automated password protected door lock system, *Advances in Industrial Engineering and Management*, Vol. **6**, No. 1, 48–52.

[5] Thoung, T. H.; Dr. Zin Ma Ma Myo (2019): Implementation of automatic door opening system with entry counter for university library, *International Journal of Trend in Scientific Research and Development* (IJTSRD), Vol. **3,** Issue 5, pp.1267–1269.

[6] Adiono, T.; Fuada, S.; Feranti Anindya, S.; Purwanda, I. G.; Fathany, M. Y. (2019): IoT-enabled door lock system, *International Journal of Advanced Computer Science and Applications* (IJACSA), Vol. **10**, No. 5.
DOI: 10.14569/IJACSA.2019.0100556

[7] Lee H.-S.; Hsieh, L.-C. (2009): Innovative design of an automatic car-door opening system, *Proceedings of the IMECS 2009*, Vol. **II.** IMECS 2009, March 18–20, Hong Kong.

[8] Downs, S.; Pollo, A.; Bredemeier, E. (2018): Residential automatic door opener. Mechanical Engineering Design Project Class. 94.

[9] Allain, Rhett (2012): *Maximum Acceleration in the 100 m Dash*. WIRED SCIENCE, Aug. 31.

[10] Lee, J. (2008): *Usain Bolt 100 m 10-meter Splits and Speed Endurance*.

Mechanical Engineering – Scientific Journal, Vol. **41,** No. 1, pp. 29–36 (2023)
Number of article: 661
Received: March 28, 2023
Accepted: May 7, 2023
In print: ISSN 1857–5293
On line: ISSN 1857–9191
UDC: 531.6.082.73:621.01]:[004.942:519.642
https://doi.org/10.55302/MESJ23411661029i

Original scientific paper

ANALYTICAL MODELING AND FEM SIMULATIONS OF ENERGY HARVESTING CANTILEVER BEAM

Anastasija Ignjatovska, Damjan Pecioski, Dejan Šiškovski, Maja Anačkova, Simona Domazetovska

Faculty of Mechanical Engineering, "Ss. Cyril and Methodius" University in Skopje, P.O.Box 464, MK-1001 Skopje, Republic of North Macedonia
anastasija.ignjatovska@mf.edu.mk

A b s t r a c t: The concept of energy harvesting systems allows sustainable energy sources, such as mechanical energy, to be harvested from the environment. The feature of piezoelectric material to generate voltage as a result of its deformation characterizes them as an energy harvesting tool, due to their robustness and efficiency characteristics. This paper shows numerical modeling of an energy harvesting cantilever beam using the Euler-Bernoulli method. The FEM simulations of the cantilever beam have been created in order to determine the optimal position of the piezoelectric transducer along the beam. Furthermore, these conclusions have been used to develop the mathematical model in MATLAB in order to investigate the effect of the geometry characteristics of the beam and the piezoelectric transducer on the output parameters. The impact of the dimensions and effective area of the piezoelectric transducer and its location on the cantilever beam as well as the effects of the dimensions of the beam have been studied in order to obtain an optimal energy harvesting model in terms of its efficiency. Once the modeling phase has been completed, the output results regarding the generated voltage and power from the energy harvesting system have been compared and models have been validated.

Key words: energy harvesting; piezoelectric materials; cantilever beam; modeling and simulation

АНАЛИТИЧКО МОДЕЛИРАЊЕ И СИМУЛАЦИИ НА КОНЗОЛЕН СИСТЕМ ЗА СОБИРАЊЕ ЕНЕРГИЈА СО МЕТОДОТ НА КОНЕЧНИ ЕЛЕМЕНТИ

А п с т р а к т: Концептот на системи за собирање енергија овозможува собирање на енергија од одржливи извори, каква што е механичката енергија. Пиезоелектричните материјали генерираат напон како резултат на нивната деформација, при што се карактеризираат со висока робусност и ефикасност, што овозможува нивна примена како алатка за собирање енергија. Во овој труд е извршено нумеричко моделирање на конзолен систем за собирање енергија користејќи го методот на Ојлер-Бернули. Симулациите кои се базирани на методот на конечни елементи на конзолен систем се изведени со цел определување оптимална положба на пиезоелектрикот по должината на конзолата. Понатаму овие заклучоци се искористени за развој на математички модел во MATLAB, со цел анализирање на влијанието на геометриските карактеристики на конзолата и пиезоелектрикот врз излезните параметри. Проучено е влијанието на димензиите и ефективната површина на пиезоелектрикот и неговата локација на конзолата, како и ефектите од димензиите на конзолата, со цел дизајнирање оптимален ефикасен модел за собирање енергија. Откако фазата на моделирање е завршена, добиените резултати во однос на генерираниот напон и моќност од системот за собирање енергија се споредени и моделите се валидирани.

Клучни зборови: собирање енергија; пиезоелектрични материјали; конзола; моделирање и симулации

1. INTRODUCTION

The energy crisis is one of the main problems facing humanity today as a result of which science and researchers are constantly trying to develop sustainable solutions in order to fulfill energy demands. Therefore, technologies that use renewable energy sources such as solar energy, kinetic energy, thermal

or bio-energy noticed rapid progress. Apart from the macro-energy harvesting technologies which include renewable energy plants, recently, continuous development has also been made in microenergy harvesting technologies. Micro-energy harvesting technology is focused on the alternatives to conventional batteries and uses energy from mechanical vibration, mechanical stress and strain, which generate low-level power expressed in mW or μW [1]. The piezoelectric energy harvesting technique has been widely researched due to its high energy conversion ability from mechanical vibration. This technique uses the properties of piezoelectric materials to generate voltage under the influence of a mechanical force.

Most research papers in the energy harvesting area, present the harvester as a cantilever beam with one or more piezoelectric layers, which is excited harmonically at its fundamental natural frequency in order to obtain maximum electrical output [2]. This is due to the fact that compared to other structures, the cantilever beam has a lower resonant frequency, and provides higher stress and strain with less ambient vibrational force [3]. There are various methods for modeling an unimorph beam, or a beam with a single piezoelectric transducer mounted on its surface. Depending on the purpose of the model, one has to determine which method is optimal. For example, Belhora *et al.* [4] use the pin-force model to develop a model that predicts the energy harvesting capabilities of an electrostrictive polymer composite. Various papers [5, 6, 7] compare the most used methods for analytical modeling: the pin-force model, the enhanced-pin force model which expands upon the pin-force concept, and the Euler-Bernoulli model. The Euler-Bernoulli method has been proven to be the most accurate representation of a real energy harvesting system out of the three methods, and for this reason it has been used in this paper. On the other hand, the finite element method has been widely used as an analysis tool for continuous systems with a finite number of concentrated masses. The discretization of the continuous systems of a finite number of elements or concentrated masses simplifies the mathematical apparatus or analytical solutions to the dynamics of the elastic structure from partial differential equations to a system of ordinary differential equations [8]. Uddin *et al*. [9] use the finite element method in determining natural frequencies, modes, and stresses along a cantilever piezoelectric energy harvesting beam. Kumar *et al*. [10] use the finite element method for coupled piezoelectric energy harvester in order to discretize the electromechanical coupling phenomenon between mechanical and electrical domains. They optimize material properties that determine the performance of piezoelectric energy harvesters such as dielectric constant, piezoelectric strain coefficient, electromechanical coupling coefficient, Young modulus, density, and electrical and mechanical quality factors [10]. An area in energy harvesting that opens up a wide research space is the optimization of the design of the energy harvesting system in order to generate maximal voltage.

In this paper, an optimization of the cantilever piezoelectric energy harvesting beam concerning the position of the piezoelectric transducer, the position of the excitation force, and the geometrical characteristics of the piezoelectric transducer and the beam have been conducted. A combination of two different modeling methods has been used: analytical modeling using the Euler-Bernoulli method and the finite element method.

2. MATHEMATICAL MODELING

a) *Mathematical modeling of the beam*

Continuous systems are mechanical systems with continuously distributed mass and theoretically have infinite degrees of freedom. In order to obtain an analytical solution for the dynamics of these systems, certain approximations and simplifications have to be adopted. In order to be able to use the Euler-Bernoulli equation, the assumptions concerning the material homogeneity of the beam and its ideally constant width are adopted. Using these assumptions, partial differential equations with constant coefficients are obtained. The solutions to these partial differential equations represent the natural frequencies of the system and the modes of oscillation of the elastic structure.

The differential equation of motion of a continuous beam according to the Euler-Bernoulli method is represented with the following relation:

$$EI_y \frac{\partial^4 y(x,t)}{\partial x^4} = f(x,t) - \rho A \frac{\partial^2 y(x,t)}{\partial t^2} \qquad (2.1)$$

where y is the deplacement of the beam, its density is ρ_b and A_b is its area of the cros-section, whereas $\rho_b A_b \frac{\partial^2 y(x,t)}{\partial t^2}$ is kinetic energy, $E_b I_b \frac{\partial^4 y(x,t)}{\partial x^4}$ is potential energy, and $f(x,t)$ is the excitation force.

If the excitation force is a harmonic function, the differential equation can be rewritten as:

$$\frac{E_b I_b}{\rho_b A_b} \frac{\partial^4 y(x,t)}{\partial x^4} + \frac{\partial^2 y(x,t)}{\partial t^2} = \frac{F_0}{\rho_b A_b} \sin(\omega t)\, \delta\left(x - L_f\right) \qquad (2.2)$$

where ω is the frequency of the excitation force and L_f is the distance from the clamped end to the point where the excitation force is applied.

The general solution of the equation (2.2) can be expressed as:

$$y(x,t) = \sum_{i=1}^{\infty} T_i(t) Y_i(x) \tag{2.3}$$

where $T_i(t)$ is the *i*-th model coordinate of shape and $Y_i(x)$ is the *i*-th mode shape of the beam.

Inman *et al*. [11] state that the first 3 modes (i = 1, 2, 3) in equation (2.3) are sufficient for generating the mode shape equation of the cantilever beam.

By replacing expression (2.3) in (2.2), the following differential equations can be obtained [12]:

$$Y(x)^{iv} - \frac{{\omega_n}^2}{c^2} Y(x) = 0, \tag{2.4}$$

$$\ddot{T}(t) + {\omega_n}^2 T(t) = 0. \tag{2.5}$$

The solution of the first characteristic equation depends only on the x coordinate:

$$Y(x) = A\sin(\beta x) + B\cos(\beta x) + \\ + C\sinh(\beta x) + D\cosh(\beta x) \tag{2.6}$$

where β is the wave number [11] and is expressed as:

$$\beta^4 = {\omega_n}^2 \frac{\rho_b A_b}{E_b I_b} \tag{2.7}$$

where ω_n is the natural frequency of the system.

In the order to obtain maximal deflections of the beam, the frequency of the excitation force has to be equal to the first natural frequency of the beam. Constants A, B, C and D can be calculated using the boundary conditions for clamped-free configuration [11]. At the clamped end, for x = 0, slope and deflection must be zero, while at the free end, for x = l, shearing force and bending moment must be equal to zero.

Finally, the general mode shape equation for a cantilever beam could be expressed as:

$$Y_i(x) = \cosh(\beta_i L_b) - \cos(\beta_i L_b) - \\ - \frac{\sinh(\beta_i L_b) - \sin(\beta_i L_b)}{\cosh(\beta_i L_b) + \cos(\beta_i L_b)} \cdot \\ \cdot [\sinh(\beta_i L_b) - \sin(\beta_i L_b)], \tag{2.8}$$

where L_b is the total length of the beam.

Solutions for β_i (Figure 1) are calculated from the characteristic equation:

$$\cos(\beta_i L_b)\cosh(\beta_i L_b) = -1. \tag{2.9}$$

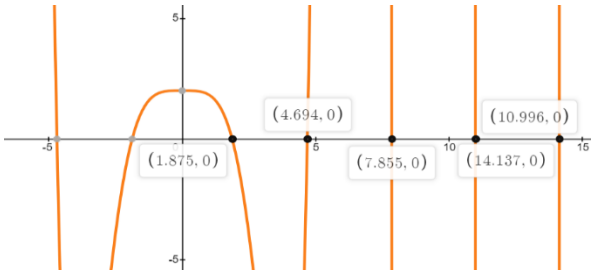

Fig. 1. Graphical representation of solutions to characteristic equation (2.9)

For the adopted value beam's length of 0.561 m. the first five natural frequencies (Table 1) can be calculated using the following expression:

$$f_i = \frac{1}{2\pi} \frac{(\beta_i L_b)^2}{{L_b}^2} \sqrt{\frac{E_b I_b}{\rho_b A_b}}. \tag{2.10}$$

The solution of equation (2.5) can be expressed as a convolutional integral:

$$T(t) = \frac{1}{\omega_{di}} e^{-\xi\omega_{ni}t} \int F_i(\tau) e^{-\xi\omega_{ni}t} \sin\left(\omega_{di}(t-\tau)\right) d\tau \tag{2.11}$$

where: ω_d is damped natural frequency,
ξ is damping ratio.

Table 1

First five natural frequencies of the beam

i	$\beta_i L_b$	Natural frequencies of the beam (Hz)
1	1.875104	3.8881
2	4.696409	24.3668
3	7.854757	68.2277
4	10.995540	133.6991
5	14.137168	221.0143

The beam curvature can be calculated as:

$$\rho(x,t) = \frac{\partial^2 y(x,t)}{\partial x^2} \tag{2.12}$$

or average beam curvature:

$$\bar{\rho}(t) = \frac{1}{L_P} \int_0^{L_P} \rho(x,t) dx \tag{2.13}$$

where L_p is the total length of the piezoelectric transducer.

The applied moment acting on the beam can be expressed as:

$$M(t) = E_b I_b \bar{\rho}(t) \tag{2.14}$$

b) *Mathematical modeling of PZT*

A general model for the piezoelectric transducer which presents the relationship between the moment of the beam and generated voltage as a function of time is:

$$V(t) = -\frac{6g_{31}\frac{E_b t_b}{E_p t_p}\left(1+\frac{t_b}{t_p}\right)}{b_p t_p\left\{1+\left(\frac{E_b t_b}{E_p t_p}\right)^2\cdot\left(\frac{t_b}{t_p}\right)^2+2\frac{E_b t_b}{E_p t_p}\left[2+3\frac{t_b}{t_p}+2\left(\frac{t_b}{t_p}\right)^2\right]\right\}}\cdot M(t), \quad (2.15)$$

where $g_{31}\left(\mathrm{V}\cdot\frac{\mathrm{m}}{\mathrm{N}}\right)$, is the voltage constant $E_b\left(\mathrm{V}\cdot\frac{\mathrm{N}}{\mathrm{mm}^2}\right)$ is Young's modulus of the material of the beam, $I_b\ (\mathrm{m}^4)$ is the axial moment of inertia of the beam and $E_p\left(\frac{\mathrm{N}}{\mathrm{m}^2}\right)$ is Young's modulus of the piezoelectric material. Concerning the geometry of the system, $t_b(\mathrm{m})$ is the beam's thickness, $t_p(\mathrm{m})$ and $b_p(\mathrm{m})$are the thickness and width of the piezoelectric transducer, respectively.

The generated power can be calculated as:

$$P(\mathrm{t}) = V(\mathrm{t})\cdot I(t) \quad (2.16)$$

$$I(t) = C_P\cdot\frac{\mathrm{d}V}{\mathrm{d}t} \quad (2.17)$$

$$C_P = \frac{d_{31}\cdot A_p}{g_{31}\cdot t_p} \quad (2.18)$$

where $I(t)$ is the current expressed as a function of time, C_P is the capacitance of the piezoelectric transducer, A_p is the effective area of the piezoelectric transducer, and d_{31} is its piezoelectric strain coefficient.

Based on these mathematical models of the cantilever beam and piezoelectric transducer, analytical modeling and simulations in MATLAB and FEM simulations have been performed in order to analyze this energy harvesting system in detail.

3. RESULTS AND DISCUSSION

Analytical modeling and FEM simulations have been conducted in order to analyze the impact of several input parameters on the generated output power. The following properties have been studied: position of the piezoelectric transducer along the beam, position of the excitation force, length ratio and thickness ratio of the beam and piezoelectric transducer, respectively. Obtained optimal values have been used as an input and an identical harmonic excitation force has been applied to both models. The analytical and FEM model have been validated by comparison of the obtained results concerning output voltage and power.

a) *Position of piezoelectric transducer*

Firstly, FEM simulations have been performed in order to determine the optimal position of the piezoelectric transducer along the beam, which would generate maximal power. According to results from FEM simulations (Figure 2), the maximal output power is generated when the distance between the clamped end of the beam and the piezoelectric transducer equals zero. One may deduct that by increasing this distance, output electric power decreases. Therefore, optimal position of the piezoelectric transducer is next to the clamped end of the beam.

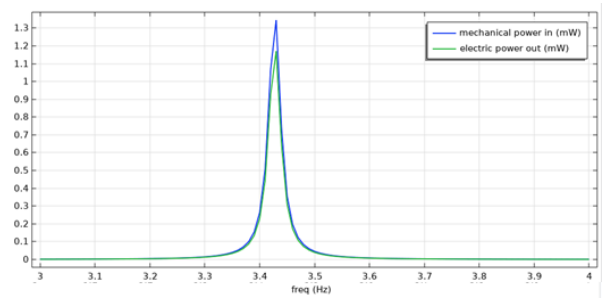

a) PZT is placed next to the clamped end

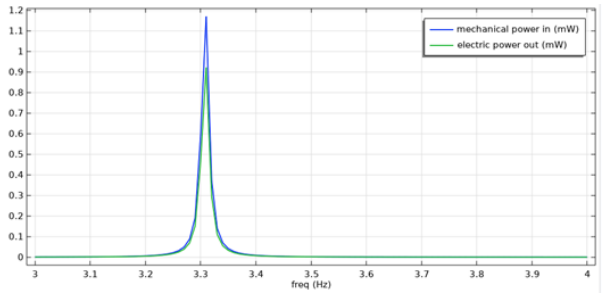

b) PZT is placed at the center of the beam

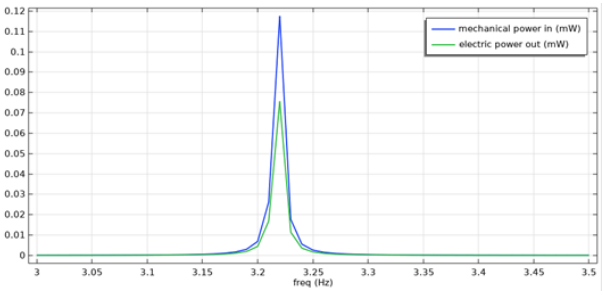

c) PZT is placed on the free end of the beam

Fig. 2. Output electric powe (mW)
Three different positions of the PZT

b) *Position of excitation force*

Output electric power is expected to change when position of the excitation force is varied. In order to discover optimal placement of excitation harmonic force, which generates maximal output electric power, analytical modeling in MATLAB

has been performed. By increasing the distance from the clamped end of the beam to the line of action of the excitation force, the applied moment to the beam amplifies. As the obtained results from the simulation (Figure 3) show, the optimal position of the excitation force is at the free end of the beam. The excitation force can be defined with the following function:

$$F(t) = 0.35 \cdot \sin(2\pi \cdot \omega_1 \cdot t) = \\ = 0.35 \cdot \sin(2\pi \cdot 3.88 \cdot t) \qquad (3.1)$$

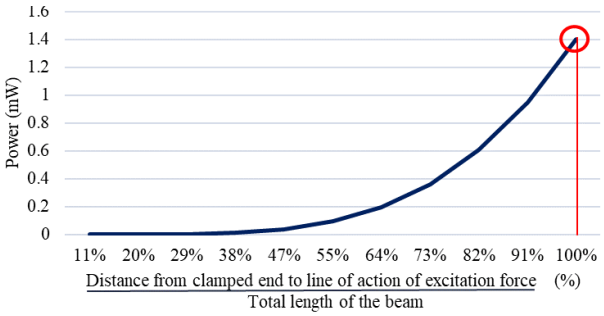

Fig. 3. Output electrical power as a function of the position of excitation force

In the optimized model the excitation force is placed at the free end of the beam and follows the function shown in (3.1).

c) *Length ratio*

Another parameter that has to be optimized is the length of the piezoelectric transducer in relation to the beam's length. Analytical simulations in MATLAB have been performed in order to determine optimal length of the piezoelectric transducer which enables maximal power generation. Results (Figure 4) show that when 47% of the length of the beam is covered by a PZT, maximal power is generated. Until certain value for the length of the piezoelectric transducer is reached, output power increases by increasing the length.

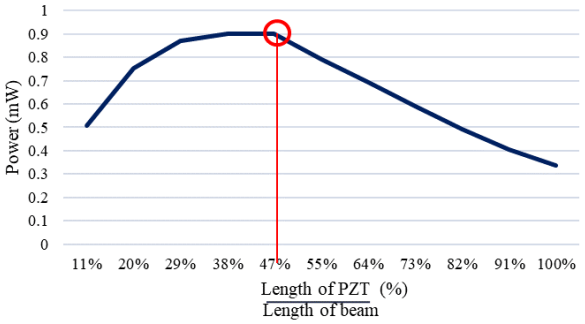

Fig. 4. Output electrical power as a function of length ratio of PZT and beam

For values of the length higher than the crossing point, overall characteristics of the system get affected and the effective cross-section, Young's modulus and natural frequencies change. Adverse effects are caused by reducing beam strain and deformation, and overall generated electric power.

d) *Thickness ratio*

Last parameter that has been optimized is thickness ratio of piezoelectric transducer and beam, respectively. Obtained results from MATLAB simulations (Figure 5) show a peak value of generated power for thickness ratio of 33%.

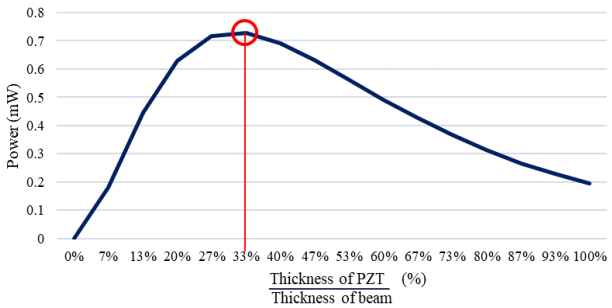

Fig. 5. Output electrical power as a function of thickness ratio of PZT and beam

For values of the thickness ratio of the piezoelectric transducer and the beam, respectively, the generated power decreases by increasing the value of thickness ratio.

e) *MATLAB and FEM simulations of optimized model*

Analytical modeling and simulations and FEM simulations of the optimized model (Figure 6) have been performed and output results have been compared. Identical input parameters which match calculated optimal values, concerning the dimensions and properties of the beam and the piezoelectric transducer (Table 2) have been used. The frequency of the excitation force matches the first natural frequency of the system (Figure. 6).

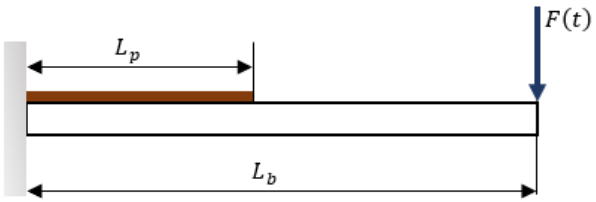

Fig. 6. Energy harvesting cantilever beam with PZT

T a b l e 2

Parameters of the beam and PZT

	Parameter	Not.	Value	Unit
Beam	Length	L_b	0.561	m
	Width	b_b	0.04	m
	Thickness	t_b	0.0015	m
	Density	ρ_b	7850	kg/m^3
	Young's modulus	E_b	$2{\cdot}10^{11}$	Pa
PZT (PZT-5A)	Voltage constant	g_{31}	$-11.3{\cdot}10^{-3}$	V·m/N
	Dielectric constant	d_{31}	$-190{\cdot}10^{-12}$	m/V
	Young's modulus	E_p	$3{\cdot}10^3$	Pa
	Length	L_p	0.263	m
	Width	b_p	0.04	m
	Thickness	t_p	0.0005	m
	Density	ρ_p	7950	kg/m^3
	Resistance	R	1000	kΩ

Output results from the analytical modeling and simulation in MATLAB (Figure 7) show that voltage of 202.63 V and electrical power of 1.34 mV have been generated in 3 seconds, at the first natural frequency of the system. The highest values for the generated voltage and power are achieved at the first natural frequency of the system and therefore the system was excited only on that frequency.

Obtained results from the FEM simulations (Figure 8) show that in 3 seconds, voltage of 190.32 V and electrical power of 1.74 mW have been generated at the first natural frequency of the system. In the FEM simulations, until the first natural frequency has been reached, the system is excited by the excitation force given in expression (3.1). After that, the frequency of the excitation force is changed in order to excite the second natural frequency of the system (24.37 Hz). Results show that maximal output is achieved at the first natural frequency as firstly stated.

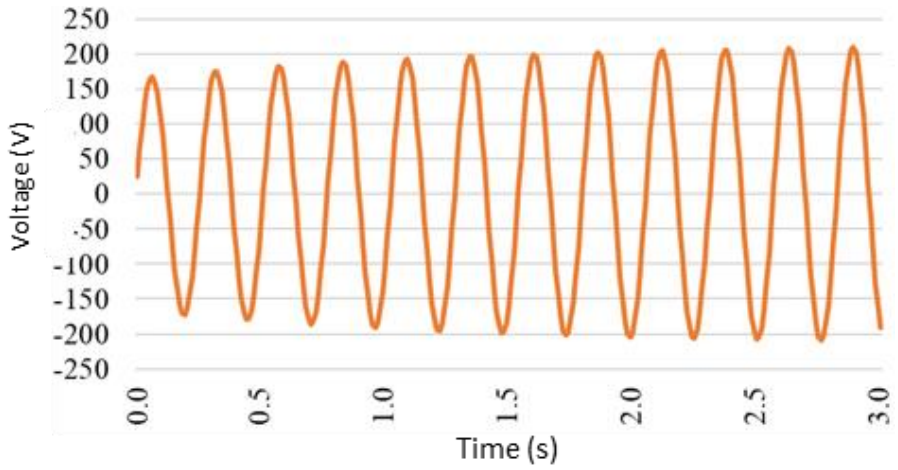

a)

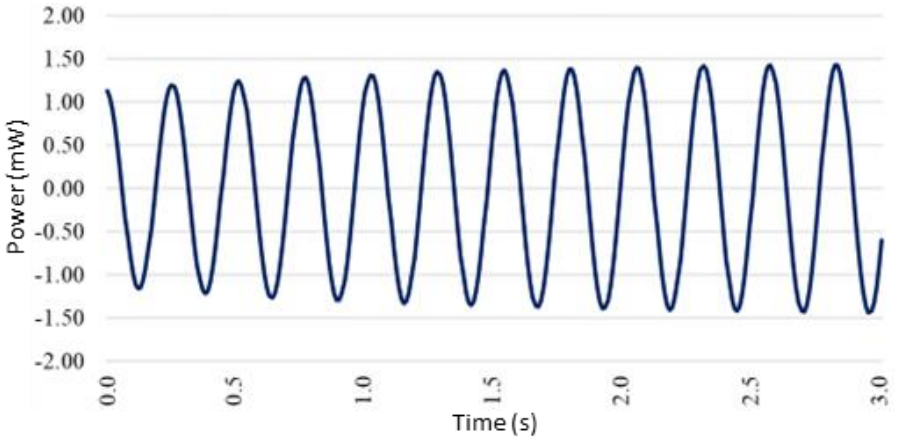

b)

Fig. 7. Generated a) voltage (V) and b) electrical power (mW) from analytical simulations in MATLAB

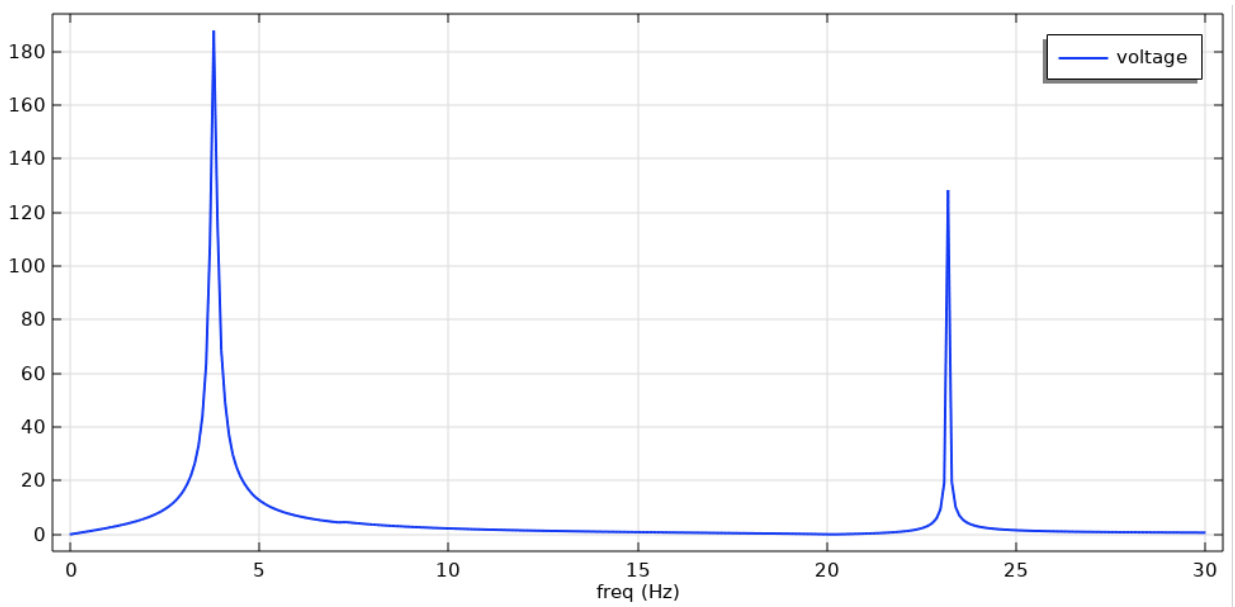

a)

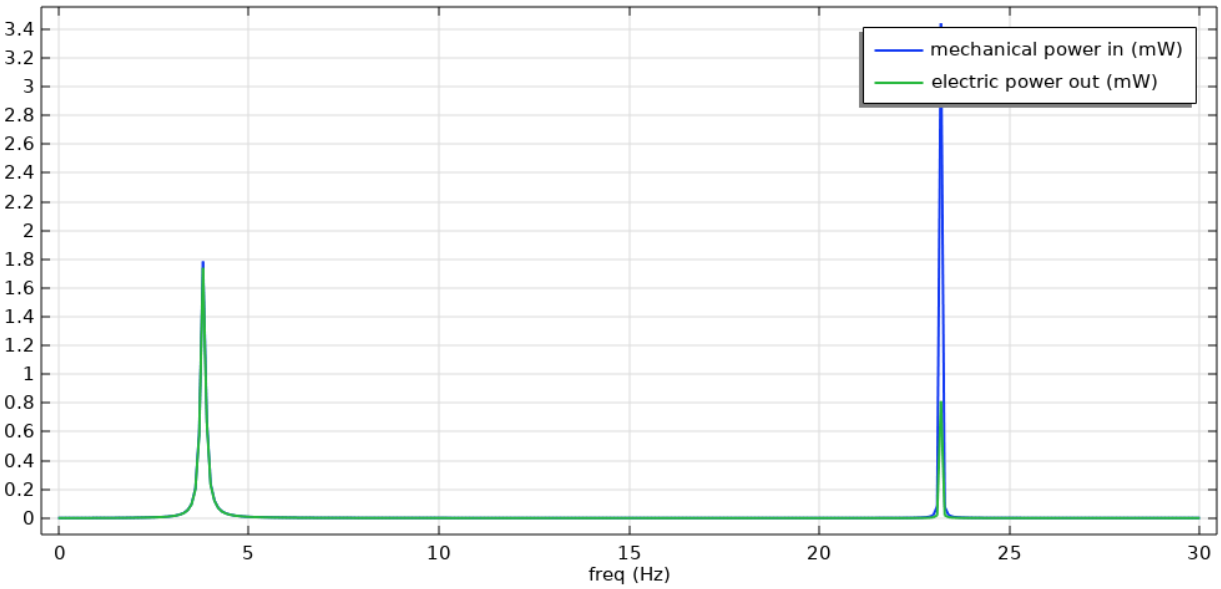

b)

Fig. 8. Generated voltage (V) and electrical power (mW) from FEM simulations

Over a certain period of time, the generated voltage and electric power are stored and their value increases. In this paper, change of stored voltage and electric power for a period of 3 seconds has been plotted (Figure 7) and calculated (Figure 8).

Validation of the models has been performed by comparison of the obtained output results concerning the generated voltage and electrical power. Acquired results from both models using two different modeling methods have similar values and therefore model is valid. Thus, model can successfully predict power generation from a cantilever unimorph vibrating beam.

4. CONCLUSION

Analytical modeling based on Euler-Bernoulli theorem and FEM simulations of energy harvesting cantilever beam have been made. Optimal parameters of the model have been determined, concerning the position of the piezoelectric transducer, position of the excitation force, length and thickness ratio of the piezoelectric transducer and the beam, respectively. Maximal electric power has been generated for: location of the piezoelectric transducer next to the clamped end of the beam, location of excitation force on the free end of the beam, length ratio of

0.47 and thickness ratio of 0.33 between the piezoelectric transducer and the beam. Once the optimal parameters have been defined, they have been used as input parameters for the model. Based on an exact model, simulations in MATLAB and FEM simulations have been performed in order to determine output voltage and electric power. Since obtained output results for the identical model using two different techniques match, a deduction can be drawn that the model is valid.

Although, this paper is purely theoretical, the authors have also been working on an experimental setup which is based on the obtained results from the conducted software analyses. On that way, created theoretical models would be validated by an experiment. Also, an energy harvesting unimorph beam, or a beam with a single piezoelectric transducer mounted on its surface is modelled in this paper. In future work, using the proposed concept, the model could analogically be upgraded in two ways in order to generate higher voltage and electric power. First way is by creating a bimorph energy harvesting beam, by placing two PZT on the top and bottom surfaces of the beam. The second approach implies placing multiple PZT on the surface of the beam, which would enable achieving the optimal calculated length ratio of 0.47. Nevertheless, whichever approach would be chosen, proper analyses must be conducted, and adequate models must be created.

REFFERENCES

[1] Kim, H. S.; Kim, J.-H.; Kim, J. (2011): A review of piezoelectric energy harvesting based on vibration. *International Journal of Precision Engineering and Manufacturing*, **12**, 1120–1141.

[2] Erturk, A.; Inman, D. J. (2008): A distributed parameter electromechanical model for cantilevered piezoelectric energy harvesters. *Journal of Vibration and Acoustics*, **130**, No. 4. https://doi.org/10.1115/1.2890402

[3] Gogoi, U. J.; Shanmuganantham. T. (2015): Energy harvesting of cantilever with silicon tip mass-based MEMS energy scavengers. In: *2nd International Conference on Electronics and Communication Systems (ICECS)*, IEEE, pp. 185–188.

[4] Belhora, F. *et al.* (2013): Mechano-electrical conversion for harvesting energy with hybridization of electrostrictive polymers and electrets. *Sensors and Actuators* A: *Physical* **201**, pp 58–65.

[5] Eggborn, T. (2003): *Analytical models to predict power harvesting with piezoelectric materials*, Master thesis, Virginia Tech. http://hdl.handle.net/10919/32981

[6] Nabavi, S.; Zhang, L. (2017): Design and optimization of piezoelectric MEMS vibration energy harvesters based on genetic algorithm. *IEEE Sensors Journal*, **17**, No. 22, pp. 7372–7382.

[7] Kim, S. H.; Ahn, J. H.; Chung, H. M.; Kang, H. W. (2011): Analysis of piezoelectric effects on various loading conditions for energy harvesting in a bridge system. *Sensors and Actuators A: Physical*, Vol. **167**, No. 2, pp 468–483.

[8] Jovanova, J.; Gavriloski, V. (2014): Analytical and experimental modeling of a smart beam. *Journal of Vibroengineering*, Vol. **16**, No. 7, pp 3409–3418.

[9] Uddin, N.; Islam, Sh.; Faisal Ryad, M.; Bhuyan, M. S. (2021): Finite element analysis of piezoelectric cantilever beam using vibration for energy harvesting devices. In: *AIP Conference Proceedings*, vol. **2324**, No. 1, pp. 030004. AIP Publishing LLC. https://doi.org/10.1063/5.0037801

[10] Kumar, A.; Sharma, A.; Kumar. R.; Vaish, R.; Chauhan, V. S. (2014): Finite element analysis of vibration energy harvesting using lead-free piezoelectric materials: A comparative study. *Journal of Asian Ceramic Societies*. Vol. **2**. No. 2, pp 139–143.

[11] Inman, D. J.; Singh, R. C. (1994): *Engineering Vibration*. (4^{th} Edition), Vol. **3**. Chapter 6. Englewood Cliffs, NJ, Prentice Hall.

[12] Šiškovski, D. (2016): *Active adaptive vibration control of beam using an electromagnetic actuator*. Master thesis, Faculty of Mechanical Engineering, Skopje.

Mechanical Engineering – Scientific Journal, Vol. **41,** No. 1, pp. 37–42 (2023)
Number of article: 662
In print: ISSN 1857–5293
Received: March 28, 2023
On line: ISSN 1857–9191
Accepted: May 25, 2023
UDC: 620.22:531.6.082.73]:621-25
https://doi.org/10.55302/MESJ23411662037p

Original scientific paper

DESIGN OF AN ENERGY HARVESTING SYSTEM USING PIEZOELECTRIC MATERIALS

Damjan Pecioski, Anastasija Ignjatovska, Dejan Šiškovski, Simona Domazetovska, Maja Anačkova

Faculty of Mechanical Engineering, "Ss. Cyril and Methodius" University in Skopje, P.O.Box 464, MK-1001 Skopje, Republic of North Macedonia
damjan.pecioski@mf.edu.mk

A b s t r a c t: Energy harvesting by using piezoelectric materials is one of the most widely used techniques for conversion of waste energy into useful. Using this technique, generated vibration energy from machines can be converted into useful electrical energy. In this paper, an energy harvesting system that supplies power for low-power consumption devices has been designed. The experimental model consists of a rotating machine that generates mechanical vibrations that actuate a cantilever beam and a piezoelectric transducer as a sensor for energy harvesting. The aim is to generate greater power as an output, which could be achieved by obtaining maximal strain for the given frequency range of the vibration source. The frequency range of the vibration machine is variable and multiple frequencies have been used. Using the Euler-Bernoulli method, the beam dimensions have been calculated so that its natural frequency matches the operating machine frequency. By reaching the resonant point of the cantilever beam, the maximal power from the designed energy harvesting system can be generated.

Key words: energy harvesting; piezoelectric transducers; vibrations of rotating machine; cantilever beam

ДИЗАЈН НА СИСТЕМ ЗА СОБИРАЊЕ ЕНЕРГИЈА СО КОРИСТЕЊЕ ПИЕЗОЕЛЕКТРИЧНИ МАТЕРИЈАЛИ

А п с т р а к т: Собирањето енергија со примена на пиезоелектрични материјали е една од најкористените техники за конверзија на генерираната неискористена енергија во корисна. Користејќи ја оваа техника, генерираната енергија од вибрациите на машините може да се претвори во корисна електрична енергија. Во овој труд е дизајниран систем за собирање енергија кој може да обезбеди енергија за уреди со мала потрошувачка на енергија. Експерименталниот модел се состои од ротирачка машина која генерира механички вибрации кои активираат конзолен носач и пиезоелектричен материјал како сензор за собирање енергија. Целта е да се генерира поголема излезна моќност, што може да се постигне со добивање максимално напрегање за дадениот опсег на фреквенција на изворот на вибрации. Опсегот на фреквенции на машината за вибрации е променлив и се користат повеќе фреквенции. Користејќи го методот на Ојлер-Бернули, пресметани се димензиите на конзолниот носач така неговата природна фреквенција да се совпаѓа со фреквенцијата на работната машина. Со достигнување на резонантната точка на конзолата се постигнува генерирање на максимална моќност од дизајнираниот систем за собирање енергија.

Клучни зборови: собирање енергија; пиезоелектрични материјали; вибрации на ротирачка машина; конзола

1. INTRODUCTION

Over the last decades, green manufacturing has attracted a great deal of attention worldwide. The use of different types of renewable energy is studied in order to replace traditional fossil fuels, which harm both the environment and public health [1, 2]. Clean energy can be achieved by using the waste energy from the ambient environment such as solar, acoustic, wind, and vibrational energy. In the fol-

lowing Table 1, a comparison of power density generated from different ambient sources has been shown. All values are normalized by volume and are reported as μW/cm^3 its high energy conversion ability from mechanical vibration. This technique uses the properties of piezoelectric materials to generate voltage under the influence of a mechanical force. The experiments done by [3, 4] show vibrations as a good source for energy harvesting, secondly only to solar energy in ideal conditions.

T a b l e 1

The power density of different energy sources [3, 4]

Energy source	Power density (μW/cm^3)
Solar (outdoors)	15 000–direct sun/150–cloudy day
Solar (indoors)	6 – office desk
Vibrations (piezoelectric conversion)	250
Vibrations (electrostatic conversion)	50
Acoustic noise	0.003 at 75 dB, 0.96 at 100 dB
Temperature gradient	15 at 10 °C gradient

Energy harvesting on a global macroscale is studied with the goal of replacing fossil fuels with clean energy, while on a microscale with the goal differs. With the recent advances in wireless and micro-electromechanical systems (MEMS) technology, the demand for portable electronics and wireless sensors grows rapidly. These sensors are portable and because of that, they require their own power supply which is usually secured by a conventional battery. However, due to their finite lifespan, problems can occur. For portable electronics or electronics within systems that are hard to physically reach, replacing the battery is problematic and extremely time-consuming activity since the electronics could fail at any time. For such systems, harvesting mechanical vibrations using piezoelectric materials are one of the best alternative sources of energy due to their implementation in various environments.

Many researchers have studied the vibration problems of piezoelectric structures, and some achievements have been made. Liu *et al*. [5] studied the dynamic analytical solution of a piezoelectric stack utilized in an actuator and a generator based on the linear piezo-elasticity theory. Parashar *et al*. [6] studied the nonlinear shear-induced flexural vibrations of piezoceramic actuators. Mukherjee and Chaudhuri [7] demonstrated the effect of large deformations on piezoelectric materials and structures under time-varying loads. Chen *et al*. [8] studied the natural vibration and transient response of a functionally graded piezoelectric material (FGPM) curved beam with a numerical method. Dong *et al*. [9] discussed the influence that piezoelectric materials exert on the vibration behavior of a stepped cantilever beam with surface bonded or embedded piezoelectric materials. Kim and Tadesse [10] stated that the generated power density of the piezoelectric transduction is more than three times greater than the power density of electrostatic and electromagnetic transducers. Jeon *et al*. [11] found that the highest power density from piezoelectric material subjected to the external vibrational source was 37 μW/mm^3. For the electromagnetic effect, Saha *et al*. [12] showed that a value of 4.375 μW/mm^3 could be generated from the electromagnetic-based generator subjected to the vibrating beam. Despesse *et al*. [13] built a system to convert the surrounding mechanical vibrations into electrical energy using the electrostatic transducer. The research within this field shows piezoelectric energy harvesting as an energy source alternative for conventional batteries.

In this paper, an experimental model is presented, where a piezoelectric transducer is used to harvest energy of mechanical vibration from a rotatory machine. The piezoelectric material is placed on a cantilever beam and coupled together with an energy harvesting module.

2. MATHEMATICAL MODELING

a) *Vibration of a cantilever beam*

Mechanical systems which have a continuously distributed mass are referred to as continuous systems. These systems theoretically have infinite degrees of freedom. An analytical solution to the dynamics of these systems is possible only for simple cases with an approximation of homogeneous material as well as constant width along the length of the system. Using these approximations, partial differential equations can be employed with constant coefficients to solve the problem. The solutions to these PDEs represent the frequency of the system and the modes of oscillation of the elastic structure. One of the most used methods for modeling continuous systems and the one which will be used in this paper is the Euler-Bernoulli method.

The Euler-Bernoulli method takes into account the bending energy of the structure and the kinetic energy of the transversal movement of the beam. The differential equation of motion of a continuous beam according to the Euler-Bernoulli method is the following mathematical dependency:

$$EIy\frac{\partial^4 y(x,t)}{\partial x^4} = f(x,t) - \rho A\frac{\partial^2 y(x,t)}{\partial t^2}, \quad (2.1)$$

where $\rho A\frac{\partial^2 y(x,t)}{\partial t^2}$ is the kinetic energy, $EIy\frac{\partial^4 y(x,t)}{\partial x^4}$ the potential energy, and $f(x,t)$ is the actuation of the system.

A full description of the modeling of a cantilever beam has been developed in greater detail by Mineto [14] and Šiškovski [15].

b) *Piezoelectric modeling*

The piezoelectric effect exists in two domains: the first is the direct piezoelectric effect that describes the material's ability to transform mechanical strain into electrical charge; the second form is the converse effect, which is the ability to convert an applied electrical potential into mechanical strain energy. The direct piezoelectric effect is responsible for the material's ability to function as a sensor which is used in this paper. The mechanical and electrical behavior of a piezoelectric material can be modeled by two linearized constitutive equations. These equations contain two mechanical and two electrical variables. The direct effect and the converse effect may be modeled by the following matrix equations:

– direct piezoelectric effect:

$$\{D\} = [e]^{\mathrm{T}}\{\mathrm{S}\} + [\alpha^s]\{\mathrm{E}\}$$

– converse piezoelectric effect:

$$\{\mathrm{T}\} = [c^E]\{\mathrm{S}\} - [e]\{\mathrm{E}\}$$

where {D} is the electric displacement vector, {T} is the stress vector, [e] is the dielectric permittivity matrix, [c^E] is the matrix of elastic coefficients at constant electric field strength, {S} is the strain vector, [α^S] is the dielectric matrix at constant mechanical strain, and {E} is the electric field vector. The matrix form of the equations for the direct and converse piezoelectric effect for a piezoceramic material which is polarized on the 3rd axis are given in the equations (2.2 and 2.3).

A full description of the piezoelectric effect and its modeling is beyond the scope of this paper. However, a significant number of published papers have developed these equations in greater detail such as Mineto [14].

$$\begin{bmatrix}\varepsilon_1\\ \varepsilon_2\\ \varepsilon_3\\ \varepsilon_4\\ \varepsilon_5\\ \varepsilon_6\end{bmatrix} = \begin{bmatrix} S_{11} & S_{12} & S_{13} & 0 & 0 & 0\\ S_{21} & S_{22} & S_{23} & 0 & 0 & 0\\ S_{31} & S_{32} & S_{33} & 0 & 0 & 0\\ 0 & 0 & 0 & S_{44} & 0 & 0\\ 0 & 0 & 0 & 0 & S_{55} & 0\\ 0 & 0 & 0 & 0 & 0 & 2(S_{22}-S_{12})\end{bmatrix}\begin{bmatrix}\sigma_1\\ \sigma_2\\ \sigma_3\\ \tau_{23}\\ \tau_{31}\\ \tau_{12}\end{bmatrix} + \begin{bmatrix}0 & 0 & d_{31}\\ 0 & 0 & d_{32}\\ 0 & 0 & d_{33}\\ 0 & d_{24} & 0\\ d_{15} & 0 & 0\\ 0 & 0 & 0\end{bmatrix}\begin{bmatrix}E_1\\ E_2\\ E_3\end{bmatrix} \quad (2.2)$$

$$\begin{bmatrix}D_1\\ D_2\\ D_3\end{bmatrix} = \begin{bmatrix}0 & 0 & 0 & 0 & d_{15} & 0\\ 0 & 0 & 0 & d_{24} & 0 & 0\\ d_{31} & d_{32} & d_{33} & 0 & 0 & 0\end{bmatrix}\begin{bmatrix}\sigma_1\\ \sigma_2\\ \sigma_3\\ \sigma_4\\ \sigma_5\\ \sigma_6\end{bmatrix} + \begin{bmatrix}e_{11}^{\sigma} & 0 & 0\\ 0 & e_{22}^{\sigma} & 0\\ 0 & 0 & e_{33}^{\sigma}\end{bmatrix}\begin{bmatrix}E_1\\ E_2\\ E_3\end{bmatrix} \quad (2.3)$$

3. EXPERIMENTAL SETUP

a) *Model description*

The experimental setup shown in Figure 2 consists of a rotational shaft whose frequency can be controlled using a frequency regulator. Coupled to the base of the machine is a cantilever beam with an attached piezoelectric transducer (PI-876-A12). The piezoelectric transducer is placed as close as possible to the clamped end, as seen in Figures 1 and 2, in order to achieve maximum deformation. The experimental setup is the following: the cantilever beam is designed at a length of 240 mm, width of 40 mm, and height of 1.5 mm. The excitation frequency of the machine is varied in order to achieve resonant conditions of the cantilever beam. In this setup, a different mass is added to the free end of the cantilever beam and the change in frequency, as well as the voltage output of the harvester, are measured. All the elements used for this experiment are shown in the Figure 2.

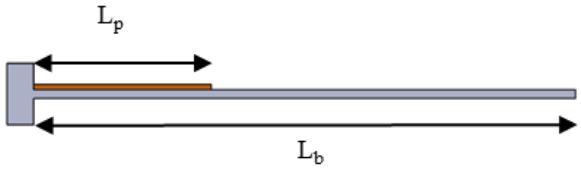

Fig. 1. Cantilever beam with attached PZT sensor

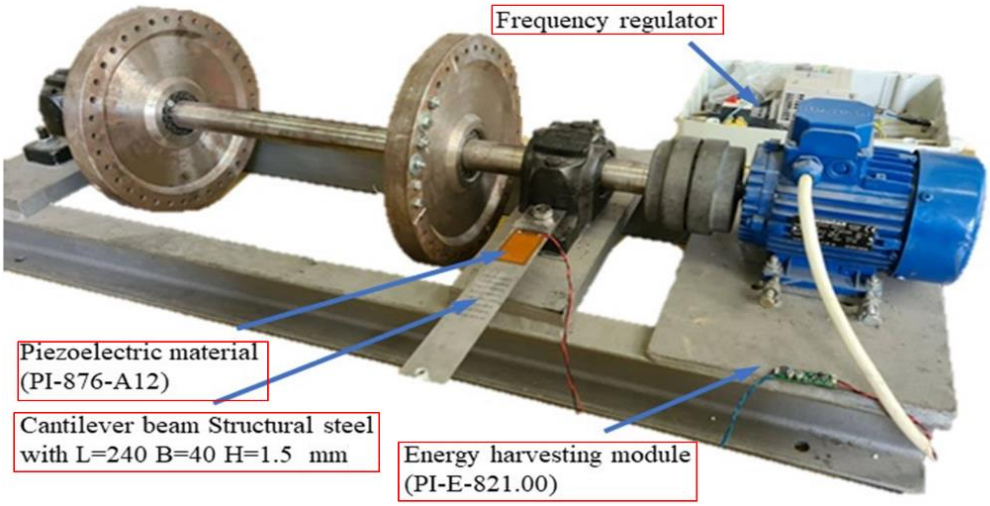

Fig. 2. Experimental model setup

b) *Energy harvesting circuit*

The piezoelectric strip generates electricity while being deformed, but if this power is not being used or stored, it will be dissipated with no utilization. Having a piezoelectric energy harvester requires a rectifier circuit in order to convert the AC wave from the harvester to the DC voltage, which is suitable for energy storage.

The used energy harvesting module is PI-E-821.00, and its electronic circuit is shown on Figure 3. Figure 3 shows a full-wave rectifier with a diode bridge. On one side the piezoelectric material is connected and on the other the output towards the battery or sensor. The harvester has two capacitors each of 100 μF and an output voltage of 3.3 V or 5 V.

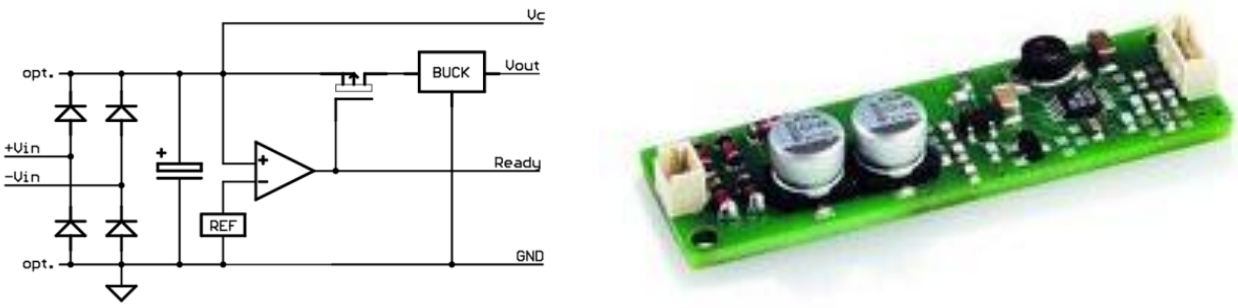

a) b)

Fig. 3. a) Electronic circuit of PI-E-821.00. **b)** Energy harvester PI-E-821.00

4. RESULTS AND DISCUSSION

In the experimental setup the dimensions of the beam are length (L = 240 mm) width (W = 40 mm) and height (H = 1.5 mm) and the angular frequency of the machine is varied. A mass is added to the end of the cantilever and the changes in the frequency and output voltage as well as the amplitude of the vibrations are measured. On the Table 2 the results of the measurements are shown.

T a b l e 2

Experimental variables

Mass (g)	Frequency of resonance (Hz)	Output voltage (V)	Amplitude of vibrations (mm/s)
0	18.5	6.2	3.62
5	17.4	6.6	3.4
10	17.9	6.39	3.1
15	16.7	6.25	2.8

Looking at the information of the Table 2. As the point mass increases the natural frequency of the beam decreases, as well as the amplitude of vibrations that can be seen. On the other hand, the output voltage behaves in a different manner. These results are presented on the Figure 4.

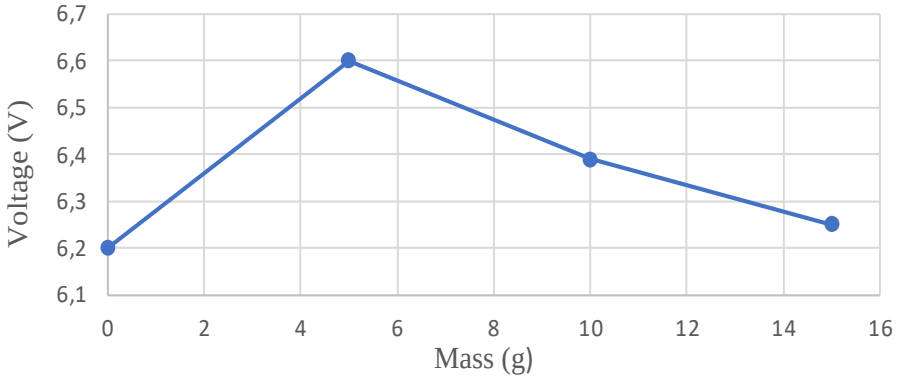

a) Voltage vs Mass

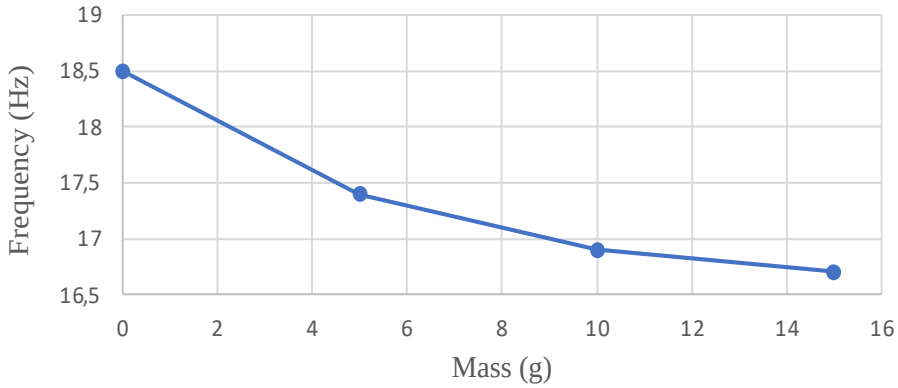

b) Frequency vs Mass

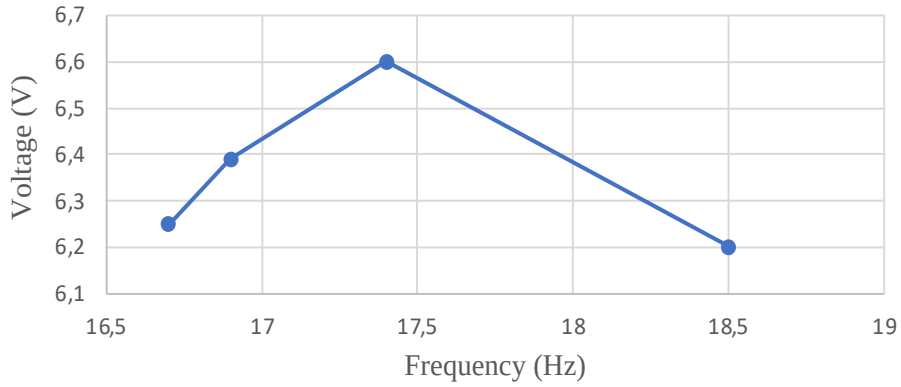

c) Frequency vs Voltage

Fig. 4. Experimental results

Looking at Figure 4a, it can be seen that having a point mass on the end of the cantilever beam increases the energy output of the piezoelectric material compared to an empty cantilever beam. This behavior is noted up until a mass of 5 grams, further increase of the mass lowers the output energy. As

expected, the addition of a mass to the end of the cantilever beam lowers the natural frequency of the cantilever beam which can be seen on Figure 4b. Having the natural frequency of the cantilever beam lowered means that in order to have a resonant condition, the frequency rotation of the machine also needs to be lowered. Having the frequency lowered affected the output voltage of the energy harvesting as can be seen on Figure 4c. Lowering the frequency of rotation of the machine correlates to lower amplitudes of vibration. These lower vibrations correspond to lower deformations of the cantilever and lower energy output of the piezoelectric material. It can be concluded that an optimal variation would be to have a point mass on the end of the cantilever beam which is in the range of 3–5 grams. Further analysis of this behavior is necessary to declare whether the point mass added is correlated to the overall mass of the beam, its length, or its width.

4. CONCLUSION

Within this paper, a proof of concept has been designed for the possibility of harvesting vibrational waste energy and converting it into useful electrical energy. Within the experiment, the system has been modeled as a unimorph cantilever harvester meaning, only a single piezoelectric transducer has been used, while the use of a bimorph harvester will yield doubled output power. The generated power can then be used to provide continuous and uninterrupted electrical power to low-power devices. It was seen that the introduction of a point mass to the system increases the deformations achieved in resonance, hence increasing the energy output of the piezoelectric material. The experiments were made in the frequency range of 16–19 Hz. It has been measured that the amplitudes of the vibrations increase as the frequency of rotation of the machine increases showing that for machines operating at higher frequencies more power can be obtained.

One of the major limitations of research within this field is the fact that the power generated by piezoelectric materials is too small to power most electronics which is the reason that in these circumstances only low-power sensors are used. Knowing this, the research focuses on new and innovative methods of accumulating the harvested energy as well as methods of further increasing the amount of energy the PZT material can harvest. Furthermore, the efficiency of the power harvesting circuit must be maximized in order to allow the full amount of energy generated to be transferred to the storage medium.

REFFERENCES

[1] Jacobson, M. Z.; Mark A. D. *et al*. (2017): 100% clean and renewable wind, water, and sunlight all-sector energy roadmaps for 139 countries of the world. *Joule* **1**, No. 1, pp. 108–121.

[2] Heard, B. P.; Barry, B. W.; Wigley, T. M. I.; Bradshaw, C. J. A. (2017): Burden of proof: A comprehensive review of the feasibility of 100% renewable-electricity systems. *Renewable and Sustainable Energy Reviews* **76**, pp. 1122–1133.

[3] Cao, S.; Li, J. (2017): A survey on ambient energy sources and harvesting methods for structural health monitoring applications. *Advances in Mechanical Engineering* **9** (4), https//doi:10.1177/1687814017696210

[4] Roundy, S.; Paul, K.; Wright, P. K.; Pister, K. S. J. (2002): Micro-electrostatic vibration-to-electricity converters. In: *ASME International Mechanical Engineering Congress and Exposition*, vol. **36428**, pp. 487–496.

[5] Liu, X.; Jianjun, W. (2018): Dynamic analytical solution of a piezoelectric stack utilized in an actuator and a generator. *Applied Sciences* **8**, No. 10.

[6] Parashar, S. K.; Von Wagner, U. (2005): Nonlinear shear-induced flexural vibrations of piezoceramic actuators: experiments and modeling. *Journal of Sound and Vibration* **285**, No. 4–5, pp. 989–1014.

[7] Mukherjee, A. B.; Chaudhuri, A. S. (2005): Nonlinear dynamic response of piezolaminated smart beams. *Computers & Structures* **83**, No. 15–16, pp. 1298–1304.

[8] Chen, M.; Chen, H. (2018): The isogeometric free vibration and transient response of functionally graded piezoelectric curved beam with elastic restraints. *Results in Physics* **11**, pp. 712–725.

[9] Dong, X. J.; Meng, G. (2005): Vibration analysis of a stepped laminated composite Timoshenko beam. *Mechanics Research Communications* **32**, No. 5, pp. 572–581.

[10] Kim, H.; Tadesse, Y. (2009): Piezoelectric energy harvesting. *Energy Harvesting Technologies*, pp. 3–39.

[11] Jeon, Y. B.; Sood, R. (2005): MEMS power generator with transverse mode thin film PZT. *Sensors and Actuators A: Physical* **122**, No. 1, pp. 16–22.

[12] Saha, C. R.; O'Donnell, T. (2006): Optimization of an electromagnetic energy harvesting device. *IEEE Transactions on Magnetics* **42**, No. 10, pp. 3509–3511.

[13] Despesse, G.; Jager, T. (2005): Fabrication and characterization of high damping electrostatic micro devices for vibration energy scavenging. In: *Proc. Design, Test, Integration and Packaging of MEMS and MOEMS*, pp. 386–390.

[14] Mineto, A.; Braun, M. P. (2010): Modeling of a cantilever beam for piezoelectric energy harvesting. In: *9th Brazilian Conference on Dynamics, Control and Their Applications, Sao Carlos, Brazil*, pp. 599–605.

[15] Šiškovski, D. (2016): *Active adaptive vibration control of beam using an electromagnetic actuator*. Master thesis, Faculty of Mechanical Engineering, Skopje.

Mechanical Engineering – Scientific Journal, Vol. **41,** No. 1, pp. 43–50 (2023)
Number of article: 663
In print: ISSN 1857–5293
Received: April 9, 2023
On line: ISSN 1857–9191
Accepted: April 22, 2023
UDC: 7.05:621.985]:[004.896:004.356-023.5
https://doi.org/10.55302/MESJ23411663043m

Original scientific paper

DESIGN PROCESS OF COMPLEX PRODUCT SHAPE WITH LATTICE VORONOI'S STRUCTURE USING CAx TOOLS

Ile Mirčeski, Dimitrij Georgievski

Faculty of Mechanical Engineering, "Ss. Cyril and Methodius" University in Skopje, P.O.Box 464, MK-1001 Skopje, Republic of North Macedonia
ile.mircheski@mf.edu.mk

A b s t r a c t: The aim of this paper is to present the design process of creating complex product shapes in industrial design with lattice Voronoi's structure using CAx tools. Complex product shapes have often been used in industrial design. Nowadays, the creation of products with complex shapes is possible using modern software package Fusion 360, using CAx tools and Additive Manufacturing (AM) technologies for rapid production and verification of prototypes. In this context, this paper focuses on a design process which incorporates the lattice Voronoi's structure as a topology optimization technique. The AM technology with Fused Filament Fabrication (FFF) 3D printing was chosen due to its ability to create products with rapid prototyping technology, as well as the complexity of the product shape. The design process includes conceptual design, 3D modeling and parametric design, preparation for production with 3D printing as well as testing to verify the product design. For prototyping of the product design an open-source system is used. The product model is designed and prototyped by the students with the use of 3D printing FFF technology.

Key words: design process; complex product shape; CAx; Fused Filament Fabrication (FFF)

ПРОЦЕС НА ДИЗАЈНИРАЊЕ СЛОЖЕНИ ОБЛИЦИ НА ПРОИЗВОД СО РЕШЕТКАВИ ВОРОНОИЕВИ СТРУКТУРИ И УПОТРЕБА НА АЛАТКИТЕ CAx

А п с т р а к т: Целта на овој труд е да се презентира процесот на дизајн за креирање сложени облици во индустрискиот дизајн со употреба на решеткава Вороноиева структура со употреба на алатките CAx. Сложените облици на производите често се употребуваат во индустрискиот дизајн. Денес креирањето на производи со сложени облици е овозможено со употреба на модерниот софтверски пакет Fusion 360, алатките CAx и адитивните технологии за брзо производство и верификација на прототипите. Во тој контекст, овој труд се фокусира на дизајнирање на процес кој вклучува решеткава Вороноиева структура како тополошка техника за оптимизација. Технологијата за адитивно производство со 3Д печатење со споени филаменти (FFF) е избрана како погодна да се креираат производи со технологија за брзо прототипирање, како и поради сложеноста на обликот на производот. Процесот на дизајнирање вклучува концептуален дизајн, 3Д моделирање и параметарски дизајн, подготовка за производство со 3Д печатење, како и верификување на дизајнот на производот. За прототипирање на дизајнот на производот се користи отворен систем. Моделот на производот е дизајниран и произведен од студент со користење на 3Д печатење со FFF технологија.

Клучни зборови: процес на дизајнирање; сложен облик на производ; CAx; 3Д печатење со споени филаменти (FFF)

1. INTRODUCTION

The complex shape of products with Voronoi structure inspired by nature has long been employed in the field of architecture, but today are employed in industrial design. The barrier for application of Voronoi structure in area of industrial design were software packages for 3D modeling and production technology of complex shape and surface. Today with the use of a several software packages such as Fusion360, Rhino & Grasshopper, Blender, nTopology, and others, as well as with application of additive manufacturing (AM) technology with FFF 3D printing, the product with complex shape can be easily fabricated. The software packages Fusion 360 and nTopology with its methodology is one of the

best for generation of lattice and porous structure for different application areas. In this research software package Fusion 360 for 3D modeling of product with Voronoi structure is used. For fabrication of product the FFF 3D printing technology with Ender 3 V.2 printer and SuperSlicer software is used.

An interesting and useful way of improving the product design shape is by using the lattice Voronoi's structure. The Voronoi pattern can be implemented to reduce the mass of products while keeping the other product functionalities intact, to reduce the manufacturing time consumption and overall cost. Additionally, thanks to the unique and interesting nature of the Voronoi pattern itself, the aesthetic design of the product's shape will be increased, which will contribute to improving the overall product quality.

Recently, 3D printing FFF technology has emerged as an effective method to produce complex structures layer by layer [1, 2]. Reducing mass of products, material and time consumption problems are still challenges for 3D printing. Creating reliable and lightweight products can be obtained by replacing solid infill materials with Voronoi porous structures.

The AM technologies supported by advanced 3D modeling of complex shapes have opened a lot of new possibilities for product designing, creativity, ergonomics, custom design, aesthetics, and efficiency in the industrial design process. Product designs with aesthetic and complex shapes can be developed, prototyped, and fabricated. To benefit from the concurrent application of these technologies in the design process, industrial designers should be educated and trained in parametric design thinking and cooperation with computer programmers and production technology experts. On the other hand, the design process itself is highly dependent on personal creativity, sensory perception of form and material, and understanding of consumer product trends [3].

Nowadays, the CAx systems and CAx engineering applications are an inseparable part of industrial design. CAx tools such as: CAD, CAM, CAE, PLM, etc., are more significantly relevant in the development process of new products and industrial design. CAx tools significantly reduce the time and costs of a new product development and fast launching the product to the market [4–6].

In summary, FFF technology enhances the design freedom in creating complex shapes of products, with improved aesthetics and modern design while keeping intact the other product functionalities, compared to the traditional manufacturing processes. When properly designed for FFF technology, parts with complex shapes can be prototyped and/or produced directly. The power and adaptability which 3D printing provides can be used to create innovative and useful products.

2. BACKGROUND

Geometric Form/Organic Matrix is an AWOL trend based on lattice Voronoi's structures, which is a specific method of achieving dynamic balance between rational and natural worlds. Geometric form based on a primitive, such as a cube or rectangle, often defines an absolute outer boundary volume of which a cellular matrix of internal structures fills in the interior void. Nowadays, this technique has been primarily used in architecture and furniture (see Figure 1), with some inroads into the product category. Also, this trend is highly related to Organic Forms/Geometric Matrix, which inverts the relationship between form and interior structure [7].

Fig. 1. Geometric Form/Organic Matrix [7]

Complex shapes and structures include complex surfaces, complex geometries, porous and lattice structures, etc., which are common in the natural environment. The most natural structures are complex structures with holes and porosities or irregular surfaces. These structures can be used as a lightweight infill, porous scaffolds, energy absorbers or micro-reactors. The novel rapid prototyping technology with 3D printing and application background is suitable to answer the current design methodologies in order to produce complex product shapes [8].

The product designers today have the possibilities to design complex geometries which can be produced with AM technology, considering there are less technological limits than before. In the research [9], Piros and Trautmann presented a new structure with complex geometries called Lightweight Voronoi Scaffold which is tested with multiaxial load case. The arrangement of Voronoi scaffold is not regular, random sampling-based Monte Carlo method is applied in order to provide proper distribution of generation of geometric instances. Piros *et al*. presented Lightweight Voronoi Scaffold which is compared to some common regular beam lattices, and results show that Lightweight Voronoi Scaffold was lighter in each case, which may open new opportunities in the field of additive manufacturing. Multilevel design for the interior of 3D fabrication is presented in the paper [10]. The aim of this work is to create lightweight 3D fabrications with lighter interior structures to minimize printing materials and supplementary to strengthen thin parts of objects. The approach allows for the composition of sparse and dense distributions of patterns of interior 3D fabrications in an efficient way, so users can fabricate their own 3D designs. Porous structures such as bone-like porous structures [10], porous Ti-based alloy prostheses [11], developed a density-aware internal porous supporting structure to improve the structural soundness of 3D fabrications [12]. The research of lattice Voronoi's structures are widely used for interior design supported with 3D print, due to its properties such as stress sustainable, lightweight, and cost-effectiveness.

The application of lattice Voronoi's structure method to construct controllable porous scaffolds is presented in the research of Wang *et al*. [13]. Their method was successful in obtaining the porous structures geometries, after which the specimens were prepared by selective laser melting technology for manufacturing and the specimens were tested with quasi-static compressive test. In the research of Lu *et al*. [14], Voronoi mesh is applied in order to reduce the material cost and weight of a given object, while providing a durable printed model that is resistant to impact and external forces.

Availability of AM technologies today has increased the application and popularity of 3D modeling of products with complex shape in industrial design to create parts with complex shape, structure, pattern, porous and lattice structures. AM technologies have applications in many areas, such as rapid prototyping and manufacturing of parts, orthopedic personalized devices [15] and others. Preparation time for AM production of parts with complex geometry is relatively short. Many industrial designers choose AM technologies as a tool for prototyping, especially for prototyping products with complex shapes such as Voronoi shapes implicated into product surfaces.

The main goal of this research is to present the design process which incorporates the lattice Voronoi's structure into the product complex shapes and the use of AM technology for prototyping of complex shapes. The design process includes identification of market needs, conceptual design, 3D modeling and parametric design, preparation for production with 3D printing FFF technology as well as testing to verify the product design. The applicability of this research is presented through illustrative example.

3. DESIGN PROCESS METHODOLOGY

The design process of a product is a complex process which consists of several phases [16]: identification of market needs, project planning, product definition or definition of the product engineering specifications, conceptual design and developing the product using CAD models, calculations, selection of materials, making technical drawings for the prototype production and defining all necessary information for manufacturing.

3.1. *Identification of market needs, product definition and project planning*

The project started at the Faculty of Mechanical Engineering in Skopje, in the study program in Industrial design. The project description was clearly defined with the set of general requirements. The project task was defined as a design of modern vase with application of AM technology and lattice Voronoi's structure. It was proposed the decorations

of the vase to be focused on small led lights, powered by a battery. Additionally, in order to understand the design problem translation of customers' requirements into a technical description of what needs to be designed was made. The development of clear requirements is a key feature for an effective design process. The customers' requirements need to be translated to engineering specifications and the design team needs to understand the problem in order to write a good set of engineering specifications. The market research showed that there are already a lot of examples of 3D printed vases with lattice Voronoi's structure. They are designed with different shapes, functions, shell thickness, holes density, etc., intended for decoration with ambient light, others intended for office equipment, others for arranging and planting flowers. In Figure 2 vases with different lattice Voronoi's structures from many designers available on the market are presented.

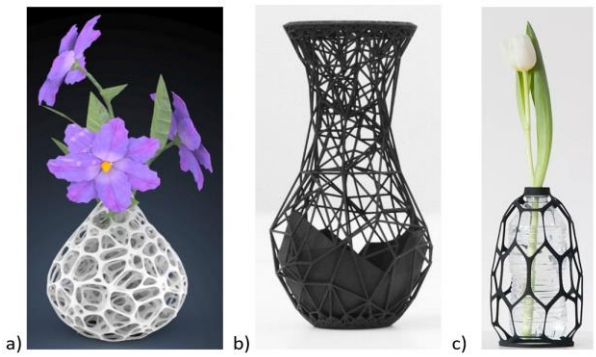

Fig. 2. a) Math Décor by Dizingof [17]. **b)** The Wire by Ivan Zhurba [18]. **c)** Knitted Vase Designlibero [19]

3.2. *Conceptual design*

A concept is an idea that is sufficiently developed to evaluate the physical principles that govern its behavior [16]. The concept of a vase with lattice Voronoi's structure is created with application of the software package Autodesk Fusion 360. Fusion 360 is CAx software for development of products with complex shapes and includes the module for creating lattice Voronoi's structures with an overall control of the mesh. The complex shape of the vase with lattice Voronoi's structures is created by the tools tessellate, reduce and pipe, incorporated in the Voronoi module. The created 3D model is parametric and the parameters which can be adjusted are Voronoi mesh, density, schedule of geometrical forms and diameter of mesh. The software Fusion 360 is not the simplest for creating lattice Voronoi's structure, but our requirements were fully satisfied. The product is intended for people who want a multi-functional eco product that can simultaneously be used as a decoration, ambient lighting, and flower vase. One concept of modern vase with lattice Voronoi's structure and complex shape was generated and is shown in Figure 3.

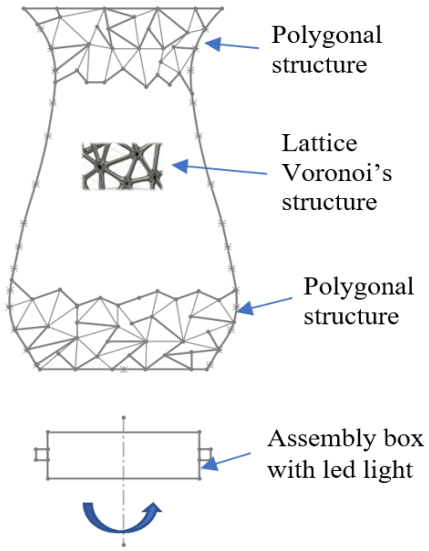

Fig. 3. Concept design of modern flower vase

3.3. *Product development*

The inspiration for the shape was a glass bottle, according to which the shape was modeled. The glass bottle inserted as an inner part of the vase with intention to achieve multi-functionality. The glass bottle in the vase serves as a flower vase.

The other function of the glass bottle in the vase is the excellent transparency and dispersion of light through the lattice Voronoi's structure. In the lower part of the vase electronics with led lights are inserted which serve as ambient lighting. The product design phase is focused on refining the concept into a hight quality product. The product's design is evaluated for its performance, robustness, quality, and cost. After all the important aspects were considered, such as performance, robustness, quality and cost, a novel design of a modern vase with lattice Voronoi's structure was created.

The vase was modeled with application of the Fusion 360 software, using the following modules: part, assembly, surface modeling, tessellate, reduce, Voronoi mesh, etc. Figure 4 presents the steps of creation of the modern vase 3D model with lattice Voronoi's structure using the Fusion 360 software.

3.4. *Prototyping*

The prototyping of the presented example, shown in Fgure 4, is with FFF 3D printing technology. For fabrication of the prototype the 3D printer Ender 3 V.2 was used, the G-code was created in the software SuperSlicer and PLA material was chosen as a prototype material. In the SuperSlicer a few parameters were adjusted, such as: printing orientation is vertical, infill is 20%, supports were used, and layer height is 0.2 mm. Printing time was 17 hours and 28 minutes.

Figure 5 presents the steps of the prototyping process: a) creating the g-code with the help of the software SuperSlicer, b) 3D printing process, c) 3D printed assembly and supports, d) the electrical circuit, and e) lower assembly with led light. The prototype of the final product of a modern vase with lattice Voronoi's structure is shown on Figure 6.

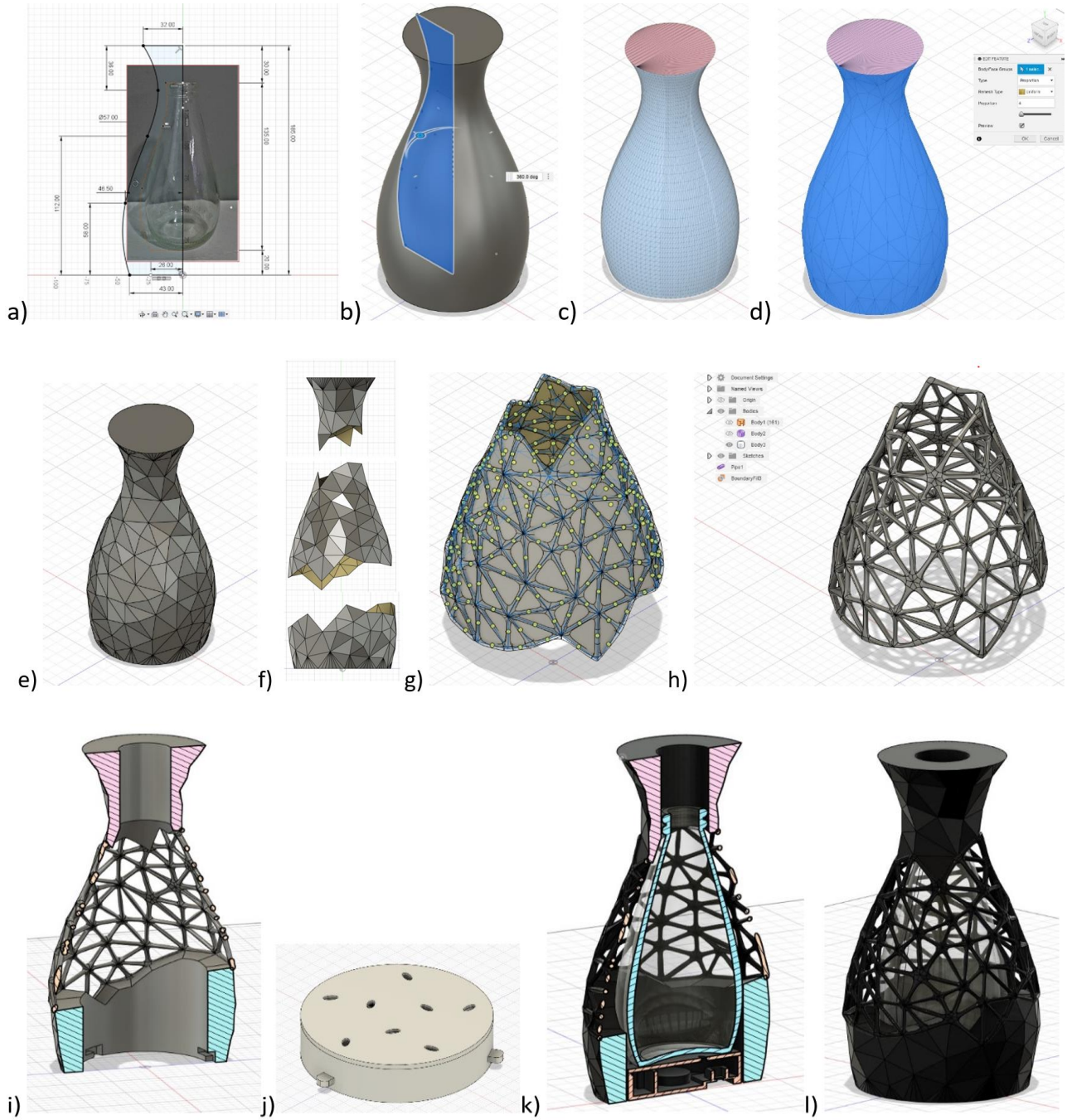

Fig. 4. Creating the 3D design of the vase with Fusion 360 in several steps: a) sketch, b) revolve, c) tessellate, d) reduce, e) create solid body, f) divide the body into 3 parts, g) lattice Voronoi's structure, i) section view of assembly, j) electronic plastic box, k) section view of vase, l) 3D model of vase assembly

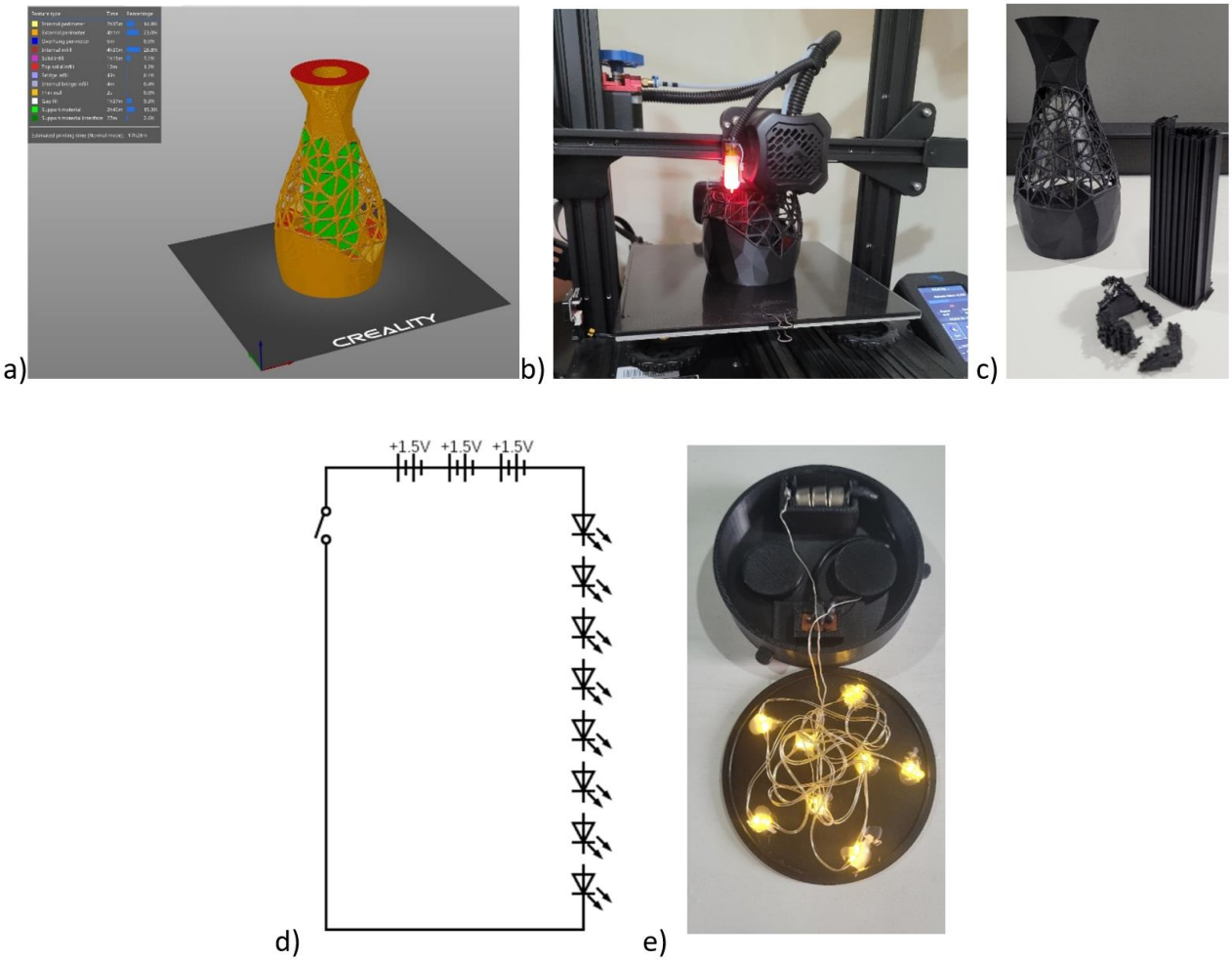

Fig. 5. Prototyping: a) creating g-code in super slicer, b) FFF process, c) the product and supports, d) electrical circuit, e) lower assembly with led ligh

Fig. 6. Final prototype of modern vase designed with lattice Voronoi's structure

4. RESULTS AND DISCUSSION

The applicability of the design process of creating complex product shapes with lattice Voronoi's structure, using CAx tools and fabrication with 3D printing technology is presented through an illustrative example. The overall design process of creation and verification of product is presented in a few steps, such as: identification of market needs, product definition and project planning, conceptual design supported by handmade sketch of a product design (see Figure 3), product development using CAD and CAx tools for 3D modeling and analysis of model (see Figure 4), and rapid prototyping of product using 3D printing technology (Figure 5). The goal is for industrial designers to predict, evaluate, and improve owner designs as early in the design stage as possible by using CAx tools and rapid fabrication process with 3d printing technology. The final prototype of product modern vase designed with lattice Voronoi's structure is presented on Figure 6 in daily and night usage with ambient led light.

5. CONCLUSIONS

This paper presented the design process of creating complex product shapes with lattice Voronoi's structure in industrial design using CAx tools. Design process stages such as identification of market needs, product definition, project planning, conceptual design, product develop-ment, and prototyping, based on selected case study are described. The new design of the modern vase implements the use of lattice Voronoi's structure, decoration elements, and ambient led lighting. The complex shape is made by using the modern software package Fusion 360, CAx tools and 3D printing technologies for rapid production and verification of prototype. The verification of the prototype provides evidential proof of efficiency of the design process. The design process supported with AM fabrication and prototyping is aimed to encourage the industrial design students to fabricate their designs early in the design process, to evaluate and present their designs in a relatively short time.

REFERENCES

[1] Gao, W.; Zhang, Y. B.; Ramanujan, D.; Ramani, K.; Chen, Y.; Williams, C. B. *et al*. (2015): The status, challenges, and future of additive manufacturing in engineering, *Computer Aided Design*, Vol. **69**, pp. 65–89. https://doi.org/10.1016/j.cad.2015.04.001

[2] Thompson, M. K.; Moroni, G.; Vaneker, T.; Fadel, G.; Campbell, R. I.; Gibson, I. *et al*. (2016): Design for Additive Manufacturing: trends, opportunities, considerations, and constraints. *CIRP Ann*., Vol. **65** (2), pp. 737–760. https://doi.org/10.1016/j.cirp. 2016.05.004

[3] Kandikjan, T.; Djokikj, J.; Mircheski, I.; Angeleska, E. (2022): Integrating parametric design and additive manufacturing knowledge in Industrial design education, *Elsevier, Materials Today: Proceedings. International Conference of Additive Manufacturing for a Better World (AM Conference)*, Singapore University of Technology and Design, pp. 470–477. https://doi.org/10.1016/j.matpr.2022.10.124

[4] Łukaszewicz, A.; Panas, K.; Szczebiot, R. (2018): Design process of technological line to vegetables packaging using CAx tools. *Proceedings of 17th International Scientific Conference on Engineering for Rural Development*, May 23–25, 2018, Jelgava, Latvia, 871–876.

[5] Łukaszewicz, A.; Skorulski, G.; Szczebiot, R. (2018): The main aspects of training in the field of computer-aided techniques (CAx) in mechanical engineering. *Proceedings of 17th International Scientific Conference on Engineering for Rural Development*, May 23–-25, 2018, Jelgava, Latvia, 865–870.

[6] Łukaszewicz, A.; Szafran, K.; Jóźwik, J. (2020): CAx techniques used in UAV design process, *2020 IEEE 7th International Workshop on Metrology for AeroSpace (MetroAeroSpace)*, pp. 95–98. DOI:10.1109/MetroAeroSpace48742.2020.9160091

[7] Organic Form/Geometric Matrix http://awoltrends.com/2012/11/organic-form-geometric-matrix/, Accessed on: 2023-04-18.

[8] Feng, J.; Fu, J.; Lin, Z.; Seang, C.; Li, B. (2018): A review of the design methods of complex topology structures for 3D printing, *Vis. Cimput.Ind. Biomed. Art*. Vol. **1**, No. 5. https://doi.org/10.1186/s42492-018-0004-3

[9] Piros, A.; Trautmann, L. (2023): Creating interior support structures with Lightweight Voronoi Scaffold, *Int J Interact Des Manuf*, Vol. 17, pp. 93–101, https://doi.org/10.1007/s12008-022-01182-8

[10] Wu, J.; Aage, N.; Westermann, R.; Sigmund, O. (2018): Infill optimization for additive manufacturing – approaching bone-like porous structures, *IEEE Trans. Visual Comput. Graphics*, Vol. **24**, pp. 1127–1140.

[11] Mircheski, I.; Gradšar, M. (2016): 3D finite element analysis of porous Ti-based alloy prostheses, *Computer Methods in Biomechanics and Biomedical Engineering (CMBBE)*, Vol. **19**, No. 14, pp. 1531–1540. https://doi.org/10.1080/10255842.2016.1167881

[12] Li, D.; Dai, N.; Jiang, X.; Shen, Z.; Chen, X. (2015): Density Aware Internal Supporting Structure Modeling of 3D Printed Objects, In: *Proceedings of the International Conference on Virtual Reality and Visualization (ICVRV)*, pp. 209–215.

[13] Wang, G.; Shen, L.; Zhao, J.; Liang, H.; Xie, D.; Tian, Z.; Wang, C. (2018): Design and compressive behavior of controllable irregular porous scaffolds: based on Voronoi-tessellation and for additive manufacturing, *ACS Biomater. Sci. Eng*., Vol. **4** (2), pp. 719–727. https://doi.org/10.1021/acsbiomaterials.7b00916.

[14] Lu, L.; Sharf, A.; Zhao, H. S.; Wei, Y.; Fan, Q. N.;, Chen, X. L. *et al*. (2014): Build-to-last: strength to weight 3D printed objects, *ACM Trans Graph.* Vol **33**, 97. https://doi.org/10.1145/2601097.2601168

[15] Kralevski, L.; Jovchevska, A.; Mircheski, I. (2022): Custom design of an orthopedic hand cast using virtual simulation, 3D printing and experimental verification, *10th International Scientific Conference "Machine Design in Context of Industry 4.0 Intelligent Products" IRMES2022,* Faculty of Mechanical Engineering in Belgrade, Serbia, pp. 205–210.

[16] Ulman, D. G. (2010): *The Mechanical Design Process*, Fourth edition, McGraw-Hill Series in Mechanical Engineering, Boston.

[17] https://www.pinterest.com/pin/3d-voronoi-vase-math-decor-by-dizingof--546976317246269611/. Accessed on: 2023-04-18

[18] https://design-milk.com/customize-print-vase-ivan-zhurba/. Accessed on: 2023-04-18

[19] https://www.designlibero.com/portfolio/3d-printed-vases-collection/. Accessed on: 2023-04-18

Mechanical Engineering – Scientific Journal, Vol. **41,** No. 1, pp. 51–58 (2023)
Number of article: 664 In print: ISSN 1857–5293
Received: September 27, 2022 On line: ISSN 1857–9191
Accepted: January 12, 2023 UDC: 004.738.5:656.13.052.43]:519.876.5
https://doi.org/10.55302/MESJ23411664051j

Original scientific paper

COMPARISON OF DIFFERENT MODELLING APPROACHES FOR VEHICLE VELOCITY CONTROL ON AN UPCOMING BOTTLENECK SECTION

Stefani Josifovska[1], **Vase Jordanoska**[2]

[1]*MSc Student at the Institute of Mechanical Construction, Mechanization Machines and Vehicles, Faculty of Mechanical Engineering, "Ss. Cyril and Methodius" University in Skopje, Skopje, Republic of North Macedonia*
[2]*Institute of Mechanical Construction, Mechanization Machines and Vehicles, Faculty of Mechanical Engineering, "Ss. Cyril and Methodius" University in Skopje, P.O.Box 464, MK-1001 Skopje, Republic of North Macedonia*
stefani.josifovska@hotmail.com

A b s t r a c t: With the development of the Internet of Things and the Smart infrastructure, simulating the traffic is not purely a mathematical question anymore, but also entails the vehicle dynamics as an important factor, due to the constant data sharing between the vehicles and the highly automated systems which control the behaviour of the vehicles. This paper aims to upgrade the traditional traffic flow model based on the Cellular Automata theory, by incorporating the positions and velocities of the vehicles, as well as introduce a longitudinal vehicle dynamics model, in order to determine the accuracy of the pure traffic model in a simulation environment (Python).

Key words: Internet of vehicles; traffic model; longitudinal dynamics; bottleneck merge

СПОРЕДБА НА РАЗЛИЧНИ НАЧИНИ НА МОДЕЛИРАЊЕ УПРАВУВАЊЕ СО БРЗИНАТА НА ВОЗИЛО ПРИ СПОЈУВАЊЕ НА ДВЕ СООБРАЌАЈНИ ЛЕНТИ ВО ЕДНА

А п с т р а к т: Со развојот на интернетот на нештата и паметната инфраструктура, симулирањето на сообраќајот повеќе не е само математички проблем, туку ја повлекува и динамиката на возилата како битен фактор, поради постојаната размена на податоци помеѓу возилата и напредните автоматизирани системи кои управуваат со однесувањето на возилата. Целта на овој труд е традиционалниот модел на сообраќаен тек базиран на теоријата на мобилни автомати, да се надгради со вклучување на позицијата и брзината на возилото вклучувајќи го и неговиот надолжен динамички модел, со цел одредување точност на чист сообраќаен модел во симулирана околина (Python).

Клучни зборови: интернет на возилата; сообраќаен модел; надолжна динамика; спојување на две ленти во една

NOMENCLATURE

IoV	Internet of Vehicles	m	mass of the vehicle
CA	Cellular Automata	F_{nf}, F_{nr}	normal force on front and rear axle
x_{new}	calculated vehicle position in the next time step	l	wheelbase
$x_{current}$	current vehicle position	V_X	vehicle longitudinal velocity
Δx	calculated vehicle displacement in the next time step	F_{xf}, F_{xr}	longitudinal tire force of front and rear axle
Δt	time step	$I_{\omega f}$, $I_{\omega r}$	moment of inertia of front and rear wheel
v_{current}	current velocity of the observed vehicle	ω_f, ω_r	front and rear wheel speed
T_f, T_r	input torque on front and rear wheel	F_{air}	air resistance
r_d	effective tire radius	μ	longitudinal friction coefficient
F_r	rolling resistance	l_f, l_r	distance from center of gravity to front and rear axles

1. INTRODUCTION

With the development of the Internet of Things and the Smart infrastructure, the idea of interconnected vehicles in the form of IoV is slowly becoming a reality. This entails the need of new models for traffic flow simulation, as well as models describing the behaviour of various automated vehicle systems that depend on the surrounding road traffic participants.

Regardless whether the observed subjects are autonomous or human-driven vehicles, one of the most common problems in the traffic flow nowadays is the traffic bottleneck situation. Merging itself is a pretty complex mathematical problem, with many possible modelling approaches, as discussed in [1]. Many authors [2, 3] suggest using the Rule 184 fuzzy cellular automation as a mathematical model of traffic flow [4]. However, this model does not take the vehicle dynamics into account, but observes the vehicles as moving points. Due to the fact that the CA modelling approach has been proven to be sufficient for traffic flow simulations, there are some authors suggesting the vehicle velocities and accelerations accompany the points in the model, using basic vehicle dynamics equations [5].

The abovementioned models could be taken one step further, by assuming that the observed vehicles are interconnected and share data via the IoV. Thus they would all be able to adjust their respective velocities in order to achieve smoother merging into a bottleneck section, as discussed in [6].

Analyzing the suggested modelling methods, the question arises whether the dynamics of the observed vehicle should necessarily be considered when simulating a bottleneck section of interconnected vehicles. The possibility exists that it is sufficient to just apply the CA model with a custom ruleset and have a discrete velocity change with a bigger time-step, i.e. that the model could capture the dynamical capabilities of a real vehicle on the road. Throughout this paper, the traffic model with the custom ruleset as well as the longitudinal vehicle dynamics model, will be presented. Furthermore, the way those two models are combined will be explained. Lastly, the simulation results will be discussed.

2. MATHEMATICAL MODELS

The main model consists of two incorporated models, one describing the behaviour of vehicles when approaching a bottleneck section, and the other describing the longitudinal vehicle dynamics. The programming language Python was used for this purpose, with the utilization of the pandas, Matplotlib and NumPy libraries.

a) *Single lane traffic model*

As mentioned earlier, the idea behind the CA model will be adopted for describing the traffic flow. However, without any modification this approach is limited, out of the scope of this research, due to the fact that it can only describe the behaviour of the vehicles in one lane. In this case, two lanes need to be observed simultaneously, since the velocity and position of the vehicles is crucial for determining the expected behaviour of the vehicles behind them.

First, a new ruleset for vehicles behaviour must be developed. It is necessary that the used algorithm takes the positions and velocities into account, meaning that a plain CA ruleset implemented on an array consisting of 0's and 1's will not suffice.

The first step in creating the traffic model would be getting a section of certain length (length of 300 meters is adopted throughout this paper), divided in equally long sections (3 meters each). An average length of a vehicle is considered 3 meters, due to the variety of vehicles with different geometric characteristics that can be found on the road. It is assumed that each vehicle can only take up one cell at each given moment.

The next step is populating the road, using a random function returning only 0's (empty slot) or 1's (populated slot), with a probability of 25%. Afterwards, looping through the slots of the lane takes place, assigning a random velocity in a certain range for every slot that contains a vehicle, as shown in Figure 1. The results are saved in a list of dictionaries, each containing two key-value pairs: one regarding the randomly assigned velocity, and the other one regarding the position (the index of the slot where the vehicle is placed).

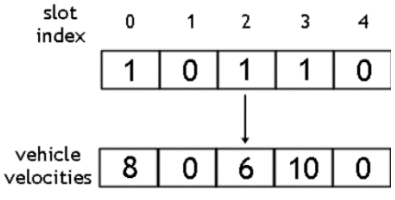

Fig. 1. Steps of populating a lane

For the purpose of the simulation, a time-step of 0.5 seconds has been adopted. After each time-

step the new position of the vehicle should be calculated as a function of the velocity, using the following expression:

$$x_{new} = x_{current} + \Delta x, \tag{1}$$

where Δx is the number of the slots the vehicle passes in the given time and is calculated according to the following expression, rounded to the closest integer:

$$\Delta x = \frac{\Delta t \cdot v_{current}}{3}. \tag{2}$$

The same logic can be applied when introducing the second lane, as shown in Figure 2.

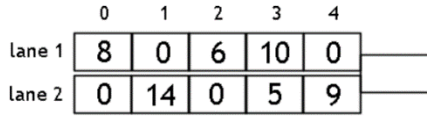

Fig. 2. Introducing a second lane to the model

However, the actual displacement of the vehicles depends on outside factors as well, such as the velocity of the vehicle in front of it, whether or not the vehicle is ready to merge or is still not in the last slot, and the situation in the neighbour lane. The algorithm for determining the new position of the vehicle is shown in Figure 3.

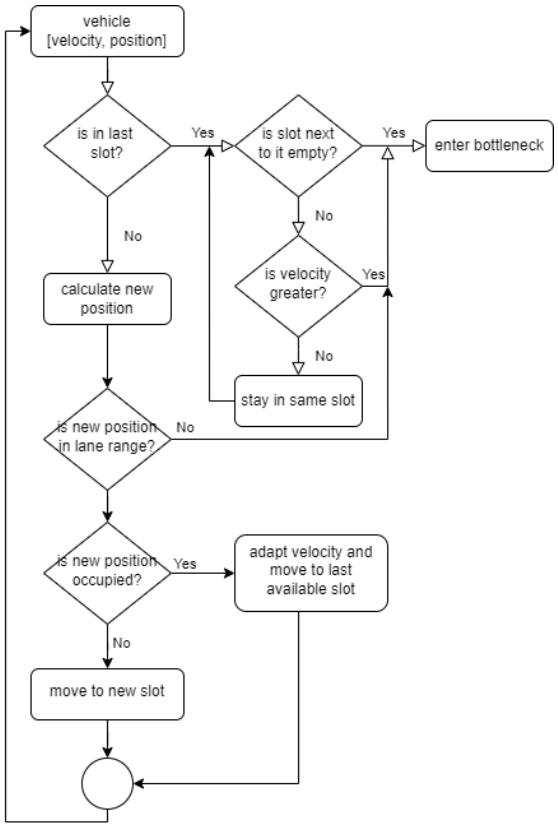

Fig. 3. Traffic flow simulation algorithm

It is important to note that when introducing the second lane, the slot with index 0 from the first lane is not randomly assigned as either 1 or 0, but is always occupied by the observed vehicle, whose dynamics should be simulated with the help of the dynamics model. Furthermore, there is a function adjusting the vehicle velocity to the one in front of it, in case of slower movement of the vehicles in the next slots of the lane and the inability to overtake, as shown in the algorithm.

If the two lanes are not observed separately, a separate function looking for the next vehicle in both lanes is to be called, and the adjusting velocity function should be called afterwards in order to slow down the vehicle, so that is could match the velocity of the vehicle which should merge before it. Doing this additional step will provide a smoother merging and traffic flow.

b) *Longitudinal vehicle dynamics model*

For the purpose of this simulation, a section with two straight lanes is observed. The vehicles in both lanes do not have the ability to overtake, nor to switch lanes, and the only time the direction of movement changes is exactly at the time of merging, which is not of interest in the simulation and is therefore neglected in the models and results. For that reason, a longitudinal dynamics model is sufficient for describing the behaviour of the vehicles in the given situation.

The longitudinal model can be applied to describe the dynamics of braking and accelerating, along with the grade angles, not considering the lateral dynamics. Moreover, the left and right wheels of the vehicle can be combined into one wheel, due to the insignificant difference between their respective wheel speeds.

The used longitudinal dynamics model can be presented with the following equations [7]:

$$\begin{cases} m \cdot \dot{v}_x = F_{xf} + F_{xr} - F_r - F_{air} \\ I_{\omega f} \cdot \omega_f = \pm T_f - r_d \cdot F_{xf} \\ I_{\omega r} \cdot \omega_r = \pm T_r - r_d \cdot F_{xr} \end{cases} \tag{3}$$

The script of the model consists of three separate classes:

1. Vehicle class, which includes the necessary vehicle parameters, such as the wheelbase, location of the centre of gravity with respect to the front and rear axles and its height, the total mass, as well as its distribution among the axes and the parameters needed to calculate the air resistance force.

2. Tire class, consisting of the necessary tire parameters, as well as functions for calculating tire slip and tire speed.

3. A Simulation class, which gets the time-step, input torque and the needed vehicle and tire parameters, in order to calculate the components describing the longitudinal behaviour of the vehicle.

The initial conditions of the vehicle dynamics simulation are shown in Table 1.

T a b l e 1

Vehicle simulation initial conditions

Symbol	Physical quantity	Initial value	Unit
x_0	Initial position	0	kg
$\dot{x}_0$	Initial velocity	inherited from traffic model	m/s
$\ddot{x}_0$	Initial acceleration	0	m/s^2
t_0	Initial time	0	s
F_{nf}	Front axle normal force	$\frac{9.81 \cdot m \cdot l_f}{l}$	N
F_{nr}	Rear axle normal force	$\frac{9.81 \cdot m \cdot l_r}{l}$	N
F_{xf}, F_{xr}	Longitudinal forces	0	N
s_f, s_r	longitudinal slip on front and rear wheel	0	–
ω_f, ω_r	Front and rear wheel speed	$\frac{\dot{v}_{xi}}{r_d}$	rad/s
T_f, T_r	Front and rear wheel torque	0	Nm

As shown in (3), the longitudinal force, which appears as a result of the input torque, needs to be calculated in order to determine the longitudinal acceleration of the vehicle. That can be achieved using the following equation:

$$F_{xi} = F_{ni} \cdot \mu. \tag{4}$$

As can be noticed from the equation (4), the longitudinal force directly depends on two factors: the normal force, which has to constantly be re-evaluated as a function of the longitudinal acceleration, and the longitudinal friction coefficient, which depends on the longitudinal slip, i.e. the relative difference between the vehicle and the tire longitudinal velocities, and cannot be expressed empirically. There are many models describing the longitudinal behaviour of a tire, based on experimental data. In this model, the Burckhardt method is used. Coefficients used in the tire model are shown in Table 2, and the longitudinal slip-friction coefficient relation is represented by the curve shown on Figure 4.

T a b l e 2

Coefficients used in the tire model

Symbol	Physical quantity	Value	Unit
r_d	Effective tire radius	0.3	m
φ	Wheel adhesion coefficient	0.8	–
f_0	Rolling resistance coefficient at v=0	0.015	–
I_f, I_r	Wheel moment of inertia	0.8	kgm^2
a	Burckhardt coefficients for dry asphalt [7]	1.28	–
b		23.99	–
c		0.52	–

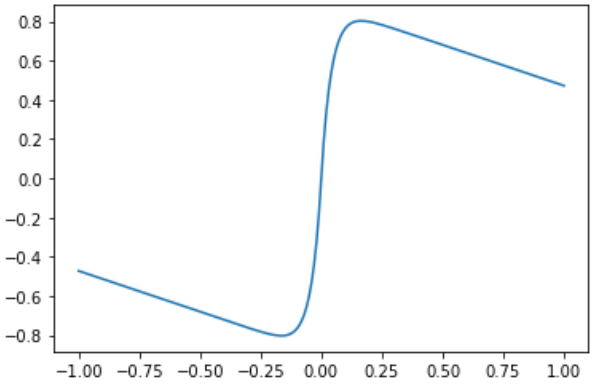

Fig. 4. Longitudinal friction coefficient in function of the wheel slip, according to the Burckhardt model (horizontal axis – wheel slip, vertical axis – friction coefficient)

c) *Incorporated model*

In order to be able to run the final simulations and get the necessary results, the two models described above need to be combined into one model, which runs according to the algorithm shown in Figure 5.

As demonstrated in the algorithm, the adopted time steps for this simulation are 0.01 seconds for the vehicle dynamics model, and 0.5 seconds for the traffic model. It is assumed that the controller gets the needed values from the surrounding vehicles twice per second, and the vehicle acts accordingly. The first check of whether the controlled vehicle is still in the lane is done by checking if the values of all the cells in lane 1, which entails our vehicle, are null. In a positive case, the observed vehicle has already gone into the merge and the simulation can be stopped, since the already presented traffic model

assumes there are no vehicles behind it, i.e. that is the last vehicle of our interest in the lane.

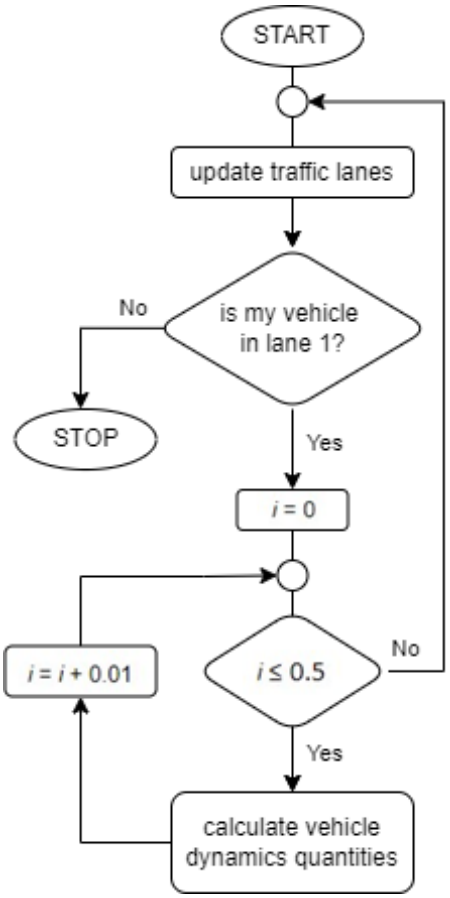

Fig. 5. Incorporated model algorithm

The outputs after every time step are stored in two separate pandas data frames, one regarding the traffic model results and the other regarding the vehicle dynamics quantities of interest, after each simulation time step.

The torque in the separate vehicle dynamics model needed to be hardcoded for each simulation, in order to imitate the behaviour of the driver. However, due to the random population of the lanes, it is impossible to know the traffic situation, and thus the needed torque, beforehand. That is why a logic for determining whether or not the torque should be increased, i.e. decreased, in the next time step and by how much, needs to be implemented. It is important to note that, in order to simplify the model, it is assumed that the vehicle has a non-zero input torque at any given time during the simulation. The velocity corrections will be done exclusively by adding a positive or negative torque, which will possibly result in unnecessary velocity dilatations that would not provide a comfortable ride, but are sufficient for the purpose of this research.

The target torque for the next time step can be calculated right after reading the velocity and position values of both the controlled vehicle and the one in front of it. Regardless of whether it is located in the same lane or not. The 2-second rule is followed in this model, meaning that if the distance between the two vehicles is greater than 2 seconds at the current velocities, the target torque should be 2000 Nm, which is achievable by most vehicles and still provides a smooth acceleration, thus allowing the vehicle to close the gap until it reaches a 2-second distance.

In case the first requirement is met, the next step should be adapting the velocity of the controlled vehicle with regards to the data gathered about the vehicle in front of it. Namely, the needed acceleration or deceleration can be calculated by simply implementing the following equation:

$$a = \frac{v_{target} - v_{current}}{\Delta t}, \tag{5}$$

where a is the target acceleration, v_{target} is the target velocity (the velocity of the vehicle in the front), $v_{current}$ is the current velocity of the controlled vehicle and Δt is the traffic model time step. Knowing the acceleration value, the inertial force F_i can be easily calculated. Furthermore, the air and rolling resistance forces can be calculated at target velocity.

Given the nature of the longitudinal dynamic vehicle model, the needed torque can be calculated by balancing the forces along the longitudinal axes, thus getting the following equation:

$$T_{target} = \pm(F_i + F_r + F_{air}) \cdot r_d. \tag{6}$$

Once the target torque is known, in order to achieve a smoother transition, provided we know the input torque from the last time step of the previous simulation cycle, T_{prev}, a slightly modified version of the Sigmoid function [8, 9] can be used:

$$sig = \frac{T_{target} - T_{prev}}{1 + e^{-0.02t+6}} + T_{prev}. \tag{7}$$

Given that the majority of the cars are front-wheel drive, but break using all four wheels, it is safe to adopt the same logic in this model. However, this entails the need to incorporate a brake torque distribution model between the front and rear axles. First of all, it needs to be determined whether the torque is increasing or decreasing, i.e. whether the vehicle is accelerating or braking. This can be done with the following check:

$$\begin{cases} T_{target} < T_{prev} => braking \\ T_{target} > T_{prev} => accelerating \end{cases} \tag{8}$$

If it is determined that the vehicle will be accelerating in the following time step, the needed torque as a whole should be applied to the front axle, whereas the rear axle gets a torque of 0. On the other hand, if the brakes need to be applied, the distribution among the axles should follow the following rule:

$$\begin{cases} T_{front} = \frac{T_{sig} \cdot F_{nf}}{9.81 \cdot m} \\ T_{rear} = T_{sig} - T_{front} \end{cases}, \quad (9)$$

where T_{sig} signifies the input torque from the Sigmoid function at the current time step.

3. SIMULATION

In this section, the simulation results will be presented and discussed.

a) *Analysis of the vehicle dynamics model output in comparison to the gathered IoV data*

As mentioned earlier, one of the goals of this simulation is to check if the vehicle on the road can follow along with other vehicles presented as simple points, in terms of dynamics. That is why two simulations with different velocity ranges have been run and only the velocity comparison between the controlled vehicle and the one in front of it will be presented, as it is the only quantity of interest.

The first simulation entails vehicles distributed among two traffic lanes, as explained in-depth in the previous section, with velocities in the range between 14 and 28 m/s, to simulate traffic flow on a motorway (Figure 6), whereas velocity range in the second simulation is between 4 and 14 m/s, to simulate city traffic (Figure 7).

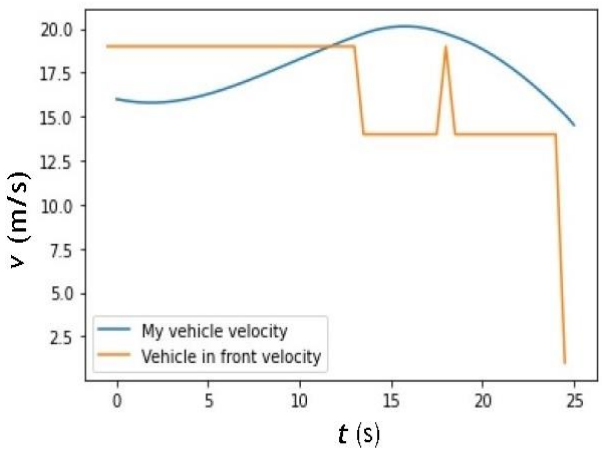

Fig. 6. Velocity comparison on a motorway

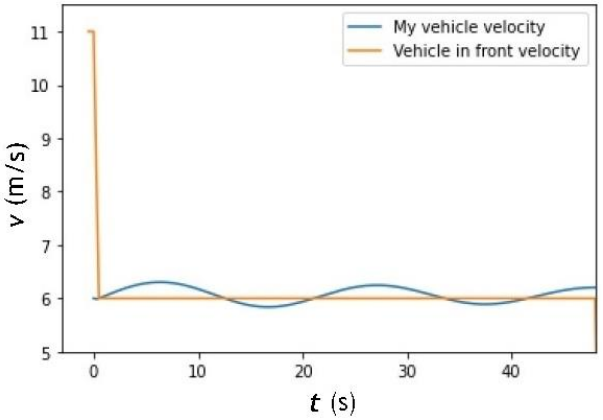

Fig. 7. Vehicle comparison on city road traffic

The same can be said about the second simulation, whose results are shown in Figure 7. Nonetheless, it is important to note that, due to the assumption that the vehicle has an input torque at any given time, as mentioned in the previous section, slight dilatations in the vehicle velocity can be noticed. One of the main reasons is the fact that the traffic situation in this instance is such that the vehicle in the front has a constant speed throughout the whole simulation, which is almost the same as the starting velocity of the controlled vehicle.

b) *Comparison between the vehicle dynamics model outputs and the behaviour of the same vehicle in the traffic model*

It is also of great significance to check whether is it really essential to incorporate the longitudinal dynamics model, given that it significantly burdens the simulation as a whole and is thus a far more expensive process. It can be determined whether the dynamics model could be omitted without disturbing the validity of the simulations, by simply comparing the results of both models (one considering the vehicle dynamics, and the other one only containing the traffic model, regardless of the dynamical capabilities of the vehicle) and checking if they are similar enough to suffice for the given purpose.

In order for this conclusion to be drawn definitely, the comparison needs to be done on a setup with more variable requirements, i.e. the velocity of the vehicle in the front should be changing frequently and thus, the response of the system can be evaluated more accurately. For this reason, a simulation where the velocity of the vehicle in the front is decreasing over time, has been chosen.

As can be noticed from the results presented on Figure 8, the controlled vehicle, due to the nature of

the traffic model, immediately adapts the velocity according to the one of the vehicle that should merge before it, and follows that velocity throughout the whole simulation. On the other hand, the model on Figure 9 presents a slightly different behaviour. Namely, the velocity of the vehicle in the front is also followed throughout the whole simulation, but that process does not happen immediately, due to the dynamical characteristics of the vehicle.

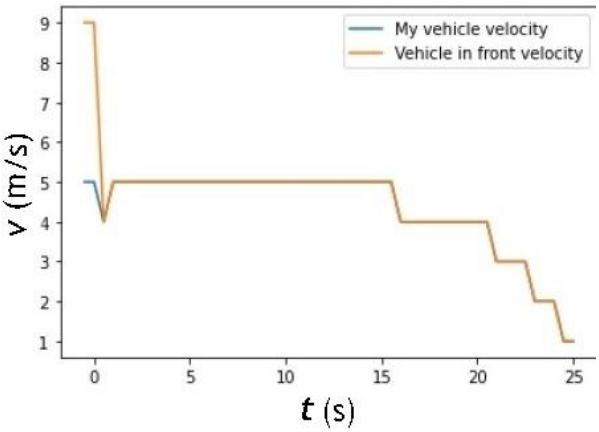

Fig. 8. Comparison between the velocities of the controlled vehicle and the one in the front, drawn from the model without the longitudinal dynamics logic

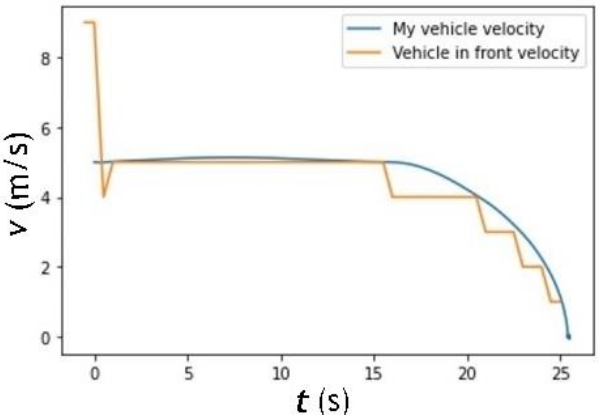

Fig. 9. Comparison between the velocities of the controlled vehicle and the one in the front, drawn from the model including the longitudinal dynamics logic

If both results are compared, such as in Figure 10, the conclusion can be drawn that, even though the first results are not as dynamically accurate and do not reflect the real behaviour of the vehicles as the second one, both curves still have clashing points throughout the whole simulation, and only differ in terms of the paths leading to those points. This leads to the conclusion that, if one is only interested in the behaviour of the vehicles in this particular traffic situation, and how they interact with each other if interconnected via the *IoV*, then the pure traffic model would suffice and does not need to be burdened with the unnecessary dynamics model. Nevertheless, if the exact behaviour of the vehicle is of significance, the results show that this way of modelling and running the simulations is necessary.

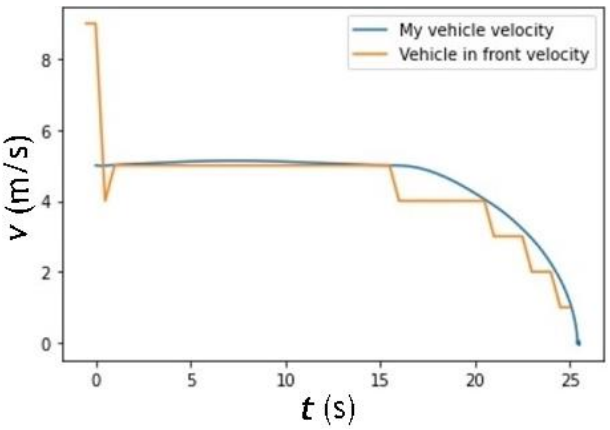

Fig. 10. Comparison between the velocities of the controlled vehicle, drawn from both models

4. SUMMARY AND CONCLUSIONS

The modelling and simulation of the control and behaviour of a vehicle, interconnected with the other vehicles on the road via the *IoV*, on a traffic section with an upcoming bottleneck merge, was shown in this paper. The modelling included both a mathematical description of a traffic flow behaviour, on the basis of the CA method, but with a new ruleset, as well as a longitudinal dynamics model for describing the behaviour of the controlled vehicle in particular.

There were mainly two points of focus, the first one being whether the vehicle is able to follow the changes introduced discretely by the traffic model, in terms of vehicle dynamics, and the second one whether this step is crucial or can it be omitted, without affecting the accuracy of the simulations.

Given the results in the last section, it can be concluded that, depending on the needs of the simulation, a pure traffic model based on the CA theory, but with a ruleset incorporating the positions and velocities of all vehicles in all given times, as well as for updating the lane cells appropriately, could be sufficient. Nevertheless, for vehicle control purposes, where many physical quantities are crucial and need to be knows at all times, the longitudinal dynamics model can be implemented, without introducing disturbances in the traffic model.

REFERENCES

[1] Haight, F. A.; Bisbee, E. F.; Wojcik, C. (1963): *Some mathematical aspects of the problem of merging*. Institute of Transportation and Traffic Engineering, University of California.

[2] Xiao, S.; Kong, L.; Liu, M. (2005): A cellular automaton model for a bridge traffic bottleneck. *Acta Mechanica Sinica*, **21** (3), pp. 305–309.

[3] Higashi, K.; Satsuma, J.; Tokihiro, T. (2021): Rule 184 fuzzy cellular automaton as a mathematical model for traffic flow. *Japan Journal of Industrial and Applied Mathematics*, **38** (2), pp. 579–609.

[4] Elefteriadou, L. (2014): *An Introduction to Traffic Flow Theory*. Springer Optimization and Its Applications (SOIA), Volume **84**, ISBN: 978-1-4614-8435-6.

[5] Zhao, H.; Zhao, X.; Feng, J. (2020): CA modeling and simulation of traffic flow in the bottleneck section of freeway under the condition of Internet of Vehicle. In: *CICTP 2020*, pp. 2290–2302.

[6] Jin, X.; Yin, G., Chen, N. (2019): Advanced estimation techniques for vehicle system dynamic state: A survey. *Sensors*, **19** (19), p. 4289.

[7] Dousti, M.; Caglar Baslamili, S.; Teoman Onder, E.; Solmaz, S. (2014): Design of a multiple-model switching controller for ABS braking dynamics, *Transactions of the Institute of Measurement and Control* **37** (5). DOI:10.1177/0142331214546522

[8] Nayak, S. (2020): *Fundamentals of Optimization Techniques with, Algorithms* (1st edition). Academic Press.

[9] Nishi, R.; Miki, H.; Tomoeda, A.; Yanagisawa, D.; Nishinari, K. (2010): Simulation and theoretical comparison between "Zipper" and "Non-Zipper" merging. In: Peper, F.; Umeo, H.; Matsui, N.; Isokawa, T. (eds): *Natural Computing. Proceedings in Information and Communications Technology*, Vol **2**. Springer, Tokyo. DOI.org/10.1007/978-4-431-53868-4_28

Mechanical Engineering – Scientific Journal, Vol. **41,** No. 1, pp. 59–70 (2023)
Number of article: 665 In print: ISSN 1857–5293
Received: May 8, 2023 On line: ISSN 1857–9191
Accepted: June 7, 2023 UDC: 656.13.052.54:629.3.027.4-526]:[004.942:519.872
https://doi.org/10.55302/MESJ23411665059ch

Original scientific paper

VEHICLE HANDLING ENHANCEMENT EMPLOYING FOUR-WHEEL INDEPENDENT STEERING SYSTEM USING SLIDING MODE CONTROL

Vasko Čangoski, Igor Ǵurkov, Darko Danev, Vase Jordanoska

Institute of Engineering Design, Mechanization and Motor Vehicles,
Faculty of Mechanical Engineering, University "Ss. Cyril and Methodius" in Skopje,
Ruđer Bošković 18, P.O. box 464, MK-1001 Skopje, Republic of North Macedonia
vasko.changoski@mf.edu.mk

A b s t r a c t: The demand for safer vehicle transportation and future automated vehicles will open the possibility for implementation of steer-by-wire (SbW) vehicle steering system. Application of this system would not be exclusive only for the front axle, but for the rear axle as well. Current four-wheel steering (4WS) systems are designed and applied using Ackermann steering geometry. Due to the vehicle designs requirements, an ideal Ackermann geometry is never achieved and steering kinematics may result in two instantaneous centres of rotation during vehicle cornering. To avoid this, a control strategy for a four-wheel independent steering (4WIS) is proposed where the four independently steered wheels attempt to achieve single instantaneous centre of rotation using sliding mode controller (SMC). As a reference model a 2DOF nonlinear vehicle bicycle model is used. The 4WS and 4WIS two-track vehicle models are created using MATLAB/Simulink and tested with manoeuvres defined by the standard ISO 7401.

Key words: 4WIS; sliding mode control; steer-by-wire; Ackermann geometry

ПОДОБРУВАЊЕ НА УПРАВЛИВОСТА КАЈ ВОЗИЛАТА СО СИСТЕМ ЗА НЕЗАВИСНО УПРАВУВАЊЕ НА ЧЕТИРИ ТРКАЛА СО ПРИМЕНА НА СТРАТЕГИЈАТА СО ЛИЗГАЧКА ПОВРШИНА

А п с т р а к т: Потребата од побезбеден транспорт и автоматизирани возила во иднина налага имплементација на системи за управување преку сигнали, без механички врски. Примената на овие системи не би била само кај предната, туку и кај задната оска. Сегашните системи за управување на четирите тркала се конструирани и применети користејќи Акерманова геометрија. Поради конструктивните барања кај возилата, идеалната Акерманова геометрија никогаш не се постигнува и кинематиката на управувачкиот механизам може да резултира со два истовремени пола на ротација при движење на возилото во кривина. За да се избегне тоа, се предлага стратегија на управување со лизгачка површина на систем за независно управување на тркалата, за сите четири тркала да бидат управувани независно со цел да се постигне единствен моментален пол на ротација. Како референтен модел е искористен нелинеарен модел-велосипед на возило со два степена на слобода. Моделите на возилата со управување на четирите тркала и со независно управување на секое тркало се креирани со помош на МАТЛАБ/Симулник и се тестирани со маневри дефинирани согласно со стандардот ISO 7401.

Клучни зборови: систем за независно управување на четири тркала; управување со лизгачка површина; управување преку сигнали; Акерманова геометрија

NOMENCLATURE

a	Distance between instantaneous centre and front axle
a_y	Lateral acceleration
B	Pacejka tire model stiffness factor
b	Distance between instantaneous centre and rear axle
b_f	Front track width
b_r	Rear track width

C Pacejka tire model shape factor
$C_{F\beta}$ Pacejka tire model stiffness
$C_{\alpha f}$ Front wheel cornering stiffness
$C_{\alpha r}$ Rear wheel cornering stiffness
D Pacejka tire model peak factor
d Distance between the instantaneous centre of rotation and vehicle longitudinal axis
d_i Distance between the instantaneous centre of rotation and vehicle inner wheels
d_o Distance between the instantaneous centre of rotation and vehicle outer wheels
E Pacejka tire model curvature factor
e_j Sliding mode error function (j = 1, 2, 3, 4)
F_n Vertical force
F_{nom} Nominal vertical force
F_{yf} Front tire lateral force
F_{yr} Rear tire lateral force
g Gravitational constant
h Distance between link and axle lateral axis
h_c Centre of mass height
I_z Material moment of inertia
i Inertia radius
k Maximum value of the signal that the SMC controller can produce (j = 1, 2, 3, 4)
K 4WS proportional control strategy constant
l Wheelbase
l_f Distance from centre of mass to front axle
l_r Distance from centre of mass to rear axle
$l_{j_{f,r}}$ Front and rear axle link length (j = 1, 2, 3, 4)
m Mass of the vehicle
R Turning radius
s_j Sliding mode surface function (j = 1, 2, 3, 4)
u_j SMC controller output (j = 1, 2, 3, 4)
u_{eq} SMC desired output signal of the controller in stationary conditions
V_x Longitudinal velocity
V_y Lateral velocity
α_f Front wheel side slip-angle
α_{fi} Front inner wheel side slip-angle
α_{fo} Front outer wheel side slip-angle
α_{fref} Reference front wheel side-slip angle
α_r Rear wheel side-slip angle
α_{ri} Rear inner wheel side-slip angle
α_{ro} Rear outer wheel side-slip angle
α_{rref} Reference rear wheel side-slip angle
β_c Side slip angle
δ_f Front steering steered angle
δ_{fi} Front inner steered wheels angle
δ_{fo} Front outer steered wheels angle
δ_{fref} Reference front steered wheel angle
δ_r Rear steered wheels angle
δ_{ri} Rear inner steered wheels angle
δ_{ro} Rear outer steered wheels angle
δ_{rref} Reference rear steered wheel angle
$\gamma_{j_{f,r}}$ Front and rear axle angle between links
λ Constant which multiplies the error in SMC controller
ϕ Thickness of the boundary layer of the sliding surface in SMC controller
φ Road surface friction coefficient
ω_z Vehicle yaw rate

1. INTRODUCTION

Increased demands for improved overall vehicle performance along with needs for safer and more sustainable transportation lead to development of new advanced vehicle systems.

Regarding vehicle steering system, Ackermann steering geometry is still the most used steering principle in modern vehicles. Beside many advantages, throughout the whole cornering process, the ideal Ackermann geometry with single centre of rotation during turning is rarely achieved. Nevertheless, this principle with mechanical linkage is still used in classic and automated steering systems, such as the Active Front Steering (AFS) and the Active Rear Steering (ARS) in 4WS or AWS vehicles.

Authors in [1] present improved vehicle dynamics and handling by implementing fuzzy-logic controller in coordinated control involving AFS and vehicle yaw control system. Feng *et al.* present coordinated chassis control [2] where the AFS system is integrated with traction control and differen-tial braking. Doumiati *et al.* suggest a phase plane approach [3] that shows improvement in vehicle handling. As AFS control strategy, model predictive control (MPC) is used by Falcone *et al.* [4]. Ding *et al.* suggest sliding mode control (SMC) [5], while authors in [6] combine SMC and extreme learning machine. Another machine learning method is proposed by Huang *et al.* [7] where a neural network controller is implemented.

Authors in [8] present comparison between integrated AFS and vehicle stability control (VSC) and integrated ARS and VSC, controlled by SMC using co-simulation. Hiraoka *et al.* [9] and authors in [8] present the idea of using reference 4WS bicycle model to improve 4WS vehicle performance. In [10] Ferrara presents the application of SMC in broader spectrum of vehicle systems.

Most of the previously mentioned research papers point out the advantages of using AFS and ARS systems which significantly improve the vehicle dynamics. These systems, together with the current type approval legislation requires a mechanical

linkage between the steering wheel and the steered wheels. In order to avoid the disadvantages of the mechanical linkage, many researchers are focused on developing a Steer-by-Wire (SbW) systems. The Steer-by-Wire system would free up more space, lower the weight of the vehicle and most importantly could potentially lead to improved vehicle dynamics and could provide steering correction in case of unwanted driver's command and need to stabilize the vehicle.

In [11] Chen *et al.* propose four-wheel independent steering (4WIS) control strategy based on wheels minimum load. Authors in [12] and [13] present improved vehicle stability of a prototype 4WIS and four-wheel independent driving (4WID) vehicle using several control algorithms. Improved vehicle manoeuvrability is also presented in [14] and [15]. Liu *et al.* present application of SMC in 4WIS system in [16]. Using yaw moment control method, Yim [17] makes a comparison between AFS, front wheel independent steering (FWIS), 4WS and 4WIS. The paper had shown that 4WIS offers the best vehicle performance. Nah and Yim present a combined method between VSC, 4WIS and 4WID [18].

Development of a 4WIS represents state-of-the-art in terms of vehicle steering and handling among researchers and engineers. The application of this system in vehicles would decrease the gap between theoretical and real steering systems performance, thus significantly improving vehicle handling and stability. Unfortunately, the biggest current problem represents the legislation limitations and the lack of redundant mechanism(s) in case of system failure.

To analyze the characteristics and the performance of the 4WIS system, in this paper a nonlinear 4WIS vehicle model is compared with a nonlinear 4WS that uses proportional rear wheel steering control algorithm. As [8] suggests, a reference nonlinear all wheel steering (AWS) bicycle model is created where the rear wheels are steered using linear control strategy to achieve vehicle side-slip angle value of zero in steady and transient state.

This study aims to analyze the potential of the SMC controllers on vehicle stability when employed to generate correction of the desired wheel steer angles in order to achieve single instantaneous centre of rotation. The correction is based on the difference between the wheels steer angles and the wheels side-slip angles because that difference defines the vehicle traveling direction and the cornering radius of the vehicle.

Therefore, by focusing on overcoming the imperfections of mechanical steering mechanism and implementation of SMC controllers in independent all-wheel steering, a control strategy concept is presented which allows more precise determination of the instantaneous centre of rotation, increased vehicle stability, smaller off-tracking and tire deformation.

2. VEHICLE MODELS

The presented concept of 4WIS is based on the aim to achieve single instantaneous centre of rotation, while maintaining the desired wheels' side-slip angles. It would increase vehicle stability, while decreasing tire wearing and loads. As a reference model for the 4WIS, a 2DOF nonlinear bicycle model is used. An additional 4WS model was created, in which both axles have Ackermann steering geometry derived from real vehicle with mechanical linkage. The geometry was chosen because it is still most widely used in passenger vehicles. The effects of implementing four-wheel independent steering are analyzed and presented by comparison between the 4WS and 4WIS vehicle model using standardized test procedures accordingly to the standard ISO 7401.

Figure 1 shows a schematic overview of the proposed concept. The driver commands different front wheel steering angles to both vehicles in order to complete the standardized manoeuvre according to ISO 7401. This is presented in greater details in the results section.

While the front wheel steer angles of the 4WS vehicle depend solely on the driver's command, the final values of the 4WIS front wheel steer angles depend on the driver's command and the correction of the SMC controllers.

On the other hand, the 4WS rear wheels are controlled using a proportional control strategy, while the 4WIS uses control strategy which attempts to achieve vehicle side-slip angle value of zero during steady and transient state. In this case that would not be literally possible because nonlinear vehicle model is being used, while the particular strategy is derived from a linear bicycle model. However, it significantly lowers the values of the vehicle side-slip angle. Beside the input from control strategy, an additional correction is being applied by the SMC controllers. The strategies used and the vehicle models are described in detail in the following subsections.

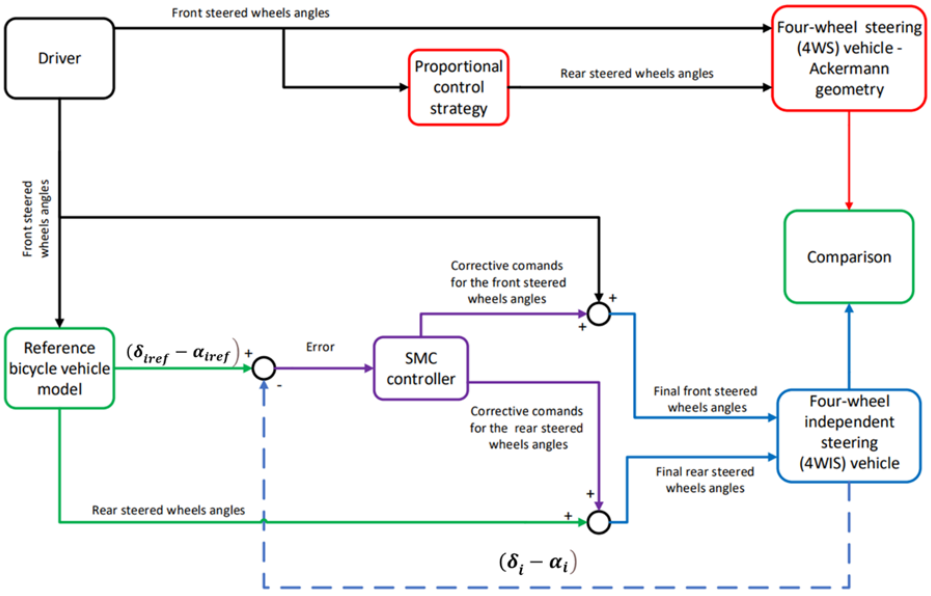

Fig. 1. Schematic overview of the presented concept

a) *Bicycle reference model*

As a reference model, a nonlinear all wheel steering (AWS) bicycle model (Figure 2) is used. The model has 2DOF, lateral velocity and yaw rate, while the longitudinal velocity is assumed to be constant. The tires are modelled using the Magic Tire Formula of Pacejka described by equations (1) and (2). Furthermore, the parameters of the reference model, 4WS and 4WIS vehicles are chosen to represent *C* vehicle segment as one of the most common vehicles. The vehicle parameters and the Pacejka model coefficients are presented in Table 1.

$$F_{yf} = D\sin\{C\arctan[B\alpha_f - E(B\alpha_f - \arctan(B\alpha_f))]\} \quad (1)$$

$$F_{yr} = D\sin\{C\arctan[B\alpha_r - E(B\alpha_r - \arctan(B\alpha_r))]\} \quad (2)$$

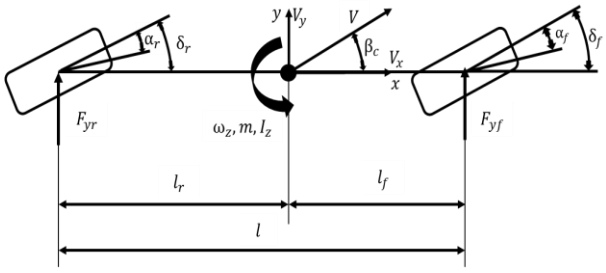

Fig. 2. 4WS bicycle vehicle model

Instead of 2WS bicycle model as a reference model, a 4WS was chosen since 2WS model has slower dynamic response and would force the 4WIS vehicle to mimic the performance of 2WS vehicle. These conclusions are presented in [8]. As, a control strategy for rear wheels, a linear control strategy is chosen which requires vehicle side-slip angle value of zero during the steady and transient state. Although the real value would never be zero, because a linear strategy is applied on a nonlinear model, nonetheless the performance of the reference model and the desired values are more favourable than some other strategies. The equations of the linear bicycle model, from which the strategy is derived, are presented in equations (3) and (4), while the control strategy itself is described by equation (5).

T a b l e 1

Vehicle bicycle model parameters

Mass (m):	1400 kg
Wheelbase (*l*):	2600 mm
Distance from centre of mass to front axle (l_f):	1200 mm
Inertia radius (iz):	1150 mm
Front wheel cornering stiffness $(C_{\alpha f})$:	50000 N/rad
Rear wheel cornering stiffness $(C_{\alpha r})$:	50000 N/rad
B	$C_{F\beta}/(CD)$
$C_{F\beta}$	$K_a \sin\left\{(2\arctan\left(\frac{F_n}{F_{nom}}\right)\right\}$
C	1.2
D	φF_n
E	0

$$\dot{V}_y = \left(\frac{-C_{\alpha f}-C_{\alpha r}}{mV_x}\right)V_y + \left(\frac{C_{\alpha r}l_r - C_{\alpha f}l_f}{mV_x} - V_x\right)\omega_z + \frac{C_{\alpha f}}{m}\delta_f + \frac{C_{\alpha r}}{m}\delta_r \quad (3)$$

$$\dot{\omega}_z = \left(\frac{C_{\alpha r}l_r - C_{\alpha f}l_f}{I_z V_x}\right)V_y + \left(\frac{-C_{\alpha f}{l_f}^2 - C_{\alpha r}{l_r}^2}{I_z V_x}\right)\omega_z + \frac{C_{\alpha f}l_f}{I_z}\delta_f - \frac{C_{\alpha r}l_r}{I_z}\delta_r \quad (4)$$

$$\delta_r = -\frac{C_{\alpha f}}{C_{\alpha r}}\delta_f + \frac{mV_x^2 + C_{\alpha f}l_f - C_{\alpha r}l_r}{C_{\alpha r}V_x}\omega_z \quad (5)$$

b) *Four-wheel steering (4WS) model using Ackermann geometry with proportional control strategy*

Figure 3 presents the Ackermann geometry of one axle. The 4WS vehicle is modelled to have identical front and rear axle, with the same geometry, the only difference being the maximum steer angle of the wheels of the front and rear axle.

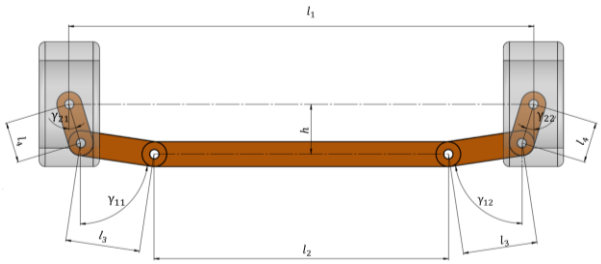

Fig. 3. 4WS vehicle's front and rear axle

For this vehicle, a proportional control algorithm is chosen and presented in equation (6), as one of simplest control strategies, combined with input delay of 0.1s in the rear wheels reaction. This delay is implemented to gain faster response from the vehicle.

$$\delta_r = K\delta_f \quad (6)$$

where $K = 0.2$. The relation between the inner and outer wheel is presented by equations (7) and (8). While it must be pointed out that the parameters of the vehicle are identical with the ones of the reference vehicle, except for the tire cornering stiffness which is assumed to be half the size of the cornering stiffness of the bicycle model. The Ackermann's geometry parameters are presented in Table 2. The values for the front and rear axle are identical.

$$\delta_{fo} = \gamma_{22f} - \arcsin\left(\frac{l_{1f} - l_{2f} - l_{3f}\sin(\gamma_{11f}) - l_{3f}\sin(\gamma_{12f}) + l_{4f}\sin(\gamma_{21f} + \delta_{fi})}{l_{4f}}\right) \quad (7)$$

$$\delta_{ro} = \gamma_{22r} - \arcsin\left(\frac{l_{1r} - l_{2r} - l_{3r}\sin(\gamma_{11r}) - l_{3r}\sin(\gamma_{12r}) + l_{4r}\sin(\gamma_{21r} + \delta_{ri})}{l_{4r}}\right) \quad (8)$$

T a b l e 2

Ackermann geometry – parameters

l_1:	1500 mm
l_2:	950 mm
l_3:	240 mm
l_4:	130 mm
h:	160 mm
$\gamma_{11}, \gamma_{12},$ (in straight ahead wheel position):	81.48°
$\gamma_{21}, \gamma_{22},$ (in straight ahead wheel position):	16.84°

In Figure 4 the turning process of the 4 WS vehicle is presented during higher velocity motion. Assuming only the steering angles of the wheels, orthogonal lines are drawn from the front wheels that intersect in point O_f and in the same way the orthogonal lines relative to the rear wheels intersect in Or. The values R_f and R_r represent the distances between the corresponding centre points and the vehicle's centre of mass. The value D_R represents the distance between those points. It must be pointed out when wheels side-slip angles are considered, the vehicle has single instantaneous centre of rotation. It's location is found in the distance between the points O_f and O_r. Smaller distance D_R means more precise positioning of instantaneous centre of rotation, while the vehicle's off- tracking, tire wear and tendency to stability loss would all be lower.

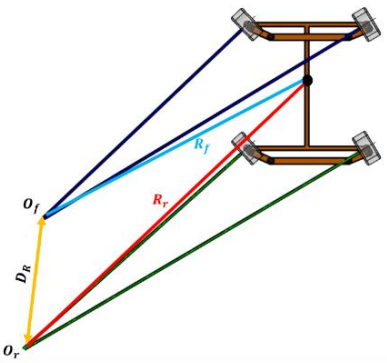

Fig. 4. Existence of two instantaneous centres of rotation using mechanical linkage of the front and the rear wheels

c) *Four-wheel independent steering (4WIS) model*

Last of the presented vehicle models is the 4WIS model (Figure 5). The vehicle has 4 wheels which can be steered independently. The input signal for the front wheels is the front wheel steering angle of the reference vehicle bicycle model. Afterwards, that value is modified using equations (9) and (10), in order to achieve the desired single instantaneous centre of rotation. Equation (9a) is derived from Figure 5 using triangle O12, while using triangle O34 equation (9b) is derived with assumption that the wheels' side-slip angles are negligible. By combining (9a) and (9b), the value of the inner front wheel steering angle is derived in eq. (10a). With the same approach, equation (10b) and rear wheels steering angles (11a and 11b) are derived.

$$\tan(\delta_{fef}) = a/d \tag{9a}$$

$$\tan(\delta_{fi}) = a/d_i \tag{9b}$$

$$\delta_{fi} = arctan\left(\frac{d}{d_i}\tan(\delta_{fref})\right); \tag{10a}$$

$$\delta_{fo} = arctan\left(\frac{d}{d_o}\tan(\delta_{fref})\right) \tag{10b}$$

$$\delta_{ri} = arctan\left(\frac{d}{d_i}\tan(\delta_{rref})\right); \tag{11a}$$

$$\delta_{ro} = arctan\left(\frac{d}{d_o}\tan(\delta_{rref})\right). \tag{11b}$$

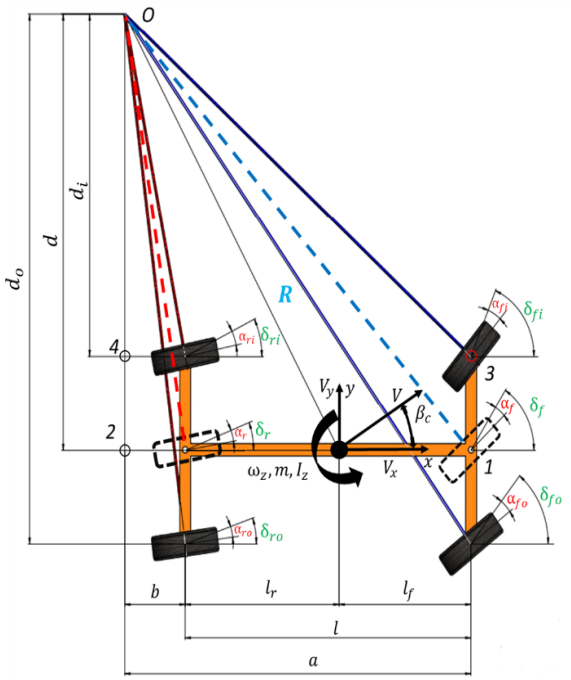

Fig. 5. 4WIS vehicle model

The variable d is obtained from the driver's command of the vehicle bicycle model and together with the values for d_i and d_o are calculated during the simulation in each integration step.

The wheel side-slip angles are taken into consideration in the SMC controllers which correct the driver's command. There, the real values of the parameters d, d_i and d_o and the turning radius are also calculated during the simulation in each integration step, but they are obtained from the 4WIS model. Those relations are presented in equations (12) and (13) and are used for the calculation of the value D_R.

$$\tan(\delta_{fj} - \alpha_{fj}) = \frac{a}{d_{4WIS}};\ \tan(\delta_{rj} - \alpha_{rj}) = \frac{b}{d_{4WIS}} \tag{12}$$

$$R = \sqrt{x^2 + (l_r + b)^2} \tag{13}$$

At the end, the wheel steering angles are corrected based on the error between the reference value from the bicycle model and the actual value of the 4WIS vehicle model. The values that are compared represent a difference between the steering angles of the wheels and the wheels' side-slip angles. Those values were chosen for the sliding mode control because in practice the traveling direction of the vehicle is determined by the difference between the wheel steering angles and the wheels side-slip angles, due to the lateral deformation of the tires.

The front and rear wheels side-slip angles of the four-wheel vehicle model are presented in equations (14) and (15). Also, these equations are used to calculate the desired reference values of the bicycle model.

$$\alpha_{fi} = \delta_{fi} - \frac{V_y - l_f\omega_z}{V_x - 0.5b_f\omega_z};\ \alpha_{fo} = \delta_{fo} - \frac{V_y - l_f\omega_z}{V_x + 0.5b_f\omega_z} \tag{14}$$

$$\alpha_{ri} = \delta_{ri} - \frac{V_y - l_r\omega_z}{V_x - 0.5b_r\omega_z};\ \alpha_{ro} = \delta_{ro} - \frac{V_y - l_r\omega_z}{V_x + 0.5b_r\omega_z} \tag{15}$$

The control strategy of SMC controllers is presented in the next section, while the comparison between the 4WS and 4WIS is presented in the results section.

It is important to mention that in both two-track vehicle models, the vertical load distribution of the wheels is taken into account. This distribution is calculated using equations (16) and (17) and it is used in Pacejka tire models.

$$F_{zfo} = \frac{0.5mgl_r}{l} + \frac{0.5ma_yh_c}{b_f} \tag{16a}$$

$$F_{zfi} = \frac{0.5mgl_r}{l} - \frac{0.5ma_yh_c}{b_f} \tag{16b}$$

$$F_{zro} = \frac{0.5mgl_f}{l} + \frac{0.5ma_y h_c}{b_r} \quad (17a)$$

$$F_{zri} = \frac{0.5mgl_f}{l} + \frac{0.5ma_y h_c}{b_r} \quad (17b)$$

3. DESIGN OF THE SLIDING MODE CONTROLLERS IN THE 4WIS MODEL

For the sliding mode control the sliding surface is defined by equation (18), while as mentioned above, the error is defined as subtraction between the actual and the reference value of the difference between the wheels' steering angle and the wheel side-slip angles (19). The control output, which is responsible for the final steering angle of the wheel is not solely dependent on the output command of the SMC (20), but also depends on the commands given by the driver. By combining equations (10), (11) and (20) the final values for the wheels' steering angles are calculated using equations 21 (21a and 21b) and 22 (22a and 22b).

$$s_j = \dot{e} + \lambda e \quad (18)$$

$$e_j = (\delta_{jref} - \alpha_{jref}) - (\delta_j - \alpha_j) \quad (19)$$

$$u_j = k\tanh\left(\frac{e_j}{\phi}\right) + u_{eq} \quad (20)$$

where $k = 1$, while $\phi = 10$, $\lambda = 50$ and $u_{eq} = 0$.

The values are chosen on basis of several conducted simulations.

$$\delta_{fi} = arctan\left(\frac{d}{d_i}\tan(\delta_{fref})\right) + k\tanh\left(\frac{e_{fi}}{\phi}\right); \quad (21a)$$

$$\delta_{fo} = arctan\left(\frac{d}{d_o}\tan(\delta_{fref})\right) + k\tanh\left(\frac{e_{fo}}{\phi}\right). \quad (21b)$$

$$\delta_{ri} = arctan\left(\frac{d}{d_i}\tan(\delta_{rref})\right) + k\tanh\left(\frac{e_{ri}}{\phi}\right); \quad (22a)$$

$$\delta_{ri} = arctan\left(\frac{d}{d_o}\tan(\delta_{rref})\right) + k\tanh\left(\frac{e_{ro}}{\phi}\right). \quad (22b)$$

4. SIMULATED MANOEUVRES AND RESULT ANALYSIS

Vehicles were tested using two manoeuvres described in the Standard ISO 7401. For the cornering manoeuvre, both vehicles are steered to achieve 4 m/s^2 of lateral acceleration in steady state, as requested by the standard, while traveling with constant longitudinal speed of 80 km/h. As recommended by the standard, the vehicles are tested for the step-steer and the single lane change manoeuvre. The road surface has friction coefficient of φ = 0.6.

The following comparative results of the 4WS and 4WIS vehicles are presented: steering angles, wheels' side-slip angles, lateral acceleration, yaw rate, vehicle side-slip angles, trajectory and radius error.

Step-steer

In the first manoeuvre, the different values of the steering angles of the 4WS and 4WIS can be observed in Figures 6 and 7, which also results in different wheels' side-slip angles presented in Figures 8 and 9. Lower values of wheel side-slip angles for the 4WIS vehicle indicate higher capability of the vehicle to withstand lateral forces.

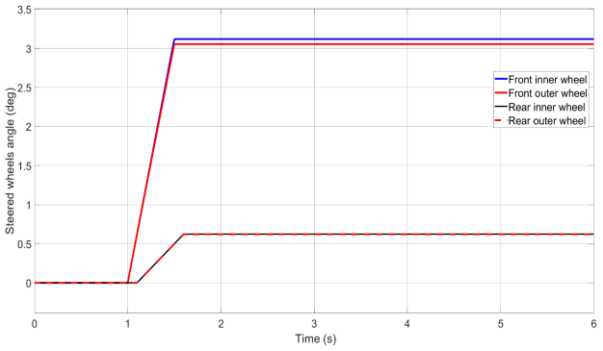

Fig. 6. Front and rear wheels' steering angles – 4WS vehicle

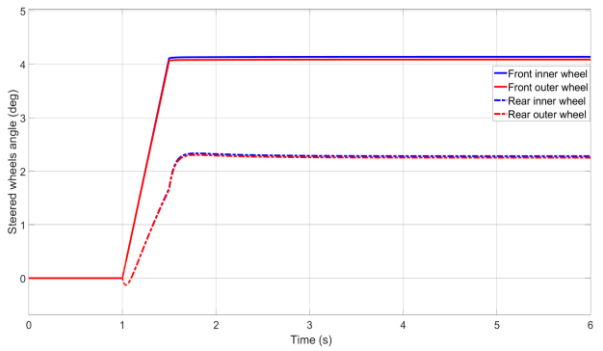

Fig. 7. Front and rear wheels' steering angles – 4WIS vehicle

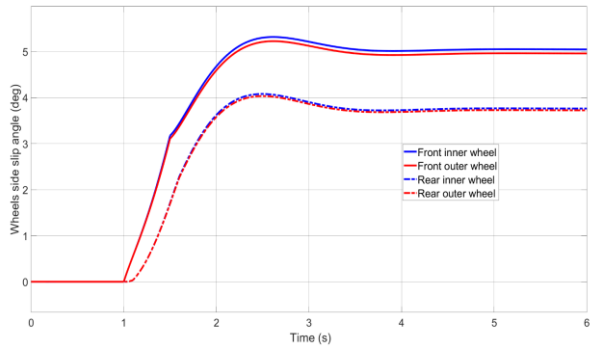

Fig. 8. Wheels' side slip angle – 4WS vehicle

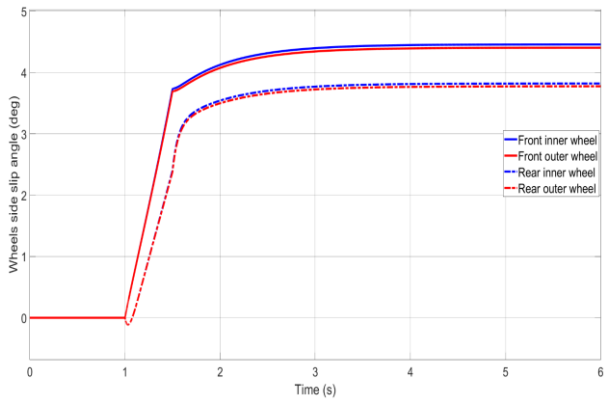

Fig. 9. Wheels' side slip angle – 4WIS vehicle

In the Figure 10, the value of the lateral acceleration is 4 m/s^2 in steady state, thus fulfilling the Standard ISO 7401. Also, it can be observed that the 4WIS has faster response than the 4WS vehicle. The same conclusion can be derived from Figure 11 with regard to the yaw rate, where the 4WIS reaches steady state after 1.5 seconds of the manoeuvre, just after driver's command reaches maximum value, while the 4WS settles after the 4th second.

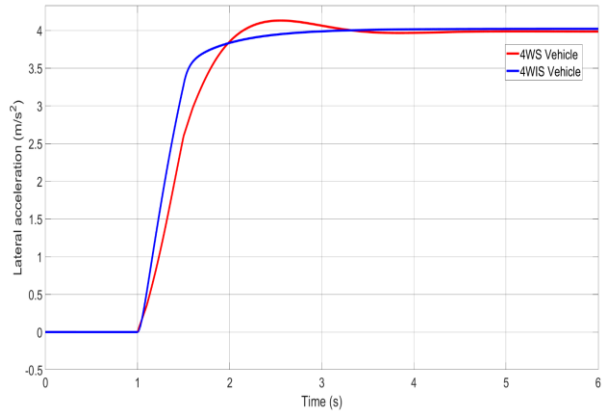

Fig. 10. Lateral acceleration

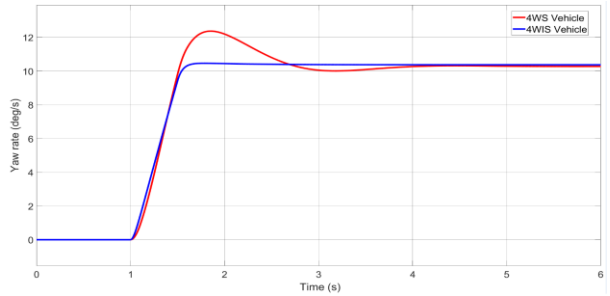

Fig. 11. Yaw rate

The biggest advantage of the proposed strategy can be noticed in the values for the vehicles side-slip angle (Figure 12), where the 4WIS achieves significantly smaller values. Therefore, it allows better driver perception and handling and increased safety. Because of the identical values of the lateral acceleration and yaw rate, the trajectory is almost identical (Figure 13). In Figure 14 the D_R parameter value is shown, where it can be observed that more than 30 mm in the transient period of the 4WS, while 4WIS possess value of approximately 3 mm. These small values are result of the smaller values of the steering angles of the wheels.

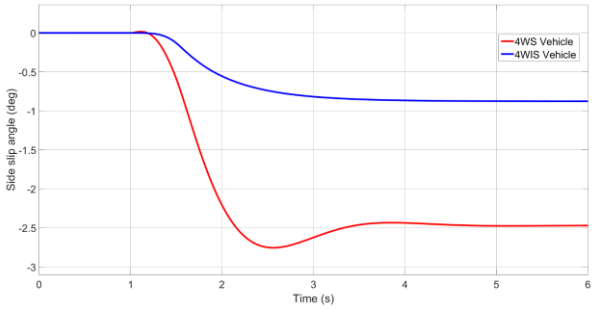

Fig. 12. Vehicle side slip angle

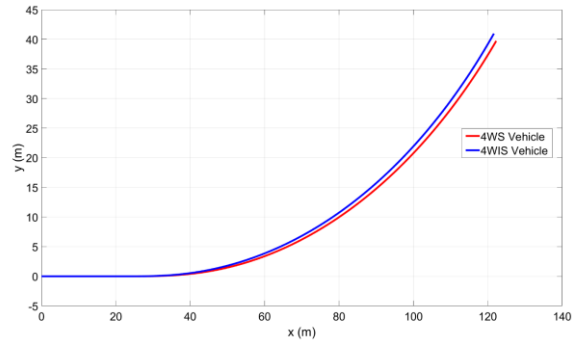

Fig. 13. Trajectory

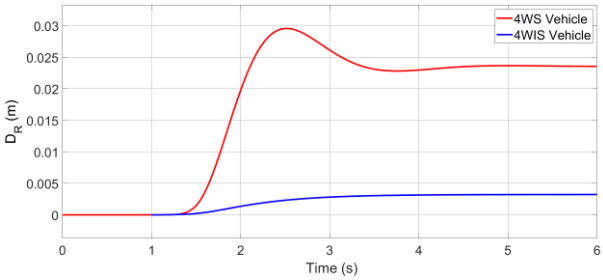

Fig. 14. D_R parameter

Single lane change

In this manoeuvre, vehicles are traveling with constant longitudinal velocity of 80 km/h and the steering angles of the wheels are assigned values so that (Figures 15 and 16) the vehicles achieve 4 m/s^2 of lateral acceleration in the first peak. Because of

the rear wheels control strategy of the 4WIS, they are turned in opposite direction at the beginning of the manoeuvre, therefore resulting in faster vehicle response (Figure 16).

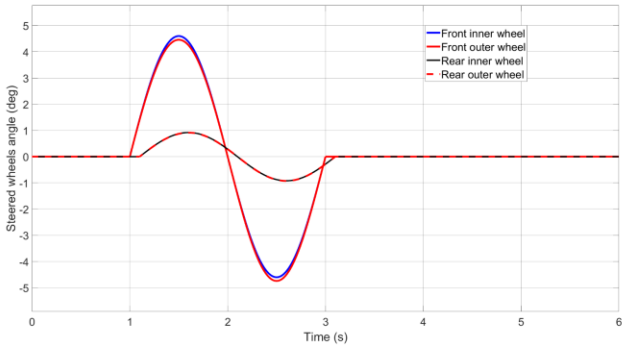

Fig. 15. Front and rear wheels steering angles – 4WS vehicle

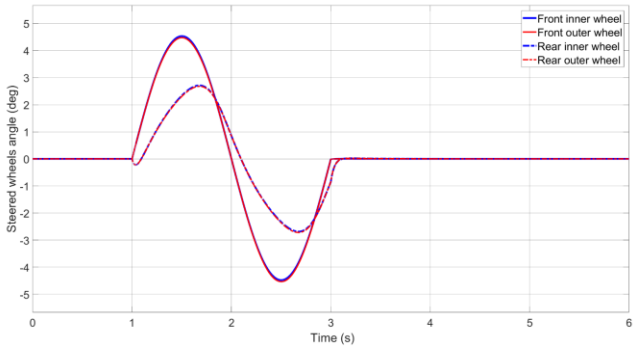

Fig. 16. Front and rear wheels steering angles - 4WIS vehicle

By observing the wheel side-slip angles (Figures 17 and 18), it can be concluded that at certain period of the manoeuvre, just before the 2nd second, the absolute values of the rear wheels side slip angles are larger than the front ones. That trend changes during the manoeuvre and the difference and the peaks are higher for the 4WS vehicle, but nevertheless, it results in a short transient period where both vehicles are showing oversteer characteristics. This period is much shorter for the 4WIS vehicle.

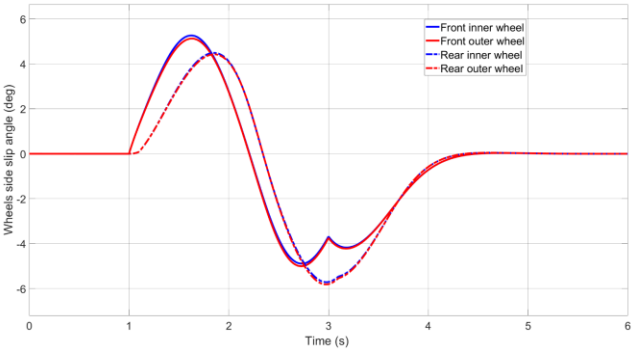

Fig. 17. Wheels side slip angle – 4WS vehicle

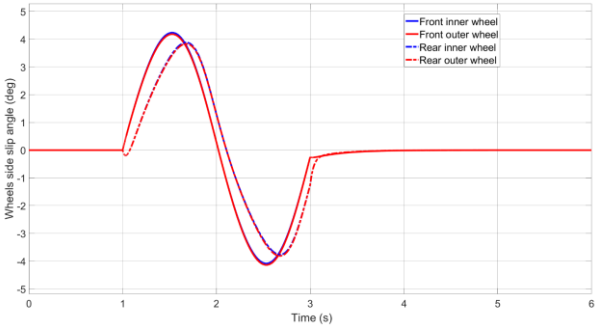

Fig. 18. Wheels side slip angle – 4WIS vehicle

This behaviour and the larger differences between the values of the rear and front wheel side-slip angles, results in requirement for longer time for the 4WS to reach steady state, around 5th second (Figure 19), while the maximum values of yaw rate (Figure 20) and side-slip angle (Figure 21) are larger, resulting in increased possibility for vehicle destabilization and deteriorated driver's perception of the vehicle's travelling direction.

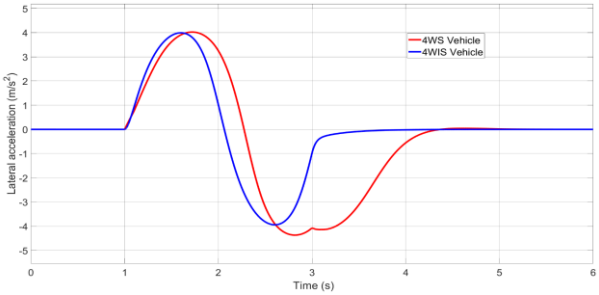

Fig. 19. Lateral acceleration

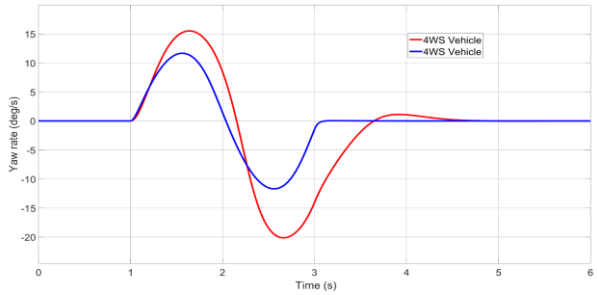

Fig. 20. Yaw rate

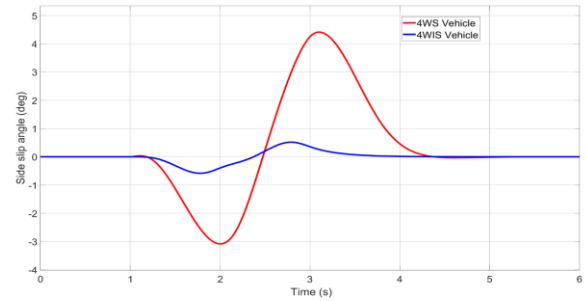

Fig. 21. Vehicle side slip angle

All of this can be confirmed with Figure 22, where the 4WS vehicle needs larger space to complete the manoeuvre (almost 4 meters) and the vehicle is moving in a direction much different than the initial lane. It must be pointed out that in real case scenario the driver would try to correct the vehicle's trajectory, thus avoiding traveling in the wrong lane and direction. In this situation the value of the D_R parameter (Figure 23) is almost 80 mm for the 4WS vehicle, while the 4WIS achieves value near to zero, having virtually single centre of rotation.

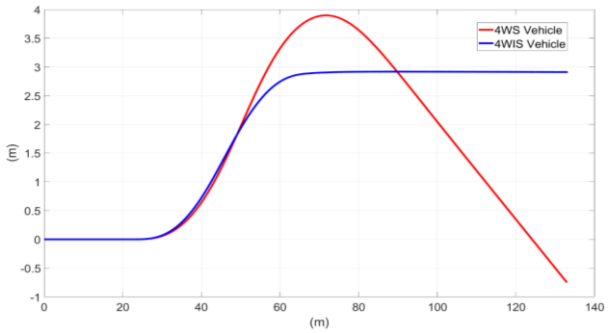

Fig. 22. Trajectory

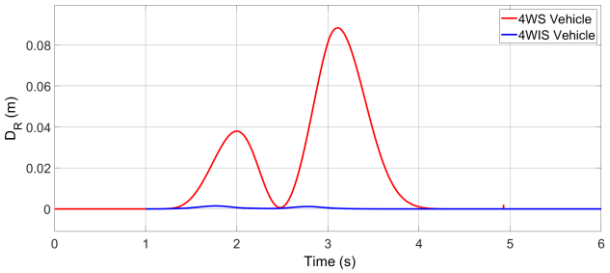

Fig. 23. D_R parameter

Single lane change – slippery road conditions

The previous results have shown better vehicle dynamic response and stability of the 4WIS vehicle over the 4WS. To further test the capabilities of the concept, tests were simulated in a case scenario of a single lane change, but the road conditions are deteriorated. Now the vehicles travel on a snow road surface with friction coefficient of $\varphi = 0.3$.

Results show that both vehicles would lose their stability in a step-steer manoeuvre because the driver's command remains constant throughout the manoeuvre, while during the single lane change the 4WIS controllers manage to prevent the vehicle from swirling out. Because of this, only the results of the single lane change manoeuvre are presented.

Figure 24 presents the steering angles of the wheels of the 4WIS vehicle, while the steering angles of the wheels for the 4WS are identical as those in Figure 15. While the front steered wheels angles are turned in similar angles like in the previous simulation, the rear steered wheels angles turn with higher intensity and are commanded with phase delay. The biggest contribution for this is SMC controllers attempting to prevent vehicle destabilization. The first indications of that and 4WS vehicle destabilization can be observed in Figure 25 and 26, where the wheels side-slip angles values of the 4WS are larger with tendency to further increase their value.

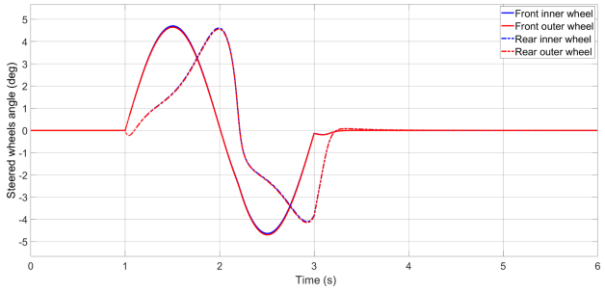

Fig. 24. Front and rear steered wheels angle – 4WIS vehicle

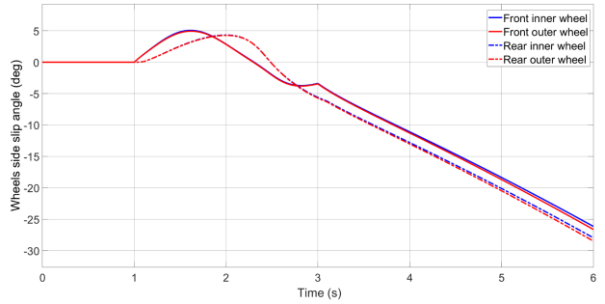

Fig. 25. Wheels side slip angle – 4WS vehicle

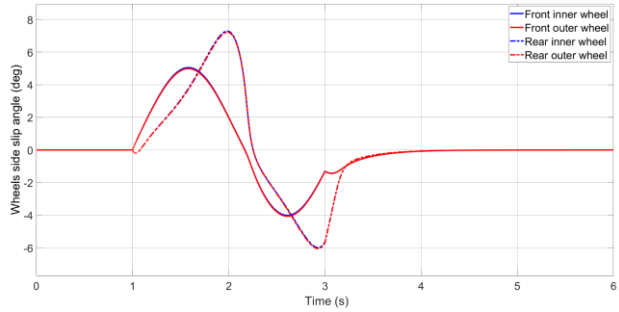

Fig. 26. Wheels side slip angle – 4WIS vehicle

The same conclusion can be drawn from Figures 27, 28 and 29 where the 4WS vehicle clearly fails to complete the manoeuvre, because the 4WS outputs don't follow sinusoidal form and don't reach steady-state value of 0. This can be only confirmed in Figure 30, where the trajectory of the 4WS shows that the vehicle starts to swerve, reaching total road width of around 10 m which is higher than

most of the standard highway lanes. Due to the larger values of the wheels side slip angles, the value D_R of the 4WS is more than fifty times higher than in the previous manoeuvre (Figure 31), resulting in larger vehicle off-tracking and tire wear and loads. On the other side the 4WIS maintains almost ideally single centre of rotation even though the vehicle is struggling to remain stable.

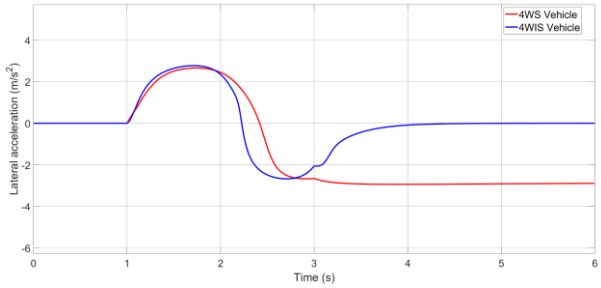

Fig. 27. Lateral acceleration

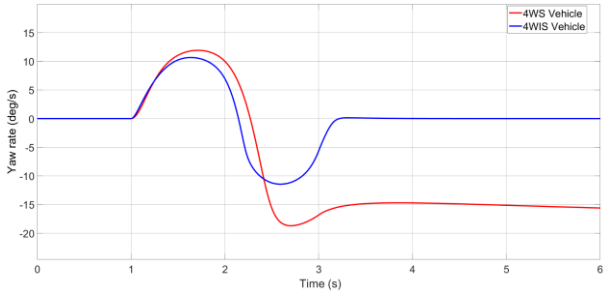

Fig. 28. Yaw rate

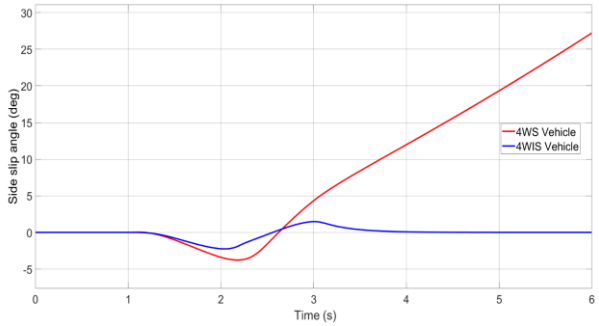

Fig. 29. Vehicle side slip angle

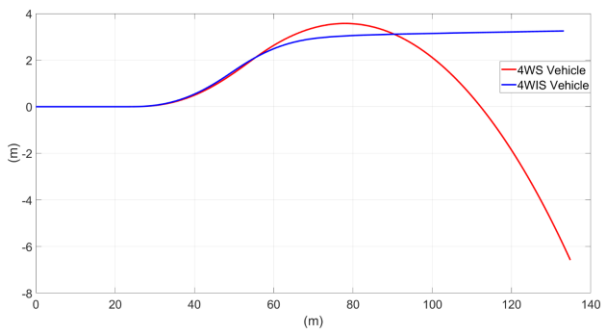

Fig. 30. Trajectory

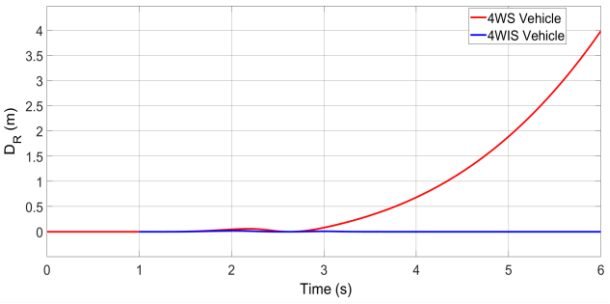

Fig. 31. D_R parameter

5. DISCUSSION AND CONCLUSIONS

The presented concept of a 4WIS vehicle had shown great potential over the 4WS vehicle. Faster vehicle response, shorter settling time and smaller vehicle side-slip angle which allows improved driver's evaluation and estimation of the vehicle traveling direction, are few of the improvements that this proposed control algorithm achieves. By conducting the same manoeuvre on a deteriorated road condition, the 4WIS manages to stabilize the vehicle while maintaining the value of the D_R almost to zero.

Implementation of SMC controllers in the 4WIS vehicle, that correct the error difference between the steering angles of the wheels and wheels side-slip angles is successfully used in the steer-by-wire steering concept that offers increased vehicle stability as well as improved handling and safety. Combined with the single instantaneous centre of rotation that this vehicle has, it results in decreased tire loads, wear and off-tracking.

With regard to the approximations made for this vehicle models, for the future work an improved vehicle model with more DOF or virtual vehicle model is planned, upgraded with additional active vehicle control systems.

REFERENCES

[1] Jordanoska, V.; Danev.; D.; Changoski, V. (2021): Evaluating coordinated cooperative control of three active car systems using fuzzy-logic, *IOP Conference Series: Materials Science and Engineering*, Vol. **1190** (1).

[2] Feng, J.; Chen, S.; Qi, Z. (2020): Coordinated chassis control of 4WD vehicles utilizing differential braking, traction distribution and active front steering, *IEEE Access***,** Vol. **8.** DOI: 10.1109/ACCESS.2020.2990729.

[3] Doumiati, M.; Sename, O.; Dugard L.; Martinez-Molina, J.; Gaspar, P.; Szabo, Z. (2023): Integrated vehicle dynamics control via coordination of active front steering and rear braking, *European Journal of Control*, Vol. **19**, Issue 2, pp. 121–143.

[4] Falcone, P.; Tseng, E. H.; Borrelli, F.; Asgari, J.; Hrovat, D. (2008): MPC-based yaw and lateral stabilisation via active front steering and braking, *Vehicle System Dynamics*, Vol. **46**, Issue sup 1, pp. 611–628.

[5] Ding, S.; Liu, L.; Park, Ju. (2019): A novel adaptive nonsingular terminal sliding mode controller design and its application to active front steering system, *International Journal of Robust and Nonlinear Control*, Vol. **29**, Issue 12.

[6] Zhang, J.; Wang, H.; Ma, M.; Yu, M.; Yazdani, A.; Chen, L. (2020): Active front steering-based electronic stability control for steer-by-wire vehicles via terminal sliding mode and extreme learning machine, *IEEE Transactions on Vehicular Technology*, Vol. **69**, Issue 12, pp. 14713–14726.

[7] Huang, W.; Wong, P. K.; Wong, K. I.; Vong, C. M.; Zhao, J. (2019): Adaptive neural control of vehicle yaw stability with active front steering using an improved random projection neural network, *Vehicle System Dynamics*, Vol. **59**, Issue 3.

[8] Changoski, V.; Gjurkov, I.; Jordanoska, V. (2022): Improving vehicle dynamics employing individual and coordinated sliding mode control in vehicle stability, active front wheel steering and active rear wheel steering systems in co-simulation environment, *IOP Conference Series: Materials Science and Engineering*, vol. **1271**.

[9] Hiraoka, T.; Nishihara, O.; Kumamoto, H. (2004): Model following sliding mode control for active four-wheel steering vehicle, *Review of Automotive Engineering*, Vol. **25**, pp. 305–313.

[10] Ferrara, A. (2017): *Sliding Mode Control of Vehicle Dynamics*, The Institution of Engineering and Technology, London.

[11] Chen, H.; Chen, S.; Zhou, R.; Huang, X.; Zhu, S. (2020): Research on four-wheel independent steering intelligent control strategy based on minimum load, *Concurrency and Computation: Practice and Experience*, Vol. **33**, Issue 9.

[12] Chen, X.; Han, Y.; Hang, P. (2020): Researches on 4WIS-4WID stability with LQR coordinated 4WS and DYC, *IAVSD 2019: Advances in Dynamics of Vehicles on Roads and Tracks*, Lecture Notes in Mechanical Engineering. Springer.

[13] Hang, P.; Xia, X.; Chen, X. (2021): Handling stability advancement with 4WS and DYC coordinated control: A gain-scheduled robust control approach, *IEEE Transactions on Vehicular Technology*, Vol. **70**, Issue 4, pp. 3164 –3174.

[14] Choi, M. W.; Park, J. S.; Lee, B. S.; Lee, M. H. (2008): The performance of independent wheels steering vehicle (4WS) applied Ackermann geometry, *2008 International Conference on Control, Automation and Systems*, Seoul, pp. 197–202.

[15] Oksanen, T.; Linkolehto, R. (2023): Control of four wheel steering using independent actuators, *IFAC Proceedings Volumes*, Vol. **46**, Issue 18, pp. 159–163.

[16] Liu, C.; Weichao Sun, W.; Zhang, J. (2020): Adaptive sliding mode control for 4-wheel SBW system with Ackermann geometry, *ISA Transactions*, Vol. **96**, pp. 103–115.

[17] Yim, S. (2020): Comparison among active front, front independent, 4-wheel and 4-wheel independent steering systems for vehicle stability control, *Electronics*, Vol. **9**, Issue 5.

[18] Nah, J.; Yim, S. (2020): Vehicle stability control with four-wheel independent braking, drive and steering on in-wheel motor-driven electric vehicles, *Electronics*, Vol. **9**, Issue 11.

Mechanical Engineering – Scientific Journal, Vol. **41,** No. 1, pp. 71–74 (2023)
CODEN: MINSC5 In print: ISSN 1857–5293
On line: ISSN 1857–9191

INSTRUCTIONS FOR AUTHORS

The *Mechanical Engineering – Scientific Journal* is published twice yearly. The journal publishes **original scientific papers, short communications, reviews** and **professional papers** from all fields of mechanical engineering.

The journal also publishes (continuously or occasionally) the bibliographies of the members of the Faculty, book reviews, reports on meetings, informations of future meetings, important events and data, and various rubrics which contribute to the development of the corresponding scientific field.

Original scientific papers should contain hitherto unpublished results of completed original scientific research. The number of pages (including tables and figures) should not exceed 15 (28 000 characters).

Short communications should also contain completed but briefly presented results of original scientific research. The number of pages should not exceed 5 (10 000 characters) including tables and figures.

Reviews are submitted at the invitation of the Editorial Board. They should be surveys of the investigations and knowledge of several authors in a given research area. The competency of the authors should be assured by their own published results.

Professional papers report on useful practical results that are not original but help the results of the original scientific research to be adopted into scientific and production use. The number of pages (including tables and figures) should not exceed 10 (18 000 characters).

Acceptance for publication in the Journal obliges the authors not to publish the same results elsewhere.

SUBMISSION

The article and annexes should be written on A4 paper with margins of 2.5 cm on each side with a standard font Times New Roman 11 points and should be named with the surname of the first author and then if more and numbered. It is strongly recommended that on MS Word 2003 or MS Word 2007 and on PDF files of the manuscript be sent by e-mail:

mesj@mf.edu.mk.

A letter must accompany all submissions, clearly indicating the following: title, author(s), corresponding author's name, addres and e-mail addres(es), suggested category of the manuscript and a suggestion of five referees (their names, e-mail and affiliation).

Articles received by the Editorial Board are sent to two referees (one in the case of professional papers). The suggestions of the referees and Editorial Board are sent to the author(s) for further action. The corrected text should be returned to the Editorial Board as soon as possible but in not more than 30 days.

PREPARATION OF MANUSCRIPT

The papers should be written in the shortest possible way and without unnecessary repetition.

The original scientific papers, short communications and reviews should be written in English, while the professional papers may also be submitted in Macedonian.

Only SI (Système Internationale d'Unites) quantities and units are to be used.

Double subscripts and superscripts should be avoided whenever possible. Thus it is better to write $\nu_3(PO_4)$ than $\nu_{3_{PO_4}}$ or exp(–E/RT) than $e^{-E/RT}$. Strokes (/) should not be used instead of parentheses.

When a large number of compounds have been analyzed, the results should be given in tabular form.

Manuscript should containt: title, author(s) full-name(s), surname(s), address(es) and e-mail of the corresponding author, short abstract, key words, introduction, experimental or theoretical background, results and discussion, acknowledgment (if desired) and references.

The **title** should correspond to the contents of the manuscript. It should be brief and informative and include the majority of the key words.

Each paper should contain an **abstract** that should not exceed 150 words, and **3–5 key words**. The abstract should include the purpose of the research, the most important results and conclusions.

The **title**, **abstract** and **key words** should be translated in Macedonian language. The ones written by foreign authors will be translated by the Editorial Board.

In the **introduction** only the most important previous results related to the problem in hand should be briefly reviewed and the aim and importance of the research should be stated.

The **experimental** section should be written as a separate section and should contain a description of the **materials used and methods** employed – in form which makes the results reproducible, but without detailed description of already known methods.

Manuscripts that are related to **theoretical studies**, instead of experimental material, should contain a sub-heading and the **theoretical background** where the necessary details for verifying the results obtained should be stated.

The **results and discussion** should be given in the same section. The discussion should contain an analysis of the results and the conclusions that can be drawn.

Figures (photographs, diagrams and sketches) and **mathematical formulae** should be inserted in the correct place in the manuscript, being horizontally reduced to 8 or 16 cm. The size of the symbols for the physical quantities and units as well as the size of the numbers and letters used in the reduced figures should be comparable with the size of the letters in the main text of the paper. Diagrams and structural formulae should be drawn in such a way (e.g. black Indian ink on white or tracing paper) as to permit high quality reproduction. The use of photographs should be avoided. The tables and the figures should be numbered in Arabic numerals (e.g., Table 1, Figure 1). Tables and figures should be self-contained, i.e. should have captions making them legible without resort to the main text. The presentation of the same results in the form of tables and figures (diagrams) is not permitted. The use of equation editor (MS Word, Microsoft Equation, Math Type 6.0 Equation) for typesetting the equations is recommended. Strokes (/) should not be used instead of parentheses.

Figures and tables must be centred in the column. Large figures and tables may span across both columns (Figure 1).

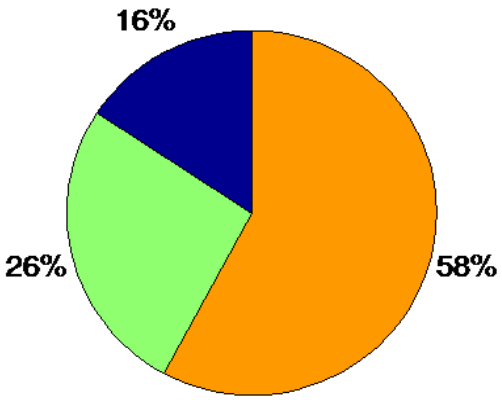

Fig. 1. Example of a graph and a single-line caption (colour)

Graphics may be full colour. Please use only colours which contrast well both on screen and on a black-and-white hardcopy because the Journal is published in black-and-white, as shown in Figure 2. The colour version is only for the electronic version of the Journal.

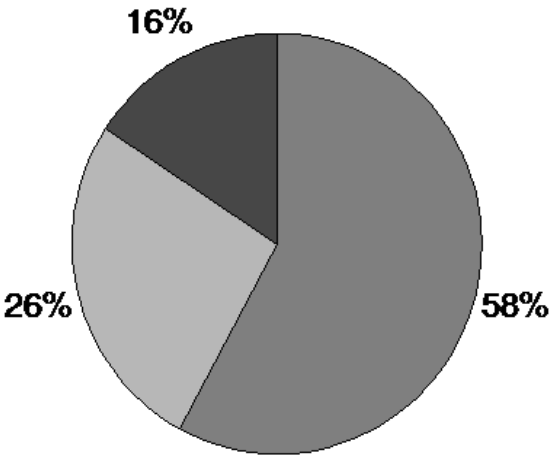

Fig. 2. Example of a graph and a single-line caption (bleck and vhite)

Please check all figures in your paper both on screen and on a black-and-white hardcopy. When you check your paper on a black-and-white hardcopy, please ensure that:

– the colours used in each figure contrast well (Figure 3),

– the image used in each figure is clear,

– all text labels in each figure are legible.

Please check all figures in your paper both on screen and on a black-and-white hardcopy. When you check your paper on a black-and-white hardcopy, please ensure that the image used in each figure is clear and all text labels in each figure are legible.

Fig. 3. Example of an image as it will appear at the electronic version of the Journal and a multi-line caption

Footnotes are also not permitted.

The **reference** should be given in a separate section in the order in which they appear in the text. The surname of one or two authors may be given in the text, whereas in the case of more than two authors they should be quoted as, for example:

Examples of reference items of different categories shown in the References section include:

- example of a book in [1]
- example of a book in a series in [2]
- example of a journal article in [3]
- example of a conference paper in [4]
- example of a patent in [5]
- example of a website in [6]
- example of a web page in [7]
- example of a databook as a manual in [8]
- example of a datasheet in [9]
- example of a master/Ph.D. thesis in [10]
- example of a technical report in [11]
- example of a standard in [12]

All reference items must be in 9 pt font. Please use Regular and Italic styles to distinguish different fields as shown in the References section. Number the reference items consecutively in square brackets (e.g. [1]).

When referring to a reference item, please simply use the reference number, as in [2]. Do not use "Ref. [3]" or "Reference [3]" except at the beginning of a sentence, e.g. "Reference [3] shows …". Multiple references are each numbered with separate brackets (e.g. [2], [3], [4–6]).

The **category** of the paper is proposed by the author(s), but the Editorial Board reserves for itself the right, on the basis of the referees' opinion, to make the final choice.

Proofs are sent to the author(s) to correct printers' errors. Except for this, alterations to the text are not permitted. The proofs should be returned to the Editorial Board in 2 days.

The author(s) will receive, free of charge, 1 reprints of every paper published in the Journal.

REFERENCES

[1] Surname, N(ame).; Surname, N(ame). (Year): *Name of the Book*, Publisher.

[2] Surname, N(ame).; Surname, N(ame). (Year): *Name of the Book*, Name of the Series. Publisher, **vol.** XXX.

[3] Surname, N(ame).; Surname N(ame). (Year): Title of the article, *Name of the Journal*, **vol. XX,** No. XX, pp. XXX–XXX.

[4] Surname, N(ame).; Surname N(ame). (Year): Title of the article, *Proceedings of the Name of the Conference*, vol. **XX,** pp. XXX–XXX.

[5] Surname, N(ame).; Surname, N(ame).: *Name of the Patent*, Institution that issued the patent and Number of the patent (Date dd. mm. yyyy).

[6] N.N. (Year): *The XXX web site*, web address.

[7] Surname, N. (Year): *XXX homepage on XXX*, web address.

[8] N.N. (Year): *Title of the Manual*, Name of the Organization.

[9] N.N.: *XXX data sheet*, Name of the Organization.

[10] Surname, N. (Year): *Title of the Thesis*, Master/Ph.D. thesis (in Language), Institution.

[11] Surname, N(ame).: Surname, N(ame). (Year): *Title of the Report*, Organization that issued the report, number of the report.

[12] Institution that issued the standard (Year): *Name of the Standard* & Number of the standard.